Few-body physics
in a Finite Volume

Dissertation

zur

Erlangung des Doktorgrades (Dr. rer. nat.)

der

Mathematisch-Naturwissenschaftlichen Fakultät

der

Rheinischen Friedrich-Wilhelms-Universität

Bonn

vorgelegt von

Simon Kreuzer

aus

Troisdorf

Bonn, Juli 2010

Angefertigt mit Genehmigung der
Mathematisch-Naturwissenschaftlichen Fakultät der
Rheinischen Friedrich-Wilhelms-Universität Bonn

1. Referent: Prof. Dr. H.-W. Hammer

2. Referent: PD Dr. B. Ch. Metsch

Tag der Promotion: 22. September 2010

"Three shalt be the number thou shalt count, and the number of the counting shalt be three. Four shalt thou not count, neither count thou two, excepting that thou then proceed to three. Five is right out."

– BOOK OF ARMAMENTS, 2:18–20,
Monty Python and the Holy Grail.

Abstract

In this work, three-body bound states were studied in finite volume using an Effective Field Theory framework. The finite volumes under consideration are cubic volumes with periodic boundary conditions. The Effective Field Theory framework used in this work employs only contact interactions and is particularly well suited for studies of universal properties, i.e. properties independent of the details of the interaction on short distances. A particular example in the three-body sector is the Efimov effect, the emergence of a geometrically spaced bound state spectrum.

In the first part, systems of three identical bosons are investigated. As a consequence of the breakdown of the spherical symmetry to cubic symmetry, the partial waves of the bound state amplitude are coupled. An infinite set of coupled integral equations for these partial waves is derived. These equations have to be solved numerically in order to obtain the binding energies in the finite volume. The dependence of the energies on the box size is calculated and the results are explicitly verified to be renormalized. Results for positive and negative scattering lengths are shown. The effects of higher partial waves are investigated. The behavior of shallow trimers near the dimer energy as well as deeply bound trimers is studied. The shallowest state investigated crosses the dimer energy at a certain volume and behaves like a scattering state for smaller volumes. Numerical evidence for a universal scaling of the finite volume corrections is provided.

Subsequently, the formalism is extended to systems of three nucleons. This case provides the main motivation for this work due to its applicability to Lattice Quantum Chromodynamics (QCD) calculations of the triton. Such calculations always take place inside a finite volume which makes control over the corresponding effects crucial for an understanding of results from the lattice. For the triton, there are two coupled channels already in the infinite volume corresponding to two different spin-isospin combinations. An infinite set of coupled integral equations for the partial waves of the bound state amplitudes is derived. The renormalization of all results is again explicitly verified. The physical triton inside a finite volume is investigated as well as the triton spectrum for unphysical pion masses. The former case qualitatively shows the same behavior as the three-boson case, and the volume dependence is calculated. The smallest volumes investigated are of the order of magnitude typical for present day Lattice calculations. The motivation for the latter part is twofold. On the one hand, Lattice QCD calculations are performed at pion masses larger than the physical one for computational reasons. On the other hand, it has been conjectured that QCD is close to the critical trajectory for an infrared renormalization group limit cycle, in which case the Efimov effect would occur for a critical pion mass. Close to this critical pion mass, the triton has excited states. The behavior of the ground state and of the excited states inside a finite volume is investigated for various pion masses around the critical one. The excited states cross the energy of the bound di-nucleon, as it was already observed for the shallowest bosonic trimer. The results for the ground state were used to provide strong numerical evidence for a universal scaling of the finite volume corrections.

Zusammenfassung

In dieser Arbeit wurden gebundene Zustände von drei Teilchen in endlichen Volumina mit der Methode der Effektiven Feldtheorie untersucht. Die betrachteten endlichen Volumina sind kubische Volumina mit periodischen Randbedingungen. Die Effektive Feldtheorie, die in dieser Arbeit verwendet wurde, verwendet ausschließlich Kontaktwechselwirkungen und ist besonders gut geeignet um die universellen, d.h. von den Details der Wechselwirkung bei kurzen Abständen unabhängigen, Eigenschaften eines Systems zu untersuchen. Ein spezielles Beispiel für eine solche Eigenschaft im Drei-Körper-Sektor ist der Efimov-Effekt, das Auftreten eines Spektrums gebundener Zustände mit einem konstanten Quotienten benachbarter Bindungsenergien.

Im ersten Teil werden Systeme aus drei identischen Bosonen untersucht. Da die sphärische Symmetrie zur kubischen Symmetrie reduziert ist, sind die Partialwellen der Amplitude des gebundenen Zustands gekoppelt. Ein System aus unendlich vielen gekoppelten Integralgleichungen für diese Partialwellen wird hergeleitet. Diese Gleichungen müssen numerisch gelöst werden um die Bindungsenergie im endlichen Volumen zu erhalten. Die Abhängigkeit dieser Energien von der Kastengröße wird berechnet und es wird explizit gezeigt, dass die Ergebnisse renormiert sind. Es werden Ergebnisse sowohl für positive als auch für negative Streulängen gezeigt. Die Effekte durch die Beimischung höherer Partialwellen werden untersucht. Sowohl das Verhalten schwach gebundener Zustände nahe der Dimer-Energie als auch tief gebundener Zustände wird studiert. Der am schwächsten gebundene der untersuchten Zustände überschreitet die Dimer-Energie bei einem bestimmten Volumen und verhält sich für kleinere Volumina wie ein Streuzustand. Numerische Belege für ein universelles Skalieren der Korrekturen durch das endliche Volumen werden präsentiert.

Anschließend wird der Formalismus auf Drei-Nukleon-Systeme erweitert. Dieser Fall liefert die Hauptmotivation für diese Arbeit, da die Ergebnisse auf Berechnungen des Tritons mit Hilfe der Gitter-Quantenchromodynamik (QCD) angewendet werden können. Solche Rechnungen verwenden stets ein endliches Volumen, was Kontrolle über die entsprechenden Effekte unverzichtbar für das Verständnis der Ergebnisse macht. Im Falle des Tritons gibt es zwei gekoppelte Amplituden bereits im unendlichen Volumen, die zwei verschiedenen Spin-Isospin-Kombinationen entsprechen. Ein System aus unendlich vielen Integralgleichungen für die Partialwellen der entsprechenden Amplituden wird hergeleitet. Es wird wiederum explizit nachgewiesen, dass alle Ergebnisse renormiert sind. Das physikalische Triton in einem endlichen Volumen wird ebenso untersucht wie das Tritonspektrum bei unphysikalischen Pionmassen. Im ersten Fall wird die Volumenabhängigkeit berechnet und qualitativ das gleiche Verhalten beobachtet wie im bosonischen Fall. Die kleinsten untersuchten Volumina sind von einer Größe die typisch ist für aktuelle Gitterrechnungen. Die Untersuchung des zweiten Falls ist zweifach motiviert. Zum einen werden aus numerischen Gründen Gitter-QCD-Rechnungen stets bei Pionmassen durchgeführt die größer sind als die physikalische. Zum anderen wurde die Vermutung aufgestellt, dass sich die QCD in der Nähe der kritischen Trajektorie für einen infraroten Renormierungsgruppen-Grenzzyklus befindet. In diesem Fall würde bei einer kritischen Pionmasse der Efimov-Effekt auftreten, und in der Nähe dieser kritischen Pionmasse besäße das Triton angeregte Zustände. Das Verhalten des Grundzustands und der angeregten Zustände in einem endlichen Volumen wird für verschiedene Pionmassen in der Nähe des kritischen Werts untersucht. Die angeregten Zustände überqueren die En-

ergie des gebundenen Zwei-Nukleon-Zustands, ähnlich dem Verhalten das im bosonischen Fall für den am schwächsten gebundenen Zustand beobachtet wurde. Die Ergebnisse für den Grundzustand wurden verwendet um starke numerische Belege für ein universelles Skalieren der Volumen-Korrekturen zu liefern.

Contents

Chapter 1

Introduction

Quantum Chromodynamics (QCD) is known to be the underlying theory of nuclear physics since almost forty years. It describes the strong interaction as an interaction between fundamental fermions, the quarks, that is mediated by vector-bosons called gluons. The notion that all the hadrons, the strongly interacting particles, observed in nature are composite objects of quarks and anti-quarks took long to develop. The first step in this direction was the development of the "Eightfold Way" [GM62, Ne'61] in the early sixties. In it, all known hadrons are arranged in multiplets of what today is called the SU(3) flavor symmetry. Group theoretical considerations led to the constituent quark model, where baryons are described as bound states of three quarks, while mesons are interpreted as quark–anti-quark bound states [GM64]. The Eightfold Way predicted the up-to-then unobserved Ω-particle and its mass. This prediction was experimentally confirmed a few years later [B$^+$64].

However, two problems remained unsolved. The first was that wave functions of the baryons seemed to violate the Pauli principle. That is, the wave functions of, e.g., the Δ^{++}, is completely symmetric, but should be antisymmetric. To solve this, it was assumed that each quark comes in one of three colors. It was then postulated that the color wave function of a hadron is always antisymmetric. This also answered the second question, namely why no free quarks are observed. A satisfactory explanation of this postulate, that is called confinement, is to date still not found and maybe the largest unanswered question in QCD.

A striking experimental confirmation for the compositeness of hadrons was provided in 1969 by deep inelastic scattering experiments [B$^+$69b, B$^+$69a]. From these experiments could be inferred that nucleons contain pointlike charged particles. These particles were shown to carry the quantum numbers of the hypothetical quarks. This evidence for the existence of quarks paved the way for QCD. It was formulated by promoting the color symmetry to a gauge symmetry [FGML73]. The quantization of such non-abelian gauge theories was known since 1967 [FP67]. In 1973, Gross and Wilczek [GW73] and Politzer [Pol73] proved that QCD is asymptotically free, i.e. that the effective charge decreases at higher energies. This explains why the deep-inelastic scattering experiments were able to probe quasi-free quarks inside hadrons, while on the other hand the strong interaction is indeed strong on the length scale of fm relevant to nuclear physics.

Since then, many experimental tests have been carried out that all confirm QCD as the underlying theory of strong interactions. Nonetheless, the determination of nuclear properties directly from the fundamental interaction of quarks and gluons remains a challenge in

theoretical physics. In particular, the coupling constant of QCD is too large to allow for a pertubative treatment of the theory in the energy regime of nuclear physics.

Nuclear physics has therefore resorted to describing the hadrons as effective degrees of freedom. Phenomenological models were successfully used to describe nuclear properties. However, a model independent approach relying directly on QCD was highly wanted. It could be found with the formulation of *Effective Field Theories* (EFTs). EFTs employ a separation of scales to describe the effective degrees of freedom in a model-independent and systematically improvable manner.

An example for an EFT of QCD, Chiral Perturbation Theory [Wei79, GL84, GL85, BKM95] is an expansion around the limit of massless quarks in the masses of the quarks or, equivalently, the masses of the lightest mesons, and in small momenta. This allows to control the pion-mass dependence of hadronic observables, which will be put to use in the course of this work. χEFT has been successfully used to describe the masses and the scattering properties of mesons as well as pion photoproduction off nucleons (see [BM07] for a review). In recent years, there has been much effort to derive few-nucleon potentials from a Chiral Effective Theory (see, e.g., [Epe06]).

A different approach employs the unnaturally largeness of the neutron-proton scattering lengths compared to the underlying length scale of ~ 1.4 fm given by the inverse pion mass. This separation of scales is employed by describing the nucleons in an EFT (sometimes called $\pi\!\!\!/$EFT) that uses only contact interactions and that corresponds to an expansion in the natural length scale over the unnaturally large scattering lengths [KSW98a, KSW98b, vK97, vK99]. The theory was subsequently extended to the three-nucleon systems [BvK98, BHvK98, BHvK00]. All three-nucleon observables depend to leading order only on three parameters. By fixing these to the two two-body scattering lengths and the neutron-deuteron scattering length, the binding energy of the triton can be predicted to a remarkable accuracy of 6% already at leading order [BHvK00]. Exploiting that calculations in this theory are easier than in χEFT, the pion-mass dependence of three-nucleon observables were studied in $\pi\!\!\!/$EFT with χEFT providing the necessary input parameters [HPP07]. In the present work, this program will be extended by placing the three nucleons inside the finite volume.

Such an EFT for resonantly interacting particles has the feature of universality, i.e. independence of the details of the underlying interaction at short distances. Therefore, there are phenomena that can be observed in *any* physical system with a large two-body scattering length. For example, if the scattering length is positive, there exists a shallow two-body bound state. In the *np*-system, this shallow bound state is identified as the deuteron. More complicated universal properties are present in the three-body system. For instance, Efimov predicted in 1970 that a sequence of geometrically spaced three-body bound states exists in the limit of infinite scattering length [Efi70, Efi79]. For a review on the universal properties of resonantly interacting few-body systems see [BH06].

This *Efimov effect* was experimentally confirmed through its impact on the recombination rate of ultracold cesium atoms [KMW$^+$05]. In such ultracold atomic atoms, the scattering length can be tuned by varying an external magnetic field through a so-called Feshbach resonance. This possibility to experimentally fine-tune the scattering length to unnaturally large values has resparked the interest in systems of resonantly interacting particles on the experimental as well as on the theoretical side.

In nuclear physics, the triton and its isospin partner, the ^{3}He nucleus can be interpreted as Efimov states. In the three-body sector of πEFT, the theory is on the critical trajectory for an ultraviolet renormalization group limit cycle [BHvK00]. The EFT for three identical bosons has the same ultraviolet behavior [BHvK99b, BHvK99a] and will therefore serve as a model case in this work.

A complimentary approach to the determination of nuclear properties is *Lattice QCD*. In this technique, going back to an idea of Wilson [Wil74], a discretized version of QCD in Euclidean space-time is solved numerically. This requires an enormous computational effort that is tackled by large CPU clusters dedicated to that task. When converting Lattice QCD results to physical results, three limits have to be taken. Firstly, the discretization has to be removed. Secondly, the calculations necessarily take place inside a finite volume. The possibility to perform a smooth extrapolation to the infinite volume was one of the main motivations for this work. Thirdly, Lattice QCD calculations are performed at unphysical quark masses due to numerical restrictions. The EFT approach is well suited to help perform these limits. The discretization introduces an ultraviolet cutoff that is present in the EFTs as a regulator anyway. In particular, the pion mass dependence is, as stated above, well under control in Chiral Perturbation Theory. The control over finite volume effects in the three-body sector is the scope of this work.

Lattice QCD has recently entered a stage where quantitative predictions become possible. For a recent review on the status of nuclear physics from Lattice QCD see [BDOS10]. The ground state masses of the mesons and the baryons can be well reproduced by modern lattice calculations, while the calculation of excitation spectra remains challenging. In the purely mesonic sector, the isospin-symmetric pion-pion scattering length was determined with remarkable precision and agrees well with the value derived from experimental results. For meson-baryon interactions, only certain channels are at the moment accessible. In particular, pion-nucleon scattering observables have not been calculated up to now. Lattice calculations of baryonic interactions are complicated by a strong exponential decay of the signal-to-noise ratio in Euclidean time. In the nucleon-nucleon interaction, the present results indicate natural values for the scattering lengths. This is in contrast to the unnaturally large values at physical pion mass. This behavior is explained by a conjecture of Braaten and Hammer [BH03] that QCD can be tuned to the critical trajectory of an infrared limit cycle by slightly varying the quark masses or, equivalently, the pion mass. The pion masses investigated in Lattice QCD are far away from this critical trajectory, therefore the nucleon-nucleon interaction is not resonant in these cases. Quantitative results for few-baryon systems have only recently been obtained for the first time [B$^+$09]. A proof of principle for calculations of three-nucleon systems with the quantum numbers of the triton was provided. As soon as these calculations reach a quantitative level, the possibility of a smooth infinite volume extrapolation as it is provided in this work will be crucial for the interpretation of the results.

As an additional motivation for the present work serves the two-body case. Here, Lüscher was able to show that the finite volume dependence of the result is not only an obstacle but also encodes infinite volume scattering properties [Lüs91b, Lüs91a]. Lüscher's general field theoretic approach relies on the fact that the two-body amplitude can be obtained analytically. Therefore, an analoguous formula for three-body sector, where the amplitude can in general only be determined numerically, is not to be expected. The finite volume results presented in this work, however, will implicitly depend on infinite volume scattering parameters.

Some properties of three-body systems in finite boxes have been studied previously. For systems where no bound states are present, Tan determined the ground-state energy of three bosons [Tan07]. This result has been generalized to systems with N bosons with repulsive or weakly attractive interactions [BDS07, DS08]. These formulas were put to use in the analysis of few-boson results from Lattice QCD. Also, systems of three identical fermions in the unitary limit of infinite scattering length inside a finite cubic box have been studied [PC07]. In this system, there are no bound states in the infinite volume due to the Pauli principle.

Chiral effective field theory has also been implemented on the lattice. Using this theory, Epelbaum et al. were able to derive several properties of the three- and four-nucleon system [EKLM09]. In particular, they were also able to derive the volume dependence of the triton energy in their approach.

Cubic volumes are not the only finite volumes that have been considered so far. When performing experiments with cold atomic gases, the atoms are located inside traps. These traps can be idealized to a harmonic oscillator potential. For certain atomic species, it is possible to experimentally tune the scattering length of the atoms by virtue of a so-called Feshbach resonance. This allows for experimental access to the regime of universal physics. Therefore, much effort is being put into the study of particles inside such a harmonic oscillator potential. EFTs are being used to derive, for example, energy spectra of particles with large scattering lengths inside harmonic oscillator potentials. As a particular example, the three-particle spectrum at the unitary limit was worked out by Werner and Castin [WC06]. The generalization to systems of N particle systems with large scattering length inside a harmonic oscillator potential is currently in progress.

The present work is focussed on the investigation of finite volume effects for three-body bound states. The case of three identical bosons will serve as a model case [KH09, KH10]. Subsequently, the formalism is extended to the three-nucleon case.

This thesis is organized as follows. In Chapter 2, the method of Lattice QCD will be introduced as well as Lüscher's formula. In the second part of this introductory chapter, the concept of EFT is introduced in detail. The application of EFTs to systems of resonantly interacting particles is discussed and universal properties of the two- and three-body sector, including the Efimov effect, are presented in detail. The $\pi\!\!\!/$EFT as special case for nucleonic systems is also described. The finite volume formalism for three identical bosons will be derived in Chapter 3. Here, also the numerical methods needed to solve for the binding energies will be discussed. The corresponding results are shown in Chapter 4. In particular, the possibility of a universal scaling of the finite volume corrections will be investigated. After the study of this model case, the formalism is extended to the three-nucleon system in Chapter 5. Results for the triton are presented in Chapter 6. Apart from the physical triton in finite volume, the pion-mass dependence of the triton spectrum was studied as well. The final chapter summarizes the main results and provides an outlook on how to proceed in the study of finite volume effects in the three-body sector.

Chapter 2

Effective Field Theory and Finite Volume Theories

The fundamental theory of strong interactions is Quantum Chromodynamics (QCD). This theory describes the interactions of quarks and gluons. In nature, however, quarks and gluons are always confined in hadrons. In particular, these are quark-antiquark bound states called mesons, like the pion, and three-quark bound states called baryons, like the nucleon. The strong coupling of QCD makes the direct calculation of hadronic properties by a perturbative approach impossible. In the last decades, two model-independent ways to circumvent this problem have emerged. The first is to solve a discretized Euclidean version of QCD numerically, an approach called *Lattice QCD*, that will be described in more detail in Section 2.1. Secondly, the Effective Field Theory (EFT) approach has been used to describe the effective degrees of freedom of the strong interaction, namely mesons and baryons. A general introduction to Effective Field Theories and their application to nuclear physics is given in Section 2.2.

2.1 Lattice QCD

The Lagrangian of QCD is given in terms of the quark fields q and the gauge fields A associated with the color group SU(3) as

$$\mathcal{L}_{\text{QCD}} = \sum_f \bar{q}_f(\slashed{D} - m_q)q_f - \frac{1}{2}\text{tr}F_{\mu\nu}F^{\mu\nu}, \tag{2.1}$$

with the covariant derivative $D_\mu = \partial_\mu - \mathrm{i}gA_\mu$ and the field strength tensor $F_{\mu\nu} = \partial_\mu A_\nu - \partial_\nu A_\mu - \mathrm{i}g[A_\mu A_\nu]$. The summation here is over the six different quark flavors. The Lagrangian is invariant under the gauge transformations $\Omega(x) \in$ SU(3), where the fields transform as

$$q \to \Omega(x)q, \tag{2.2a}$$

$$A_\mu \to \Omega(x)A_\mu\Omega^\dagger(x) - \mathrm{i}\left[\partial_\mu\Omega(x)\right]\Omega^\dagger(x). \tag{2.2b}$$

On the energy scale of hadronization, the coupling constant of QCD is of order 1. This makes a perturbative treatment of the quark-gluon-interaction leading to confined hadrons

5

impossible. A non-perturbative way to gain quantitative results on hadron properties directly from QCD was pointed out by Wilson in 1974 [Wil74]. At present, this technique that goes by the name of *Lattice QCD*, is the only way to determine hadronic properties directly from QCD. For a review on the current status of obtaining nuclear physics from Lattice QCD, see [BDOS10].

The main idea of Lattice QCD is to rewrite the path integral of QCD

$$\langle \mathcal{O} \rangle = \frac{1}{Z} \int \mathcal{D}\bar{q}\mathcal{D}q\mathcal{D}A\, \mathcal{O}[\bar{q}, q, A] \mathrm{e}^{\mathrm{i}S[\bar{q},q,A]} \tag{2.3}$$

$$Z = \int \mathcal{D}\bar{q}\mathcal{D}q\mathcal{D}A\, \mathrm{e}^{\mathrm{i}S}, \qquad S = \int \mathrm{d}t\mathrm{d}^3x \mathcal{L}_{\mathrm{QCD}} \tag{2.4}$$

such that it becomes accessible for a numerical treatment. The strongly oscillating phase factor $\mathrm{e}^{\mathrm{i}S}$ hinders the convergence of the integrals. To remedy this, the theory is analytically continued to imaginary time. Thus, Lattice QCD is formulated in Euclidean rather than Minkowski space-time. In imaginary time, the phase fator becomes e^{-S}. For positive action, this serves as a convergence factor. But still, the path integral measure corresponds to an infinite number of integrations. For the numerical calculations, space-time therefore has to be discretized. The lattice spacing will be denoted b. A typical size for the lattice spacing is at present $b \lesssim 0.12$ fm. Due to the finiteness of computer memory, only a finite number of lattice points can be used. This places every lattice calculation inevitably inside a finite volume. Most calculations are performed in a cubic volume with periodic boundary conditions, while the extend in Euclidean time is in general much larger. State-of-the-art lattice calculations use volumes of $32^3 \times 256$ in lattice units. In physical units, typical volume side lengths for present lattice calculations are $2.5 - 4$ fm.

The finite lattice spacing introduces a minimal accessible wave length. It therefore corresponds to an ultraviolet cutoff that regulates the theory. Such a cutoff is always present in EFT. Therefore, effects from the finite lattice spacing are not considered in this work. The finite volume, on the other hand, modifies the infrared physics of the system. These effects have to be removed by extrapolating to the infinite volume.

The fermions in this approach are residing on the lattice sites. The discretization of fermions is a challenging task because of the so-called fermion doubling problem. A naive discretization of the fermion field yields 16 light fermion fields. In order to resolve this, the fermionic part of the action has to be modified. Several of these lattice fermion actions are now on the market. Of special interest in modern lattice calculations are fermionic actions that respect a Lattice version of chiral symmetry. Examples are Kogut-Susskind fermions, domain wall fermions and overlap fermions.

The gauge fields are given by elements of the gauge group residing on the links between adjacent lattice sites. Gauge invariant quantities can be formed by building closed loops. In particular, the squares with minimal area are called plaquettes. The gauge action can be given by summing the real part of the trace of the plaquette over all possible plaquettes. The continuum limit of this action is indeed the Yang-Mills action, as the plaquettes are reduced to Wilson loops if the lattice spacing goes to zero. In the lattice path integral, the integration over the gauge fields has to be replaced by an integration over the gauge group for each link. The integrational measure is given by the Haar measure of the group, which guarantees gauge invariance.

The functional integration over the fermionic part of the action can be carried out by recognizing that this part of the Euclidean QCD action is always a quadratic form $\bar{q}D(U)q$ of the fermion fields. The price for this, however, is that in this case the calculation of the fermion determinant $\det(D(U)^\dagger D(U))$ is required. When calculating expectation values of fermionic operators, it is necessary to invert the fermion matrix $D(U)$. Both tasks are numerically expensive. Even worse, the inversion problem is the more ill-conditioned the smaller the quark masses are. For this reason, Lattice QCD calculations are carried out at quark masses greater than the physical ones. Higher quark masses correspond to larger pion masses, as stated by the Gell-Mann–Oakes–Renner relation $m_q \sim m_\pi^2$. Pion masses of about 250 MeV are typical in present day lattice calculations. The remaining integration over possible gauge field configuration still involves $\approx 10^9$ degrees of freedom. Integrations of this dimesionality are performed in a Monte Carlo approach.

Current Lattice calculations are able to reproduce ground state masses of mesons and baryons to good accuracies. Two-body states are also investigated. The extraction of two-body scattering parameters is made possible by Lüscher's formula that will be discussed in the following.

By generalizing a result from non-relativistic quantum mechanics to quantum field theory, Lüscher was able to derive a powerful connection between the volume dependence of two-body states inside finite cubic volumes on the one side and the scattering amplitude in infinite volume on the other side [Lüs91b]. Before stating Lüscher's formula, it is important to understand how energy levels and, in particular, masses can be extracted from correlation functions.

Inside a finite volume, momentum quantization dictates that the energy spectrum is discrete. In particular, the scattering continuum in the infinite volume corresponds to well separated energy levels. The position of the finite volume scattering levels depends on the size of the volume under consideration.

The pion two-point function, $C_{\pi^+}(t)$, is generated by a source and a sink for a pion of the form $\pi^+(\vec{x}, t) = \bar{u}(\vec{x}, t)\gamma_5 d(\vec{x}, t)$ by

$$C_{\pi^+}(t) = \sum_{\vec{x}} \langle 0|\pi^-(\vec{x}, t)\pi^+(\vec{0}, 0)|0\rangle, \tag{2.5}$$

where the sum runs over all lattice sites. This corresponds to a projection on zero momentum states. The time evolution of the pion fields is given by the Hamiltonian. Inserting a complete set of states yields

$$C_{\pi^+}(t) = \sum_n \frac{\mathrm{e}^{-E_n t}}{2E_n} \sum_{\vec{x}} \langle 0|\pi^-(\vec{x}, 0)|n\rangle\langle n|\pi^+(\vec{0}, 0)|0\rangle \xrightarrow[\text{large } t]{} A\frac{\mathrm{e}^{-m_\pi t}}{2m_\pi},$$

where in the large t limit only the contribution from the lowest lying state survives. This large time behavior allows to extract the pion mass by fitting an exponential decay. A different method is to identify a plateau in the so called Effective Mass function, which is defined as the logarithm of the ratio of correlation functions at different times. It is important to note that, in practice, the signal-to-noise ratio strongly decreases with time. Therefore, the simulations parameters always have to be tuned such that there is a large enough window in Euclidean time that allows to clearly identify such a plateau.
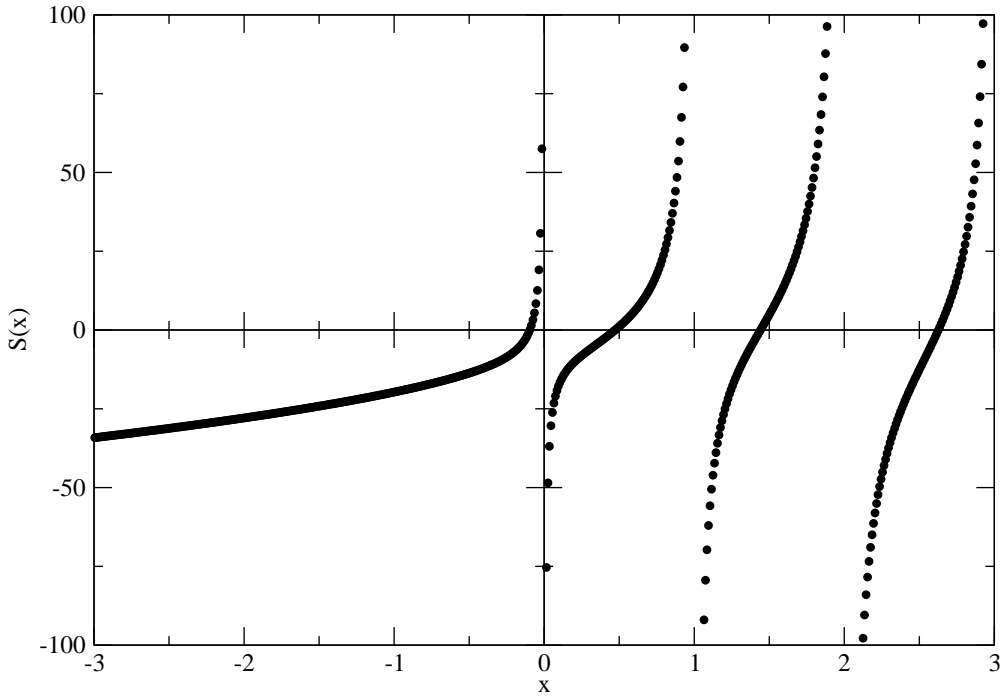
Figure 2.1: The function $S(x)$ as it appears in the version of Lüscher's formula given in Eq. (2.7).

In order to investigate two-body scattering states, four-point correlators like

$$C_{\pi^+\pi^+}(t) = \sum_{\vec{x},\vec{y}} \left\langle \pi^-(\vec{x},t)\pi^-(\vec{y},t)\pi^+(\vec{0},0)\pi^+(\vec{0},0) \right\rangle \qquad (2.6)$$

have to be computed. In large volumes, the difference between the energies of the interacting and non-interacting two-body levels is supposed to be small in comparison to the total energy of the system, which is dominated by the meson masses. This difference is extracted from a ratio of correlation functions by

$$\frac{C_{\pi^+\pi^+}(t)}{C_{\pi^+}(t)C_{\pi^+}(t)} \xrightarrow[\text{large } t]{} B_0 \mathrm{e}^{-\Delta E_0 t}.$$

This shift is connected to a momentum p by

$$\Delta E_0 = E_0 - 2m_\pi = 2\sqrt{p^2 + m_\pi^2} - 2m_\pi.$$

For this p-value, $p\cot\delta(p)$ can be obtained from Lüscher's formula

$$p\cot\delta(p) = \frac{1}{\pi L} S\left(\left(\frac{pL}{2\pi}\right)^2\right), \qquad S(x) = \sum_{\vec{n}\in\mathbb{Z}^3}^{|\vec{n}|<\Lambda} \frac{1}{|\vec{n}|^2 - x} - 4\pi\Lambda. \qquad (2.7)$$

For a short introduction into scattering theory that includes the definition of the scattering phase $\delta(p)$, see Subsection 2.2.3. In the definition of S, the limit $\Lambda \to \infty$ is implicit. The function S is plotted in Figure 2.1. By varying the volume, different values of p are obtained and consequently it is possible to map out the momentum dependence of the scattering phase

shift. The formula has been derived in a fully relativistic framework. However, there are two caveats. Firstly, the formula only holds below any inelastic thresholds, which would render the scattering phase complex. Secondly, in the derivation was assumed that the volume is large compared to the range of the interaction. Since this range is for nucleonic interactions given by m_π^{-1}, Lüscher's method can only be applied to lattice calculations with $m_\pi L \gg 1$.

Lüscher's method is frequently applied when studying two-body scattering in lattice calculations. As an example, results for the $I = 2$ pion-pion scattering length $a_{\pi\pi}^{I=2}$ are quoted here. This system is very cleanly accessible for Lattice calculations, allowing for a very precise extraction of $a_{\pi\pi}^{I=2}$. The value given by the NPLQCD collaboration is [B$^+$08]

$$m_\pi a_{\pi\pi}^{I=2} = -0.04330 \pm 0.00042,$$

while a recent determination by the ETM collaboration yielded [FJR10]

$$m_\pi a_{\pi\pi}^{I=2} = -0.04385 \pm 0.00028 \pm 0.00038,$$

where the first error is statistical and the second is an estimate of systematic uncertainties. There are no direct experimental constraints for these values. However, the scattering length can be determined very precisely from high energy scattering data in a dispersion theoretical approach by virtue of the Roy equations [Roy71]. The result is [CGL01]

$$m_\pi a_{\pi\pi}^{I=2} = -0.0444 \pm 0.0001,$$

which is in good agreement with both values obtained from the Lattice.

The nucleon-nucleon interactions were also studied in Lattice calculations. For the pion masses used in these calculations, however, the accidental fine tuning that renders the NN scattering lengths unnaturally large is not expected to be present. Indeed, the calculations yielded scattering lengths of natural size [BBOS06]. The strong pion-mass dependence of the NN-interactions can be understood from a renormalization group point of view, that will be explained in more detail in Section 6.2.

The EFT approach described in the second part of this chapter is well suited to assess the effects of finite volume physics. The form of Lüschers formula given above was derived in an EFT for two-nucleon interactions by Beane et al. [BBPS04].

Lüscher's method of phase shift determination can be extended in order to obtain resonance properties from the volume dependence of energy levels on the lattice [Lüs91a]. Recently, this has been used to study the $\Delta(1232)$ resonance [BLMR08, BLRM08].

First results of three- and four-body systems from Lattice QCD are now reported. A proof of principle for lattice calculations in the triton channel was recently provided [B$^+$09]. As can be seen from Figure 2.2, a conclusive extraction of the triton binding is not yet possible. Nonetheless, with the increasing computational resources dedicated to this field, Lattice QCD might be used for studies of few-nucleon systems at physical quark masses a decade from now.

2.2 Effective Field Theory (EFT)

Effective Field Theory (EFT) is a powerful tool that can be applied to a vast variety of physical systems. In the following, the general concept of Effective theories will be introduced. The
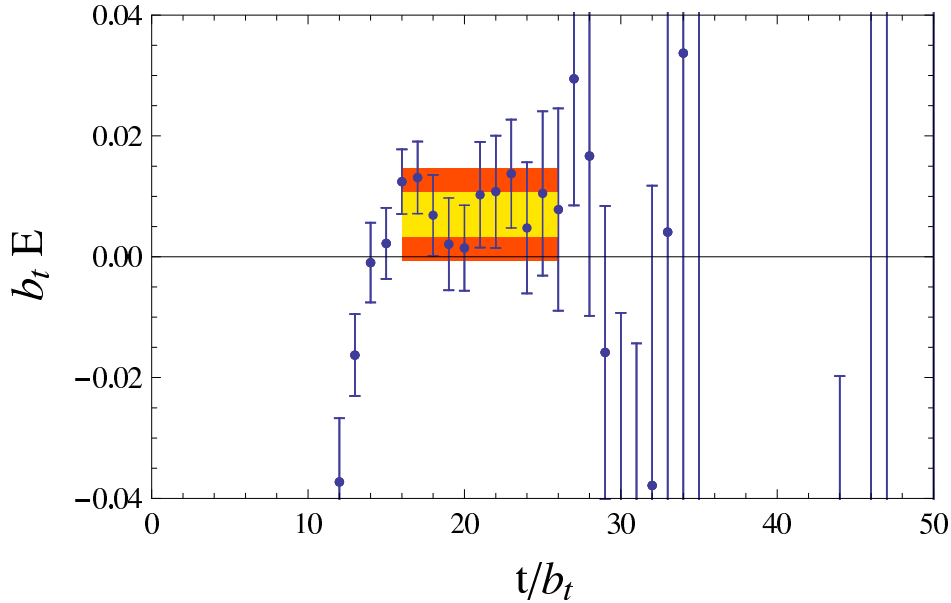
Figure 2.2: Effective Mass plot for the difference between the ground state energy in the triton channel and three times the nucleon mass. The band corresponds to the identified plateau. Figure taken from [BDOS10].

application of this approach to the theory of strong interactions is discussed in detail in Subsection 2.2.2. The EFTs under consideration in this work describe systems of resonantly interacting particles, like the few-nucleon system at very low energies. Such systems exhibit universal properties, such as the Efimov effect, that will be highlighted in Subsection 2.2.3.

2.2.1   An Introduction to Effective Theories

Effective Theories provide a model-independent way to describe low-energy properties of a physical system by exploiting a separation of scales in the problem. This separation allows to describe the relevant low-energy degrees of freedom and their interactions explicitly, while the unresolved short-distance physics are absorbed into a few low-energy constants.

As an example, consider an object with mass m in a height h above earth's surface. Its potential energy can be well described by $V = mgh$, where g is an acceleration constant. This, however, is just an Effective Theory for Newton's gravitational theory. This theory yields $V_{\mathrm{Newton}} = -GMm/(R + h)$, where G is the gravitational constant, and M and R are mass and radius of the earth. Since it is assumed that $h \ll R$, there is a separation of scales that can be exploited. Expanding V_{Newton} in powers of h/R yields an irrelevant constant, a linear term $m(GM/R^2)h$ and corrections of higher order. The combination GM/R^2 gives just the acceleration constant g.

This small example already illustrates several key features of Effective theories. First of all, the separation of scales alluded to above is used to construct one or more small dimensionless parameters. The small parameters provide a way to keep track of the accuracy of the Effective Theory by a so-called *power-counting scheme*. The power-counting is what makes Effective Theories *systematically* improvable, because the corrections from higher order terms become

smaller order by order. Moreover, this provides a way to estimate the accuracy of the result, which is of the order of the first omitted term, namely $(h/R)^2$ in the example above. Secondly, it can be seen how effects from high-energy scales are incorporated into a low-energy constant, namely g. The low-energy constants can in principle be calculated from the fundamental theory. In practice, however, this is not always possible because the fundamental theory is not known or because the underlying theory is too complicated. An example for the first case is the Standard Model, which is supposed to be an Effective Theory itself. An example for the second case is Quantum Chromodynamics (QCD), the theory of strong interactions, that will be discussed in more detail below. In these cases, the low-energy constants have to be determined by matching observables to experimental input. In nuclear physics, also results from Lattice QCD might be used to fix the low-energy constants [Nec08].

Another reason for the tremendous success of the Effective Theory approach is *universality*. Because the short-range behavior of the theory is hidden in the low-energy constants, systems with similar long-range behavior are described by the same Effective Theory. The results from such a theory are then universal in the sense that they are valid for all systems with this long-range behavior. This allows for a wide range of applications of the EFT technique to systems with very different length scales, such as particle physics, nuclear physics and physics of ultracold gases and Bose-Einstein condensates.

Effective Field Theory (EFT) is the application of the Effective Theory method to a field theory. Historically, EFTs have often been found before the corresponding fundamental theory was discovered. A particular example for this is found in the theory of weak interactions. In 1934, Fermi proposed a four-fermion contact interaction as a model for weak interactions. Three decades later, Glashow, Salam and Weinberg discovered electroweak theory, in which the weak interaction is mediated by the exchange of W- and Z-bosons. Due to their large masses, these fields can be integrated out reproducing just Fermi's contact interaction with the correct coupling constant. Therefore, the success of Fermi's theory could be explained a posteriori by the fact that Fermi guessed the correct Effective Theory for weak interactions. The technique of integrating out heavy intermediate fields will be revisited in this work when pionless Effective theory will be introduced.

2.2.2   EFTs of QCD

Historically, the EFT approach was formalized in the field of nuclear physics. The motivation for this was to overcome the stage of phenomenological descriptions of hadronic and nuclear properties and establish model-independent formulations of the strong interactions for the effective degrees of freedom, namely the hadrons.

There are two EFTs describing the strong interaction in different energy regimes. These are Chiral Effective Field Theory (χEFT) and the pionless EFT ($\not{\pi}$EFT). The former exploits the smallness of the light quark masses in QCD in comparison to hadronic scales. In the limit of massless light quarks, the QCD Lagrangian (2.1) exhibits a SU(3)$_L\times$SU(3)$_R$ symmetry called chrial symmetry. This symmetry is broken spontaneously as well as explicitly, the latter due to the quark mass terms. The spontaneous breaking of chiral symmetry gives rise to massless Goldstone bosons. These are identified with the pions, kaons and the η particle. All of these obtain masses as soon as quark masses are introduced. In χEFT, hadronic observables are

expanded around the chiral limit in powers of the small parameters

$$\frac{m_\pi, p}{4\pi f_\pi, m_\rho},$$

where the low-energy scales are the small pion mass m_π and the typical momentum p of the considered process. The high-energy scales are given by the pion decay constant $f_\pi = 92.4$ MeV and the mass of the ρ meson $m_\rho \approx 770$ MeV. The expansion in the pion-mass is equivalent to an expansion in quark masses due to the Gell-Mann–Oakes–Renner relation, $m_\pi^2 \sim m_q$.

In the purely mesonic sector, χEFT is perturbative. The inclusion of baryons introduces a new energy scale in to the problem, specifically the baryon mass in the chiral limit. This demands to be taken into account by the power counting scheme. To present date, several ways to define a consistent power counting scheme in the presence of baryons are on the market. Nonetheless, the single-nucleon sector is also accessible for a perturbative treatment. This is not the case for two or more nucleons, as can be seen by the existence of bound states. These states correspond to poles in the scattering amplitude, a behavior that can not be generated in a perturbative expansion.

Summarizing, χEFT provides a systematic access to the quark mass dependence of hadronic observables. This will be put to use in Section 6.2 where the pion-mass dependence of the triton spectrum in finite volume will be discussed.

The $\slashed{\pi}$EFT is the specifically built to deal with the fact that two nucleons interact resonantly. Resonantly interacting means that the two-body scattering length is large compared to the natural length scale of the system. This applies not only to nuclear physics but also, for example, to ultracold gases of certain atomic species. The EFTs describing systems of resonantly interacting particles share certain universal properties. Therefore, the generalities of this special class of EFTs and its application to nuclear physics, namely $\slashed{\pi}$EFT, are described in the following subsection.

2.2.3   EFTs for resonantly interacting particles

The two-body scattering length is a parameter describing the low-energy scattering properties of a system. For a precise definition, some basic concepts of scattering theory will be reviewed in the following. The stationary wave function for an elastic scattering process

$$\psi_{\vec{k}}(\vec{r}) = \mathrm{e}^{\mathrm{i}\vec{k}\cdot\vec{r}} + f_k(\theta)\frac{e^{\mathrm{i}kr}}{r} \tag{2.8}$$

is the sum of an incoming plane wave and an outgoing spherical wave. In this expression, $r = |\vec{r}|$ and $k = |\vec{k}|$. The parameter $\vec{k}$ relates to the energy of the scattering process by $E = \vec{k}^2/2m$. The factor $f_k(\theta)$ which describes the angular distribution of the outgoing wave is called the *scattering amplitude*. The scattering amplitude completely determines the differential cross section via

$$\frac{\mathrm{d}\sigma}{\mathrm{d}\Omega} = |f_k(\theta)|^2. \tag{2.9}$$

The dependence of the scattering amplitude on the scattering angle can be expanded in Legendre polynomials, yielding the so-called partial-wave expansion

$$f_k(\theta) = \sum_{\ell=0}^{\infty}(2\ell + 1)f_\ell(k)P_\ell(\cos\theta). \tag{2.10}$$

Probability conservation, or unitarity in the field theory language, poses a powerful constraint on the form the partial amplitudes f_ℓ. Exploiting this constraint, they can be shown to be of the form

$$f_\ell(k) = \frac{1}{k \cot \delta_\ell(k) - \mathrm{i}k}, \tag{2.11}$$

where the functions δ_ℓ are known as scattering phase shifts. The phase shifts are real for elastic scattering. For low scattering energies, i.e. near the threshold, the phase shifts behave as $\delta_\ell \sim k^{2\ell+1}$. Accordingly, the dominant contribution near threshold comes from the $\ell = 0$- or s-wave. The combination $k \cot \delta_0$ is then finite and can be expanded in even powers of the small quantity k as

$$k \cot \delta_0 = -\frac{1}{a} + \frac{r_0}{2} k^2 + \sum_{n=2}^{\infty} P_n k^{2n} \tag{2.12}$$

This expansion is called the *effective range expansion*. The parameters of this expansion are the scattering length a, the effective range r_0 and the shape parameters P_n. For $\ell \neq 0$, similar expansions exist for the quantities $k^{2\ell+1} \cot \delta_\ell$. At threshold, the cross section is completely determined by the scattering length to be $\sigma = 4\pi a^2$ for distinguishable particles and twice as large for indistinguishable particles.

In order to decide whether a given scattering length is large, it has to be compared to the natural length scale of the problem. For low-energies, the scattering amplitude f_k can be expanded in powers of the momentum k. Since f_k has the dimension of a length, a length scale is included to make the expansion coefficients dimensionless, yielding

$$(f_k/l) = a_0 + a_1(kl) + a_2(kl)^2 + \ldots \tag{2.13}$$

For a generic potential, there exists a length scale l such that the coefficients a_n are of order 1. This length scale is called the *natural low-energy length scale.*

A scattering length that is much larger than the natural low-energy length scale of the system is called *unnaturally large*. There are several examples for systems with unnaturally large scattering lengths. A bosonic example is a system of ^{4}He atoms that interact via the van der Waals force. The natural length scale for this interaction of He atoms is given by $l_{\mathrm{vdW}} \approx 10a_0$, where a_0 is the Bohr radius. The scattering length, on the other hand, is $a \approx 200a_0$ and therefore an order of magnitude larger. Other examples for atoms with unnaturally large scattering length are ^{85}Rb, ^{133}Cs and the triplet channel of ^{6}Li. In the scattering of α-particles, the scattering length $a \approx 5$ fm is significantly larger than the natural length scale $l \approx 1.4$ fm set by one-pion exchange. As has been stated, the unnaturally large scattering length present in both channels of the neutron-proton interaction makes it possible to apply this EFT also to NN-interactions as will be described below.

In all of the previous examples, the unnatural size of the scattering length is the result of an accidental fine tuning. The fundamental constants of nature have values in such a way that the long range part of the interaction is dominated by the unnaturally large scattering length. There are also ways to tune the scattering length to an unnaturally large value by adjusting experimental parameters, a technique called experimental fine-tuning. A prominent example where such an experimental fine tuning is possible are Feshbach resonances. In systems where a Feshbach resonance is present, an external magnetic field can be used to tune the scattering length over many orders of magnitudes. This method has become widely used for the study of universal properties in ultracold atomic systems in the course of the last years.

If an unnaturally large scattering length is present, this separation of scales can be well exploited by describing the system by an Effective Field Theory. The leading order of this EFT is given by setting the expansion parameter l/a to zero. This can be achieved by taking two limits. The *resonant limit* is taken by letting $a \to \pm\infty$, depending on the sign of a. This limit is most useful to study universal properties of the system, since the leading order EFT becomes scale-independent. The *scaling limit*, which will be used throughout this work, corresponds to setting $l = 0$ in leading order and leaving the scattering length unchanged. The advantage of this formulation is that the physical scattering length is reproduced already at leading order.

In the scaling limit, the interactions are reduced to contact interactions. To leading order, these contact interactions are momentum-independent. This corresponds to truncating the effective range expansion (2.12) after the first term. Accordingly, leading order scattering is described by the scattering length alone. Because of this, the scaling limit is sometimes also called the zero-range limit.

When setting $k \cot \delta_0 = -1/a$, the scattering amplitude f_0 as given in Eq. (2.11) has a pole at $k = \mathrm{i}/a$ for positive scattering length. This pole corresponds to a shallow two-body bound state with binding energy

$$B_2 = \frac{\hbar^2}{ma^2}. \tag{2.14}$$

This binding energy obtains corrections when incorporating higher orders of l/a into the theory.

In the three-body sector, systems in the scaling limit also exhibit universal properties. For illustration, the variable $K = \mathrm{sgn}(E)\sqrt{mE/\hbar^2}$ representing the energy of the system is plotted against the inverse scattering length for a system of three identical bosons in Figure 2.3.[1] Note that both axes are scaled by a power $1/4$ in order to show more of this plane. The $K = 0$ axis is the threshold for 3-atom scattering, denoted AAA. For positive scattering lengths, the shallow dimer described above is the threshold for the breakup of three-body bound states. For energies greater than the dimer binding energy, scattering between a single atom and a physical dimer, denoted AD, is possible. Of particular interest for the present work is the spectrum of three-body bound states, or trimers. There are infinitely many trimers present in this theory. A specific physical system has a fixed value of the scattering length a, corresponding to a vertical line. Where this line intersects the trimer branches, a three-body bound state is present. The resonant limit corresponds to the K-axis. In this limit, the system contains infinitely many trimers with an accumulation point at threshold. Moreover, the binding energies $E_T^{(n)}$ are spaced geometrically and the ratio is given by a universal number, namely

$$\frac{E_T^{(n+1)}}{E_T^{(n)}} = \mathrm{e}^{2\pi/s_0} \approx 515. \tag{2.15}$$

The universal constant s_0 has a numerical value of $1.00624\ldots$ This remarkable behavior of the trimer energies is called the Efimov effect and was predicted already in the 1970s. It was observed experimentally for the first time a few years ago using ultracold atomic gases that were tuned to the resonant limit with the help of a Feshbach resonance. The Efimov effect

---

[1]Because such a theory is prominently used in the description of ultracold atomic gases, the bosons will be referred to as atoms in the following. Accordingly, the shallow two-body bound state described in the previous paragraph will be called dimer.
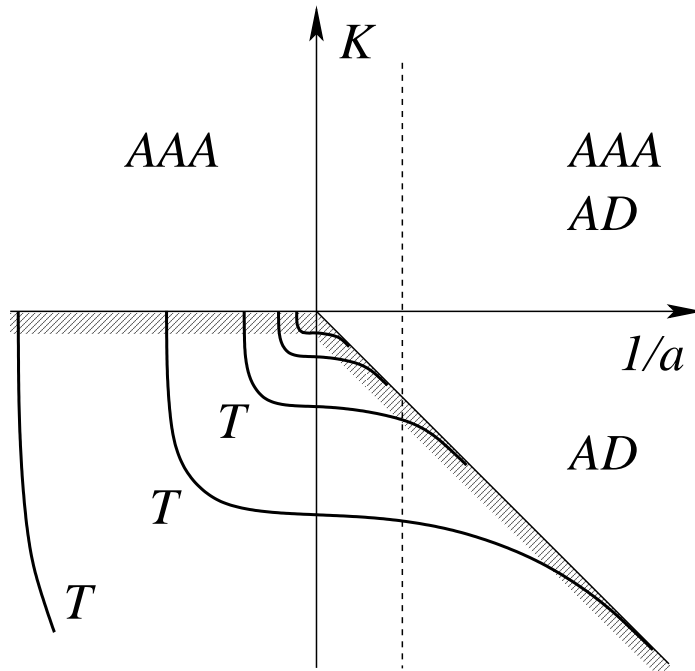
Figure 2.3: The plane spanned by the inverse scattering length $1/a$ and $K = \mathrm{sign}(E)(m|E|/\hbar^2)^{1/2}$ for the 3-body problem. The allowed regions for atom-dimer scattering states and three-atom scattering are marked AD and AAA, respectively. The lines labeled T are the infinitely many branches of Efimov trimers. The shaded area marks the threshold for trimer breakup. Note that the axes have been scaled in order to show more trimer branches.

is the signature of a discrete scaling symmetry in the three-body sector. A single three-body parameter is needed to fix the position of one of the trimer branches and therefore, because of the discrete scaling symmetry, all trimer branches. In the EFT formulation, this discrete scaling symmetry means that the EFT is close to an ultraviolet renormalization group limit cycle. Accordingly, there will be need for a single three-body input to determine the cutoff dependence of the three-body interaction. This will be discussed in detail in Section 3.1.

In the following, it will be shown how to apply the previously described approach in order to describe the interaction of two or more nucleons, yielding the so-called $\not{\pi}$EFT. Because of isospin symmetry, there are two independent two-body scattering lengths governing the NN-interaction in few-nucleon systems. They correspond to proton-neutron scattering in the isospin-triplet $^1S_0$ and isospin-singlet $^3S_1$ channel and are denoted a_s and a_t, respectively. Experimentally, they are found to be $a_s = -23.8$ fm and $a_t = 5.4$ fm. Both are large compared to the natural length scale of NN-interactions which is determined by the pion mass via $l = \hbar/(m_\pi c) \approx 1.4$ fm. As described above, an unnaturally large positive scattering length implies the existence of a shallow two-body bound state. In the $^3S_1$ channel, this bound state is identified as the deuteron with its small binding energy $B_d = 2.2$ MeV. Comparing this value to the prediction from Eq. (2.14), yields a discrepancy of 37%. This shows the importance of range corrections in this channel.

The description of nucleonic interactions by this EFT naturally extends to the three-nucleon sector along the lines discussed before. The Efimov trimers discussed there are in this approach identified with the triton and the ^{3}He nucleus. In the latter, the Coulomb interaction

between the two protons is important. Therefore, it will not be considered in this work. As described above, a single three-body input is needed to fix the Efimov spectrum. By using the neutron-deuteron scattering length as input, the binding energy of the triton is predicted to an accuracy of 6% already at leading order. In the calculations presented in this work, the input will mostly be given by the triton binding energy in infinite volume.

Chapter 3

EFT for three identical bosons in finite volume

In this chapter, it is shown how to apply the framework of Effective Field Theory as described in the previous chapter to the problem of three identical bosons. After a short review of the infinite volume case, the development of the finite volume formalism is described in detail. Starting from the effective Lagrangian, an integral equation for the central three-body quantity, namely the boson-diboson scattering amplitude, is derived. After taking into account the consequences of the cubic symmetry of the finite volume, a set of coupled integral equations describing three-boson bound states is obtained. In the final section, the numerical methods needed to calculate binding energies from these equations are discussed in detail.

3.1 Infinite volume

In this section, the treatment of bound-states of three resonantly interacting identical bosons in infinite volume within the framework of Effective Field Theory is presented. A detailed review can be found in [BH06].

The most intuitive way to describe a system of three identical bosons that interact resonantly is to use a Lagrangian density including 2- and 3-boson contact interactions:

$$\mathcal{L}_{\text{contact}} = \psi^\dagger \left(i\partial_t + \frac{1}{2}\nabla^2 \right) \psi - \frac{g_2}{4}(\psi^\dagger\psi)^2 - \frac{g_3}{36}(\psi^\dagger\psi)^3. \qquad (3.1)$$

The only degree of freedom in this Effective Field Theory is the boson field ψ. For simplicity, units are chosen such that $\hbar = m = 1$ here and in the following. However, it is very difficult to numerically calculate observables from this Lagrangian. In practice, it is useful to employ the fact that the 2-body subsystem is solvable analytically. This can be done by including an auxiliary diboson field d [BHvK99b, BH06]. The Lagrangian then reads to leading order

$$\mathcal{L} = \psi^\dagger \left(i\partial_t + \frac{1}{2}\nabla^2 \right) \psi + \frac{g_2}{4}d^\dagger d - \frac{g_2}{4}\left(d^\dagger\psi^2 + \text{h.c.} \right) - \frac{g_3}{36}d^\dagger d\psi^\dagger\psi. \qquad (3.2)$$

By solving the equation of motion for the field d and inserting the solution back into Eq. (3.2), it can be seen that this Lagrangian is indeed equivalent in the 2- and 3-body sector to the one

$$\frac{i}{k_0-\vec{k}^2/2+i\varepsilon} \qquad\qquad \frac{4i}{g_2}$$

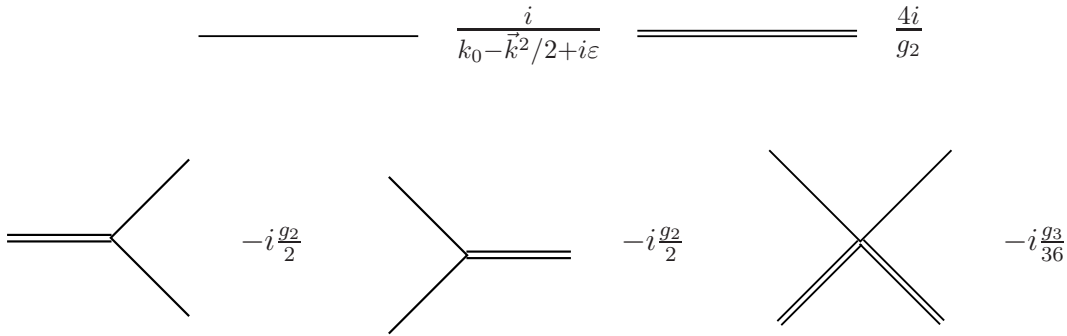$$-i\frac{g_2}{2} \qquad\qquad -i\frac{g_2}{2} \qquad\qquad -i\frac{g_3}{36}$$

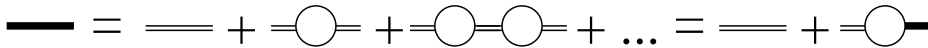Figure 3.1: Feynman rules for the Lagrangian in Eq. (3.2).

Figure 3.2: Dressing of the bare dimer propagator with bosonic loops. The thick solid line depicts the full dimer propagator.

given in Eq. (3.1). This Lagrangian corresponds to the zero-range limit. Corrections from finite range can be taken into account by including higher order terms into the Lagrangian.

The Feynman rules derived from the Lagranian (3.2) are shown in Fig. 3.1. The bare dimer propagator is a constant, corresponding to no propagation in space or time. By dressing this quantity with bosonic loops as shown in Fig. 3.2, one obtains the full dimer propagator when solving the corresponding integral equation. The loop integration has to be regulated by a momentum cutoff. The explicit dependence on the cutoff and the two-body coupling constant g_2 can be eliminated by a renormalization procedure in favor of a low-energy datum. This can be the two-body scattering length a or the binding momentum of the physical dimer, if applicable. The resulting full dimer propagator D is

$$D(E) = \frac{32\pi}{g_2^2}\left[\frac{1}{a} - \sqrt{-E}\right]^{-1}. \tag{3.3}$$

For $a > 0$, this propagator has a pole at $E = -1/a^2$, which is just the leading order result for the energy of the physical dimer state.

The central quantity in the three-body sector of this EFT is the boson-diboson scattering amplitude. It determines all three-body observables and is given as the solution of an inhomogeneous integral equation, depicted diagramtically in Fig. 3.3. For the treatment of this integral equation, it is of practical use to put the bosonic legs on-shell while the diboson legs remain off-shell. This introduces the total energy of the system, E, as an additional parameter. The loop integrals have again to be regulated by a cutoff. The resulting cutoff dependence is compensated by making the three-body coupling constant g_3 cutoff dependent as well. For convenience, a dimensionless function $H(\Lambda)$ is introduced by setting

$$g_3 = -\frac{9g_2^2}{\Lambda^2}H(\Lambda). \tag{3.4}$$

By investigating the ultraviolet behavior of the theory it can be shown that H depends log-periodically on Λ via [BH06]

$$H(\Lambda) = \frac{\cos\left[s_0\log(\Lambda/\Lambda_*) + \arctan s_0\right]}{\cos\left[s_0\log(\Lambda/\Lambda_*) - \arctan s_0\right]}. \tag{3.5}$$
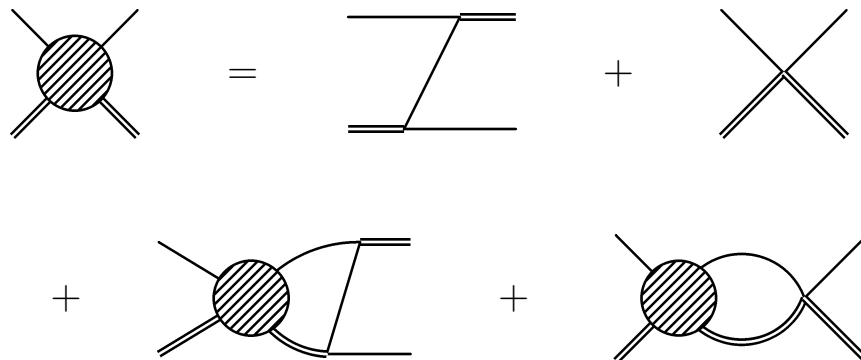
Figure 3.3: Integral equation for the boson-diboson amplitude. The single lines denote the boson propagator and the double lines denote the full dimer propagator.

Here, $s_0 \approx 1.00624\ldots$ is a universal constant and $\Lambda_* \approx 2.62\kappa_*$ is a three-body parameter that can be fixed from a trimer binding energy or any other three-body datum. The choice of Λ_* fixes the position of the Efimov trimer branches as shown in Fig. 2.3. Rescaling Λ_* by a factor $\exp(\pi/s_0)$ leaves all observables invariant. Up to this freedom, the dimensionless combination $\Lambda_* a$ characterizes a given system. This behavior of the coupling constant comes about because the three-body sector of the theory in the resonant limit lies on the critical trajectory of an ultraviolet renormalization group limit cycle.

In order to illustrate the RG limit cycle, consider the dimesionless three-body coupling

$$\hat{g}_3(\Lambda) = \frac{g_3 \Lambda^4}{144\pi^4}.$$

For several values of a and Λ_*, the Λ-dependence of $\hat{g}_3$ is shown in Fig. 3.4. By letting $\Lambda \to \infty$, the trajectories mapped out for the different physical systems are all focused on the limit cycle given by $H(\Lambda)$, given by the solid line.

Bound states appear as poles in the boson-diboson scattering amplitude at the trimer binding energy. Matching the residues of this pole on both sides of the integral equation and projecting on s-waves yields a homogeneous integral equation for the bound state amplitude that serves as a consistency condition. Values of the energy parameter E, for which this integral equation has a solution, are interpreted as trimer binding energies. The resulting trimer spectrum is the Efimov spectrum that has been described in the previous chapter. The question how this spectrum changes inside a finite cubic volume is one of the main motivations for the present work.

3.2 Finite volume

In this section, the derivation of an infinite set of coupled equations for the partial waves of the bound state amplitudes in finite volume is presented. Placing a system inside a finite volume leads to the quantization of momenta. Along with this comes the breakdown of the rotational symmetry of the infinite volume to the point symmetry of the finite volume. The consequences of these modifications are described in detail in the following.
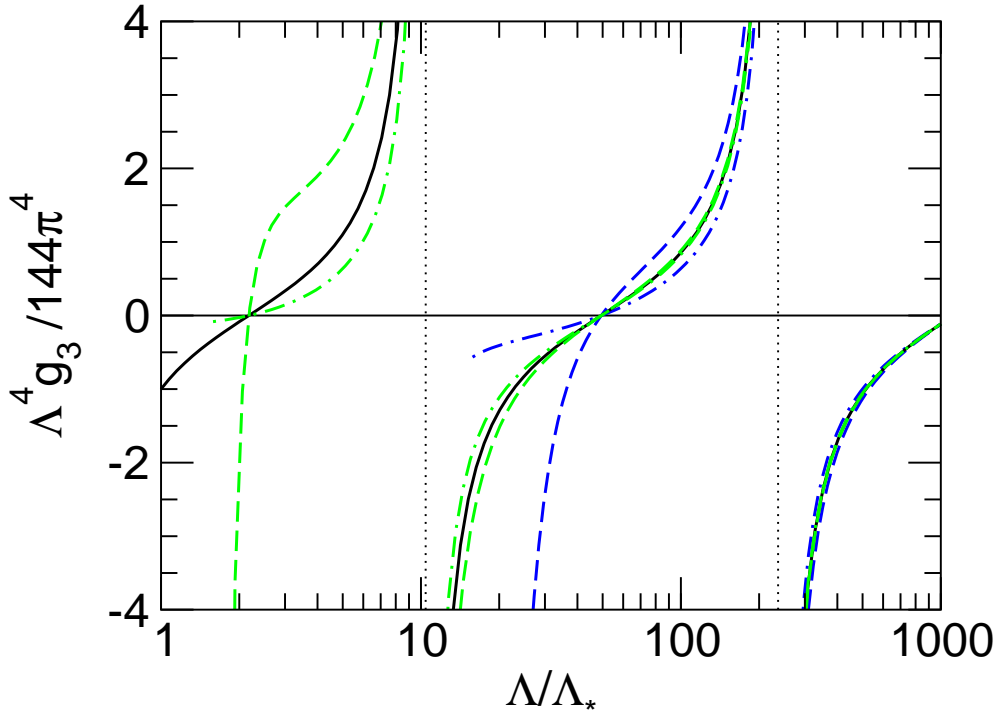
Figure 3.4: RG trajectories for different physical systems characterized by a fixed value of Λ_* and several values of the scattering length a. Shown is the dimensionless 3-body coupling as a function of the cutoff. The solid line is the RG limit cycle given by $H(\Lambda)$. For $\Lambda \to \infty$, the trajectories are approaching the limit cycle. Figure taken from [BH06].

3.2.1 Consequences of momentum quantization

The finite volumes considered in this work are cubic boxes with side length L and periodic boundary conditions. Inside such volumes, momenta are quantized and can only take the discrete values

$$\vec{p} = \frac{2\pi}{L}\vec{n}, \; \vec{n} \in \mathbb{Z}^3. \tag{3.6}$$

There is now a minimal accessible momentum. Accordingly, the infrared properties of the system are modified. On the other hand, the finite volume does not affect the ultraviolet behavior of the amplitudes. Therefore, the renormalization of the theory is the same in the infinite and the finite volume case. Of course, this statement only holds under the premise that the momentum cutoff Λ is large compared to the momentum scale set by the size of the volume, namely $2\pi/L$, such that the infrared and the ultraviolet regime of the theory are well separated. In the numerical calculations presented in this work, the renormalization was done in the infinite volume and the consistent renormalization of the finite volume results was always verified explicitly.

As in the infinite volume case, all informations on physical observables in the three-body sector are encoded in the boson-diboson scattering amplitude. This amplitude is determined by the same inhomogeneous integral equation depicted in Fig.3.3 as in the infinite volume. But, due to momentum quantization, the momenta running around in the loops can only take discrete values. Accordingly, a discrete sum over the loop momenta has to be performed

instead of a continuous integration. The summation has to be regulated by a momentum cutoff Λ.

For the diboson lines in the three-body equation depicted in Fig. 3.3, the full, interacting diboson propagator D has to be used. This quantity corresponds to the exact two-body scattering amplitude. This quantity has to be recalulated in the finite volume case since its derivation involves a loop integration. This integration is also replaced by a discrete sum that can be evaluated analytically. For a diboson with energy E, the propagator is given by

$$D(E) = \frac{32\pi}{g_2^2} \left[\frac{1}{a} - \sqrt{-E} + \frac{1}{L} \sum_{\substack{\vec{\jmath} \in \mathbb{Z}^3 \\ \vec{\jmath} \neq \vec{0}}} \frac{1}{|\vec{\jmath}|} e^{-|\vec{\jmath}|L\sqrt{-E}} \right]^{-1}. \tag{3.7}$$

In the limit $L \to \infty$, this expression reduces to the full dimer propagator in the infinite volume case given in Eq. (3.3).

Having obtained the full diboson propagator, the integral equation for the boson-diboson scattering amplitude can be written down explicitly. Using the diagrammatical representation in Fig. 3.3 and the Feynman rules in Fig. 3.1 derived from the effective Lagrangian (3.2), one obtains

$$\mathcal{A}(\vec{p}, \vec{k}; E) = -\frac{g_2^2}{4} \frac{1}{E - p^2/2 - k^2/2 - (\vec{p} + \vec{k})^2/2} - \frac{g_3}{36}$$

$$+ i \int \frac{dq_0}{(2\pi)} L^{-3} \sum_{\vec{q} \in \frac{2\pi}{L}\mathbb{Z}^3} \left[\frac{g_2^2}{4} \frac{1}{E - p^2/2 - q_0 - (\vec{p} + \vec{q})^2/2} + \frac{g_3}{36} \right] \tag{3.8}$$

$$\times \frac{D(E - q_0 + q^2/4)}{q_0 - q^2/2} \mathcal{A}(\vec{q}, \vec{k}; E).$$

Here, $\vec{p}$ $(\vec{k})$ is the momentum of the incoming (outgoing) diboson, while the momentum of the incoming (outgoing) boson is $-\vec{p}$ $(-\vec{k})$. The bosonic legs have been put on shell but the diboson legs remain off-shell. This introduces the total energy E of the system as a parameter of the equation. The integration over the unquantized loop energy can be performed by virtue of the residue theorem. This yields the sum equation

$$\mathcal{A}(\vec{p}, \vec{k}; E) = -\frac{g_2^2}{4} \mathcal{Z}_E(\vec{p}, \vec{k}) + \frac{8\pi}{L^3} \sum_{\vec{q} \in \frac{2\pi}{L}\mathbb{Z}^3} \mathcal{Z}_E(\vec{p}, \vec{q}) d(q; E) \mathcal{A}(\vec{q}, \vec{k}; E), \tag{3.9}$$

with

$$\mathcal{Z}_E(\vec{p}, \vec{k}) = \left[\left(p^2 + \vec{p} \cdot \vec{k} + k^2 - E \right)^{-1} + \frac{H(\Lambda)}{\Lambda^2} \right], \tag{3.10}$$

where $H(\Lambda)$ is given in Eq. (3.5), and $d(q; E) = \frac{32\pi}{g_2^2} D(E - 3/4q^2)$.

If the energy E is near a trimer energy $E_3^{(n)} < 0$, the amplitude $\mathcal{A}$ exhibits a simple pole and the dependence on the momenta separates:

$$\mathcal{A}(\vec{p}, \vec{k}; E) \longrightarrow \frac{\mathcal{F}(\vec{p})\mathcal{F}(\vec{k})}{E - E_3^{(n)}} + \text{regular terms}, \quad \text{as } E \to E_3^{(n)}. \tag{3.11}$$

Matching the residues on both sides of Eq. (3.9), the bound-state equation

$$\mathcal{F}(\vec{p}) = \frac{8\pi}{L^3} \sum_{\vec{q} \in \frac{2\pi}{L}\mathbb{Z}^3} \mathcal{Z}_{E_3^{(n)}}(\vec{p}, \vec{q})\, d(q; E_3^{(n)})\, \mathcal{F}(\vec{q}) \tag{3.12}$$

is obtained. This equation serves as a consistency condition. Values of the energy E, for which this homogeneous sum equation has a solution, are identified with the energies $E_3^{(n)}$ of the trimer states.

3.2.2   Consequences of cubic symmetry

In the infinite volume case, only s-wave bound states are formed. However, in a finite cubic volume, the spherical symmetry of the infinite volume is broken to a cubic symmetry. In the language of group theory, the infinitely many irreducible representations of the spherical symmtery group $O(3)$ are mapped onto the five irreducible representations of the cubic group O. The representations of the spherical symmetry group are now reducible and can therefore be decomposed in terms of the five irreducible representations of the cubic group. On the other hand, a quantity ψ_s transforming according to the irreducible representation s of O can be written in terms of the basis functions of the spherical symmetry, i. e. the spherical harmonics $Y_{\ell m}$, via

$$\psi_s(\vec{r}) = \sum_{\ell,t} R_{\ell t}(r) K_{s\ell t}(\hat{r}) = \sum_{\ell,t} R_{\ell t}(r) \left[\sum_m C_{\ell m} Y_{\ell m}(\hat{r}) \right], \tag{3.13}$$

where $\hat{r} = \vec{r}/|\vec{r}|$ and t is an additional index needed if the representation labeled by ℓ appears in the irreducible representation s more than once [vdLB47]. The linear combinations $K_{s\ell t}$ of spherical harmonics are called "kubic harmonics" [vdLB47]. The values of the coefficients $C_{s\ell m}^{(t)}$ are known for values of ℓ as large as 12 [AC65]. Details on the construction of these functions together with the group theoretical background are presented in Appendix A.

In order to make contact with the infinite volume formalism, Eq. (3.12) is rewritten using Poisson's resummation formula in three dimensions. This identity states that, when summing over all possible integer vectors, the sum over function values equals the sum over the Fourier transformed function, i.e.

$$\sum_{\vec{n} \in \mathbb{Z}^3} f(\vec{n}) = \sum_{\vec{m} \in \mathbb{Z}^3} \hat{f}(\vec{m}), \tag{3.14}$$

where $\hat{f}(\vec{m}) = \int_{\mathbb{R}^3} \mathrm{d}^3 y\, \mathrm{e}^{\mathrm{i}2\pi\vec{m}\cdot\vec{y}} f(\vec{y})$ is the Fourier transform of f. Applying the identity (3.14) to Eq. (3.12) yields

$$\mathcal{F}(\vec{p}) = \frac{1}{\pi^2} \sum_{\vec{n} \in \mathbb{Z}^3} \int \mathrm{d}^3 y\, \mathrm{e}^{\mathrm{i}L\vec{n}\cdot\vec{y}} \mathcal{Z}_{E_3^{(n)}}(\vec{p}, \vec{y}) d(y; E_3^{(n)}) \mathcal{F}(\vec{y}). \tag{3.15}$$

The term with $\vec{n} = \vec{0}$ yields the infinite volume equation , while the other terms of the infinite sum may be seen as corrections due to momentum quantization and the breakdown of the spherical symmetry. The explicit recovery of the infinite volume term is useful for bound states, since in this case the analytic structure of the amplitude, i.e. the pole at the binding

energy, is identical and only the position of the pole is changed. This approach may be inappropriate for states belonging to the continuous scattering region of the infinite volume.

In order to evaluate the angular integration in Eq. (3.15), all quantities with angular dependence are expanded in terms of the basis functions of the irreducible representations of $O(3)$, namely in spherical harmonics. The amplitude $\mathcal{F}$ itself is assumed to transform under the trivial representation A_1 of the cubic group, since the $\ell = 0$ representation is solely contained in A_1. The amplitude can therefore be written as

$$\mathcal{F}(\vec{p}) = \sum_{\ell,t} F_{\ell t}(p) K_{A_1 \ell t}(\hat{p}) = \sum_{\ell,t} F_{\ell t}(p) \sum_{m=-\ell}^{\ell^{(A_1)}} C_{A_1 \ell m}^{(t)} Y_{\ell m}(\hat{p}). \qquad (3.16)$$

The sum runs over those values of ℓ associated with the A_1-representation of O. The first values are $\ell = 0, 4, 6, 8, \ldots$ Since the first occasion where an ℓ-value appears more than once is $\ell = 12$, the summation over the multiplicity and hence the index t will be suppressed in the following. Also, the index A_1 will be dropped.

The only angular dependence of the quantity $\mathcal{Z}_E(\vec{p}, \vec{q})$ is on the cosine of the angle $\theta_{\vec{p}\vec{q}}$ between $\vec{p}$ and $\vec{q}$. Therefore, $\mathcal{Z}_E(\vec{p}, \vec{q})$ can be expanded in Legendre polynomials $P_\ell(\cos \theta_{\vec{p}\vec{q}})$. These polynomials can in turn be expressed in spherical harmonics via the addition theorem, yielding

$$\mathcal{Z}_E(\vec{p}, \vec{y}) = \sum_{\ell=0}^{\infty} Z_E^{(\ell)}(p, y) P_\ell(\cos \theta_{\vec{p}\vec{y}}) = \sum_{\ell=0}^{\infty} Z_E^{(\ell)}(p, y) \frac{4\pi}{2\ell+1} \sum_{m=-\ell}^{\ell} Y_{\ell m}^*(\hat{p}) Y_{\ell m}(\hat{y}). \qquad (3.17)$$

The exponential function in Eq. (3.15) can be rewritten using the identity

$$e^{iL\vec{n}\cdot\vec{y}} = 4\pi \sum_{\ell=0}^{\infty} i^\ell j_\ell(L|\vec{n}|y) \sum_{m=-\ell}^{\ell} Y_{\ell m}^*(\hat{n}) Y_{\ell m}(\hat{y}), \qquad (3.18)$$

where j_ℓ is the spherical Bessel function of order ℓ.

With these expansions at hand, the angular integration in Eq. (3.15) can be performed. The integral over the three spherical harmonics depending on $\hat{y}$ yields Wigner 3-j symbols or, equivalently, Clebsch-Gordan symbols. Projecting on the ℓth partial wave results in an infinite set of coupled integral equations for the quantities F_ℓ:

$$\begin{aligned}
F_\ell(p) = \frac{4}{\pi} \int_0^\Lambda \mathrm{d}y\, y^2 &\Big[Z_{E_3^{(n)}}^{(\ell)}(p, y) d(y; E_3^{(n)}) \frac{1}{2\ell+1} F_\ell(y) \\
&+ 2\sqrt{\pi} \sum_{\substack{\vec{n}\in\mathbb{Z}^3 \\ \vec{n}\neq\vec{0}}} \sum_{\ell',m'}^{(A_1)} \sum_{\ell'',m''} \begin{pmatrix} \ell' & \ell'' & \ell \\ 0 & 0 & 0 \end{pmatrix} \begin{pmatrix} \ell' & \ell'' & \ell \\ m' & m'' & 0 \end{pmatrix} \frac{C_{\ell'm'}}{C_{\ell 0}} Y_{\ell''m''}(\hat{n}) \\
&\times \sqrt{\frac{(2\ell'+1)(2\ell''+1)}{2\ell+1}}\, i^{\ell''} j_{\ell''}(L|\vec{n}|y) Z_{E_3^{(n)}}^{(\ell)}(p, y) d(y; E_3^{(n)}) F_{\ell'}(y) \Big].
\end{aligned} \qquad (3.19)$$

The ℓ' sum runs over the partial waves associated with the A_1 representation. The quantity $Z_E^{(\ell)}(p, y)$ can be calculated from Eq. (3.17) to be

$$Z_E^{(\ell)}(p, y) = (2\ell+1) \left[\frac{1}{py} Q_\ell \left(\frac{p^2 + y^2 - E}{pq} \right) + \frac{H(\Lambda)}{\Lambda^2} \delta_{\ell 0} \right]. \qquad (3.20)$$

n	$\sum_{\substack{\vec{n}\in\mathbb{Z}^3 \\ |\vec{n}|=n}} \frac{1}{2}\left(Y_{\ell m} + Y_{\ell,-m}\right)$		
	$\ell = 0, m = 0$	$\ell = 4, m = 0$	$\ell = 4, m = 4$
101	606	96.23	81.33
1001	9126	-94.05	20.69
3501	39678	118.67	-15.73

Table 3.1: Integer vector sums over real combinations of $Y_{\ell m}$ for a given absolute value n ("angular sums"). For higher partial waves, the value of the sum is smaller and the contribution of the partial wave is suppressed.

Here, Q_ℓ is a Legendre function of the second kind. The three-body contact interaction contributes only to the s-wave, as expected.

Since the bound states in the infinite volume are s-wave states, Eq. (3.19) is specialized to the case $\ell = 0$, yielding

$$
F_0(p) = \frac{4}{\pi} \int_0^\Lambda \mathrm{d}y\, y^2 \Bigg[Z_{E_3^{(n)}}^{(0)}(p,y) d(y; E_3^{(n)}) \bigg(1 + \sum_{\substack{\vec{n}\in\mathbb{Z}^3 \\ \vec{n}\neq\vec{0}}} \frac{\sin(L|\vec{n}|y)}{L|\vec{n}|y} \bigg) F_0(y)
$$
$$
+ 2\sqrt{\pi} \sum_{\substack{\vec{n}\in\mathbb{Z}^3 \\ \vec{n}\neq\vec{0}}} \sum_{\ell'=4,6,\ldots}^{(A_1)} \sum_{m'=-\ell'}^{\ell'} \mathrm{i}^{\ell'} j_{\ell'}(L|\vec{n}|y) Y_{\ell' m'}^*(\hat{n}) Z_{E_3^{(n)}}^{(0)}(p,y) d(y; E_3^{(n)}) C_{\ell' m'} F_{\ell'}(y) \Bigg].
$$
(3.21)

The specialization of Eq. (3.20) to the case $\ell = 0$ reads

$$
Z_E^{(0)}(p,y) = \frac{1}{2py} \log\left(\frac{p^2 + py + y^2 - E}{p^2 - py + y^2 - E} \right) + \frac{H(\Lambda)}{\Lambda^2}.
$$
(3.22)

The second line of Eq. (3.21) indicates admixtures from higher partial waves. Since the leading term in the expansion of the spherical Bessel function is $1/(L|\vec{n}|y)$, these contributions are suppressed by at least a/L. They will therefore be small for volumes not too small compared to the size of the bound state. Moreover, contributions from higher partial waves will be kinematically suppressed for shallow states with small binding momentum. This is ensured by the spherical harmonic in the second line of Eq. (3.21). For higher partial waves, the angular sum yields smaller prefactors relative to the s-wave ($\ell = 0$) for a given absolute value n (see Table 3.1). Only for small lattices, i.e. when a/L is large, this behavior is counteracted by terms stemming from the spherical Bessel function and higher partial waves may contribute significantly.

Therefore, it is reasonable to neglect the contributions of higher partial waves in a first approach. This yields a homogeneous integral equation for F_0:

$$
F_0(p) = \frac{4}{\pi} \int_0^\Lambda \mathrm{d}y\, y^2 Z_{E_3^{(n)}}^{(0)}(p,y) d(y; E_3^{(n)}) \bigg(1 + \sum_{\substack{\vec{n}\in\mathbb{Z}^3 \\ \vec{n}\neq\vec{0}}} \frac{\sin(L|\vec{n}|y)}{L|\vec{n}|y} \bigg) F_0(y).
$$
(3.23)

This means to consider only the effects of momentum quantization for the s-wave. Eq. (3.23) can now be solved numerically in order to yield the bound state spectrum. The numerical methods used to do so are outlined in Section 3.3.

Of course, it is necessary to assess the size of the corrections brought about by the inclusion of higher partial waves. The next higher partial wave in the representation A_1 is $\ell = 4$. In order to take this partial wave into account, the sum over ℓ' in Eq. (3.21) is truncated after $\ell' = 4$, yielding an inhomogeneous term containing the amplitude F_4. This amplitude is the solution of Eq. (3.19), specialized to $\ell = 4$, where we will only consider terms containing F_0 and F_4 itself. The resulting coupled equations are

$$F_0(y) = \frac{4}{\pi} \int_0^\Lambda \mathrm{d}y \, y^2 Z^{(0)}_{E_3^{(n)}}(p, y) d(y; E_3^{(n)}) \left[\left(1 + \sum_{\substack{\vec{n} \in \mathbb{Z}^3 \\ \vec{n} \neq \vec{0}}} \frac{\sin(L|\vec{n}|y)}{L|\vec{n}|y} \right) F_0(y) \right.$$

$$\left. + 2\sqrt{\pi} \sum_{\substack{\vec{n} \in \mathbb{Z}^3 \\ \vec{n} \neq \vec{0}}} j_4(L|\vec{n}|y) \left(Y_{40}(\hat{n}) C_{40} + Y_{44}(\hat{n}) C_{44} + Y_{4,-4}(\hat{n}) C_{4,-4} \right) F_4(y) \right],$$

(3.24a)

$$F_4(y) C_{40} = \frac{4}{3\pi} \int_0^\Lambda \mathrm{d}y \, y^2 Z^{(4)}_{E_3^{(n)}}(p, y) d(y; E_3^{(n)}) \left[\left(\frac{1}{3} + \sum_{\substack{\vec{n} \in \mathbb{Z}^3 \\ \vec{n} \neq \vec{0}}} \frac{\sin(L|\vec{n}|y)}{L|\vec{n}|y} \right) C_{40} F_4(y) \right.$$

$$\left. + 2\sqrt{\pi} \sum_{\substack{\vec{n} \in \mathbb{Z}^3 \\ \vec{n} \neq \vec{0}}} j_4(L|\vec{n}|y) Y_{40}(\hat{n}) F_0(y) \right].$$

(3.24b)

The Bessel function of order 4 is given by

$$j_4(x) = \frac{5(2x^2 - 21)}{x^4} \cos x + \frac{(x^4 - 45x^2 + 105)}{x^5} \sin x. \tag{3.25}$$

Its oscillating behavior demands for a careful numerical treatment, that will be discussed in Section 3.3. The function $Z^{(4)}_E$ is given by the specialization of Eq. (3.20) as

$$Z^{(4)}_E(p, y) = \frac{9}{py} Q_4 \left(\frac{p^2 + y^2 - E}{py} \right), \text{ with} \tag{3.26}$$

$$Q_4(x) = \frac{55x}{24} - \frac{35x^3}{8} + \frac{1}{16} \left(3 - 30x^2 + 35x^4 \right) \log \left(\frac{x-1}{x+1} \right).$$

The Eqs. (3.24) are solved in a coupled channel approach that is also discussed in the following section.

3.3 Numerical methods

The integral equations derived in the previous section have to be solved numerically in order to determine the binding energies in the finite volume. The numerical methods needed to do so are presented in the following.

The starting point for a first numerical treatment of the formalism is the homogeneous integral equation Eq. (3.23). The first step is to transform this equation into a finite-dimensional
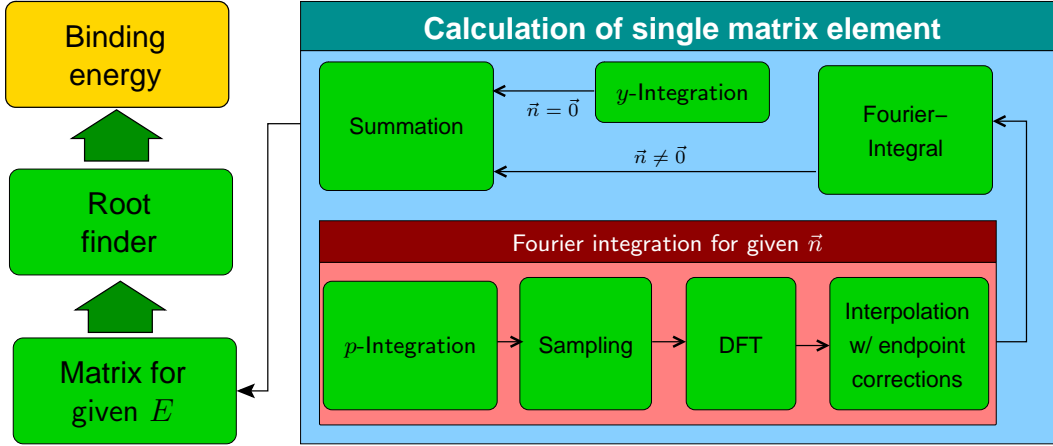
Figure 3.5: Schematic overview of the numerical procedure.

problem. Due to the oscillatory nature of the integrand, it is not sensible to use a finite number of sampling points. Instead, a set of basis functions is specified. The choice of basis functions is guided by the knowledge of the bound-state amplitude in the infinite volume case. Asymptotically, the amplitude behaves like [BHvK99b, BH06]

$$F_0(p) \rightarrow \frac{1}{p} \cos\left(s_0 \log(p/p_*)\right),$$

with the universal number $s_0 = 1.00624\ldots$ and a momentum scale p_*. The bound-state amplitude obtained by the infinite volume formalism has precisely such a form, with only a few zeros in the interval $[0; \Lambda]$. Therefore, the basis functions chosen are Legendre functions P_i with logarithmic arguments as follows:

$$\xi_i(p) = \frac{1}{p} P_i(2 \log_2(p/\Lambda + 1) - 1). \tag{3.27}$$

These basis functions are orthogonal with respect to the scalar product

$$\int_0^\Lambda \mathrm{d}p \, \frac{p^2}{p + \Lambda} \xi_i(p)\xi_j(p) = (\log 2) \frac{1}{2i + 1}\delta_{ij}. \tag{3.28}$$

The amplitude F_0 in (3.23) is replaced by its expansion in the basis functions $\sum_{j=0}^\infty f_j \xi_j(p)$ and the ith component is projected out using the scalar product. The resulting equation

$$\frac{\log 2}{2i + 1} f_i = \sum_{j=0}^\infty K_{ij}(E) f_j, \tag{3.29}$$

with

$$K_{ij}(E) = \frac{4}{\pi} \int_0^\Lambda \mathrm{d}y \, y^2 \left[\int_0^\Lambda \mathrm{d}p \, \frac{p^2}{p + \Lambda} \xi_i(p) Z_E^{(0)}(p, y) \right] d(y; E) \left(1 + \sum_{\substack{\vec{n} \in \mathbb{Z}^3 \\ \vec{n} \neq \vec{0}}} \frac{\sin(L|\vec{n}|y)}{L|\vec{n}|y} \right) \xi_j(y),$$

$$\tag{3.30}$$

can be interpreted as a matrix equation when truncating the set of basis functions.

A necessary and sufficient condition for the existence of a non-trivial solution of Eq. (3.29) is

$$\det\left[K_{ij}(E) - \frac{\log 2}{2i+1}\delta_{ij}\right] = 0. \tag{3.31}$$

Values of E that fulfill this condition are interpreted as binding energies in the finite volume. This is only a valid interpretation if the truncation of the basis and the neglect of the higher partial waves induce only small corrections for the result. In practice, the use of 40 basis functions is sufficient to yield results independent of the basis size.

A schematic overview on the numerical procedure is given in Fig. 3.5. The values of the parameter E for which the condition (3.31) is satisfied are found via Ridders' root finding algorithm. This requires the calculation of $K_{ij}(E)$ in each iteration. To save numerical effort, it is possible to expand the kernel around the binding energy in the infinite volume if the shift in the binding energy is small. The expansion is done up to first order:

$$K_{ij}(E) \approx K_{ij}(E^\infty) + \left.\frac{\mathrm{d}K_{ij}}{\mathrm{d}E}\right|_{E=E^\infty} \cdot (E - E^\infty), \quad \text{for } \frac{E - E^\infty}{E^\infty} \ll 1. \tag{3.32}$$

Naively, this expansion should work for shifts of 10-20%. The applicability of the expansion will be discussed in the next chapter where results obtained using the expanded kernel are compared to results of full calculations.

In the following, details on the numerical methods used to calculate the kernel matrix elements $K_{ij}(E)$ as defined in Eq. (3.30) are presented. This is represented by the box on the right hand side in Fig. 3.5. The calculation of a single matrix elements involves a summation over integer vectors. The term for the zero-vector is just an integration over the variable. For vectors unequal zero, a Fourier-Integral has to be evaluated. This requires to sample the integral kernel without the oscillating term, to perform a discrete Fourier transform (DFT) and applying enpoint corrections. The sampling step requires an integration over the variable p for each sampled point.

The integration over p in the sampling is performed using a logarithmically distributed Gauss-Legendre quadrature with 64 points. The integration over y for the $\vec{n} = \vec{0}$ term of the summation is done with a Gauss-Legendre quadrature with 64 points.

For $\vec{n} \neq \vec{0}$, the integrand of the y-integration is strongly oscillating due to the $\sin(L|\vec{n}|y)$ term. This motivates to evaluate this integral using the Fast Fourier Transformation technique (FFT). The computation of Fourier integrals via FFT as well as the idea of FFT itself are explained in detail in Appendix B. The technique presented there takes care of some subtleties that hinder approaching this problem by a naive discretization of the integral. The sampling for the FFT is the most time-consuming part of the calculation. The number of points to sample, M, is determined by the highest "frequency" that is to be accessed. The frequencies in the present case are the values of $L|\vec{n}|$. The highest possible frequency is connected to M and the integration range given by the cutoff Λ by

$$L|\vec{n}_{\max}|\frac{\Lambda}{M} \lesssim \pi \quad \Rightarrow \quad M > \frac{L|\vec{n}_{\max}|\Lambda}{\pi}. \tag{3.33}$$

For realistic values of these parameters, namely box sizes of a few a, an $|\vec{n}_{\max}|$ of about 3000 and cutoff values of several hundred a^{-1}, a typical value for M is 2^{20} or about one million sampled points.
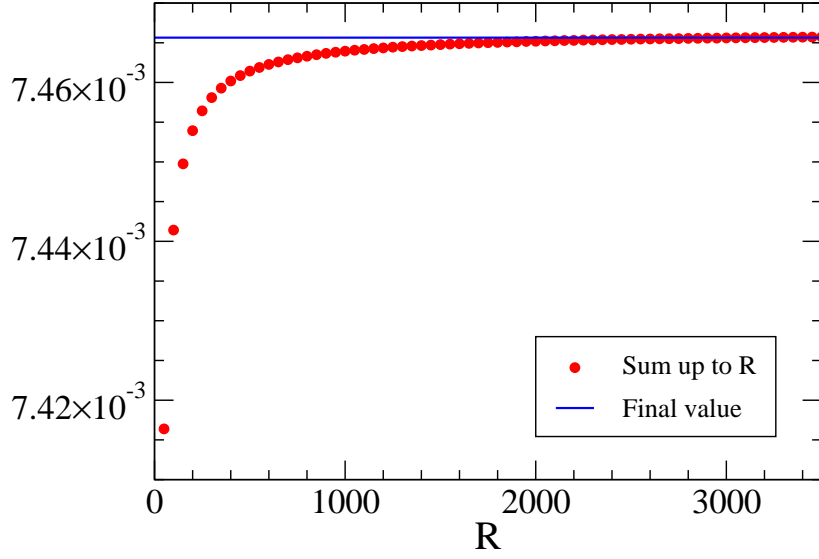
Figure 3.6: Convergence of the summation over all vectors $\vec{n} \in \mathbb{Z}^3$ in Eq. (3.30) in a specific example. Plotted are the intermediate sums for all $|\vec{n}| < R$ for values of R up to 3500.

A summation over three-dimensional integer vectors of a quantity depending only on the absolute value of the vector involves, when naively done, a lot of double counting. To circumvent this, an ordered list with absolute values that are possible for vectors in $\mathbb{Z}^3$ and their multiplicity has been created. The result of the summation can be viewed as converged when going to absolute values of about 5000. For radii from about 2000 on, the intermediate sums oscillate around the converged result. To reduce runtime, the result of the summation is calculated as a mean of 15 intermediate sums for radii from 2750 to 3500 (Fig. 3.6).

The inclusion of higher partial waves requires the solution of coupled integral equations. This is done in a coupled channel-like approach. The vectors containing the expansion coefficients of F_0 and F_4 with respect to the basis functions (3.27) are combined into a single vector. This vector again has to fulfill an eigenvalue equation similar to the truncated version of Eq. (3.29), that can be solved by the previously described methods. The kernel matrix $\tilde{K}$ of the eigenvalue equation then consists of four blocks

$$\tilde{K} = \left(\begin{array}{c|c} K & K^{(1)} \\ \hline K^{(2)} & K^{(4)} \end{array} \right). \tag{3.34}$$

The matrix K in the upper left is identical to the matrix (3.30). The other matrices can be derived from the integrands in Eq. (3.24) and read

$$K_{ij}^{(1)}(E) = \frac{8}{\sqrt{\pi}} \sum_{\substack{\vec{n} \in \mathbb{Z}^3 \\ \vec{n} \neq \vec{0}}} \int_0^\Lambda \mathrm{d}y\, y^2 \left[\int_0^\Lambda \mathrm{d}p\, \frac{p^2}{p + \Lambda} \xi_i(p) Z_E^{(0)}(p, y) \right] d(y; E) j_4(L|\vec{n}|y) \tag{3.35a}$$

$$\times (Y_{40}(\hat{n}) C_{40} + Y_{44}(\hat{n}) C_{44} + Y_{4,-4}(\hat{n}) C_{4,-4}) \xi_j(y),$$

$$K_{ij}^{(2)}(E) = \frac{8}{3\sqrt{\pi} C_{40}} \sum_{\substack{\vec{n} \in \mathbb{Z}^3 \\ \vec{n} \neq \vec{0}}} \int_0^\Lambda \mathrm{d}y\, y^2 \left[\int_0^\Lambda \mathrm{d}p\, \frac{p^2}{p + \Lambda} \xi_i(p) Z_E^{(4)}(p, y) \right] d(y; E) j_4(L|\vec{n}|y) Y_{40}(\hat{n}) \xi_j(y),$$

$$\tag{3.35b}$$

$$K_{ij}^{(4)}(E) = \frac{4}{3\pi} \int_0^\Lambda \mathrm{d}y\, y^2 \left[\int_0^\Lambda \mathrm{d}p\, \frac{p^2}{p+\Lambda} \xi_i(p) Z_E^{(4)}(p,y) \right] d(y;E) \left(\frac{1}{3} + \sum_{\substack{\vec{n}\in\mathbb{Z}^3 \\ \vec{n}\neq\vec{0}}} \frac{\sin(L|\vec{n}|y)}{L|\vec{n}|y} \right) \xi_j(y).$$

(3.35c)

The spherical Bessel function of order 4 requires a careful numerical treatment. The form (3.25) is not suited for small arguments since, in this case, large cancellations take place that are reflected in large numerical noise in the FFT. Therefore, the y-integration is split at y_{cut}. The value of y_{cut} is determined on runtime depending on the present values of Λ and $|\vec{n}|$ such that a polynomial expansion of j_4 can be used to good approximation for $y < y_{\mathrm{cut}}$. For each absolute value $|\vec{n}|$, the integration from 0 to y_{cut} is performed using a Gauss-Legendre quadrature with 64 points, while the integration from y_{cut} to Λ is done by the FFT technique.

In the summation over $\vec{n}$ in the formulae for $K^{(1)}$ (3.35a) and $K^{(2)}$ (3.35b), the only dependence on the angular part of $\vec{n}$ is in the spherical harmonics. Accordingly, an ordered list was created with the angular sum evaluated for each absolute value $|\vec{n}|$. This drastically reduces the runtime of the code.

The calculation of the matrix elements has been performed on the cluster of the Helmholtz-Institut für Strahlen- und Kernphysik (HISKP) at the University of Bonn.

As has been stated above, the number of sampling points for the FFT is the parameter with the largest influence on the runtime. When using the expanded integral kernel, the matrix and the derivative matrix have to be calculated only once. For a typical sample size of 2^{20}, this takes about 100 minutes. When going to smaller volumes, the shifts in the binding energy become larger and the Taylor expansion of the integral kernel breaks down. In this case, it is inevitable to recalculate the kernel matrix in each iteration of the root finding algorithm. This amounts to 10 to 15 evaluations of the kernel matrix and a runtime of 8 to 10 hours per data point. The higher numerical effort needed when including the $\ell = 4$ wave is reflected in an increased runtime. It is approximately four times as large as in the s-wave only case due to the coupled channel approach.

With this formalism at hand, it is now possible to study the bound-state spectrum of systems with three identical bosons. The results of these calculations are presented in the following chapter.

Chapter 4

Results for three-boson bound states in finite volume

Using the formalism laid out in the previous section, energy levels of three-boson bound states in finite cubic volumes of varying side lengths have been calculated. In the following, results for systems with negative and positive scattering length are presented. Of particular interest is whether the finite volume reslts show universal features and how the universal features of the infinite volume are modified when going to the finite volume. For convenience, the dependence of the energies on the boson mass m is reinstated in this chapter.

4.1 Positive scattering length

First, results for systems with $a > 0$ are presented. In this regime, a physical diboson state with binding energy $E_D = -1/(ma^2)$ exists. This energy is therefore identical with the threshold for the break-up of a trimer into a diboson and a single boson. In the following, five states with different energies in the infinite volume, including shallow as well as deeply bound states, will be investigated exemplarily:

$$
\begin{aligned}
\text{Ia:} \quad & E_3^\infty = -1.18907/(ma^2), \quad \Lambda_* a = 5.66, \\
\text{Ib:} \quad & E_3^\infty = -27.4427/(ma^2), \quad \Lambda_* a = 5.66, \\
\text{Ic:} \quad & E_3^\infty = -9440.91/(ma^2), \quad \Lambda_* a = 5.66, \\
\text{II:} \quad & E_3^\infty = -5.04626/(ma^2), \quad \Lambda_* a = 1.66, \\
\text{III:} \quad & E_3^\infty = -11.1322/(ma^2), \quad \Lambda_* a = 3.66.
\end{aligned}
$$

Here, E_3^∞ is the trimer energy in the infinite volume. Note that the states Ia, Ib and Ic appear in the same physical system characterized by $\Lambda_* a = 5.66$. For each of these states, its energy in a finite cubic volume has been calculated for various values of the box side length L. In order to verify the consistent renormalization of our results, the calculation was carried out for several cutoff momenta Λ. For each cutoff, the three-body interaction parameterized by $H(\Lambda)$ has been adjusted such that the infinite volume binding energies are identical to the values given above for all considered cutoffs Λ. If our results are properly
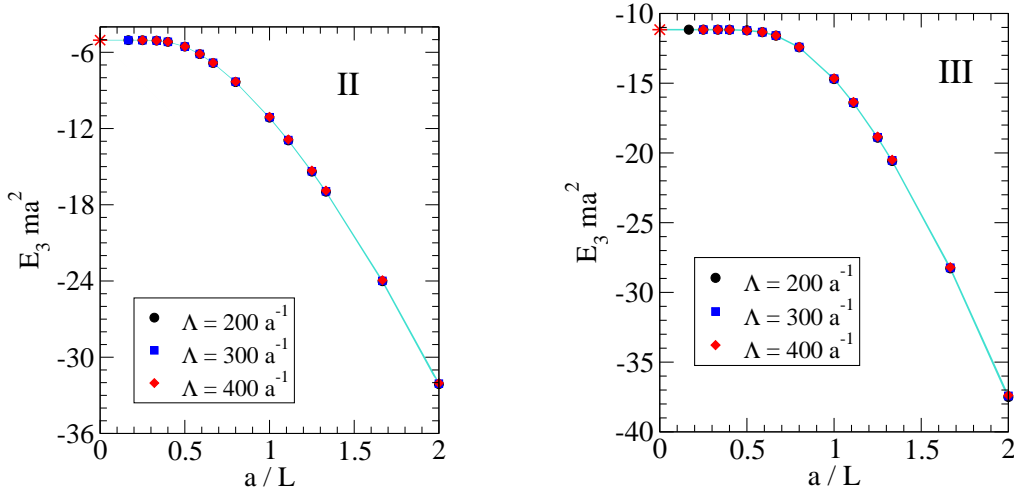
Figure 4.1: Variation of the trimer energy E_3 with the side length L of the cubic volume for the states II (left) and III (right). Plotted are three datasets for different values of the cutoff parameter Λ, together with the $1/(\Lambda a)$ bands. The point $a/L = 0$ corresponds to the infinite volume limit.

renormalized, the finite volume results for the different cutoffs should agree with each other up to an uncertainty of order $1/(\Lambda a)$ stemming from the finiteness of the cutoff.

The results for the states II and III are depicted in Fig. 4.1 for box sizes between $L = 6a$ and $L = a/2$. The values obtained for different cutoffs indeed agree with each other within the depicted uncertainty bands. Note that these bands do not represent corrections from higher orders of the EFT. For both states, the infinite volume limit is smoothly approached. As the volume becomes smaller, the energy of the states is more and more diminished. This corresponds to an increased binding with decreasing box size, i.e. the finite volume "squeezes" the bound state.

In the infinite volume, state III is more deeply bound than state II. Naively, one therefore expects the former to have a smaller spatial extent than the latter. The size of the state can be estimated via the formula $(-mE_3^\infty)^{-1/2}$, yielding $0.45a$ for state II and $0.3a$ for state III. Hence, a given finite volume should affect state II more strongly than the smaller state III. This behavior can indeed be observed. For example, considering a volume with side length $L = 2a$, the energy of state II deviates 10% from the infinite volume value, whereas the corresponding difference for state III is less than one percent. On the other hand, the energy shift of state III amounts to 10% for a smaller volume with a side length of roughly $1.3a$. This behavior is summarized in Table 4.1.

For both states, we can now form the dimensionless number $r = -mE_3^\infty L_{10\%}^2$, where $L_{10\%}$ is the box size at which the energy differs by 10% from the infinite volume value. This yields $r \approx 20$ for state II and $r \approx 19$ for state III. The approximate equality of the two values of r may indicate the presence of universal scaling in the finite volume version of the Effective Theory.

In Fig. 4.2, the three datasets obtained for state II are plotted again, this time compared to the results from calculations performed using the expansion of the kernel described in Section 3.3. For more results obtained using this expanded kernel see Ref. [KH09]. For large

State	Ia	II	III	Ib
$E_3^\infty\, ma^2$	-1.18907	-5.04626	-11.1322	-27.4427
$E_3(L=a)\, ma^2$	-4.6	-11.1	-14.66	-27.6
δ_{rel}	287%	120%	32%	0.6%
$L_{10\%}/a$	6	2	1.3	0.79
$L_{100\%}/a$	2.32	1.09	0.71	0.47

Table 4.1: For the states Ia, II, III and Ib, the infinite volume energy E_3^∞ and the energy in a finite volume with side length $L = a$ are shown together with the relative deviation from the infinite volume value $\delta_{rel} = (E_3(L=a) - E_3^\infty)/E_3^\infty$. Also given are the box sizes leading to an energy shift of 10% and 100%, respectively.
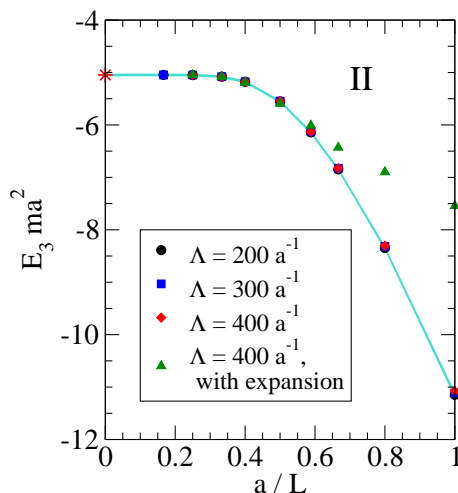

Figure 4.2: Variation of the trimer energy E_3 with the side length L of the cubic volume for state II. Plotted are three datasets for different values of the cutoff parameter Λ, together with the $1/(\Lambda a)$ bands, and one dataset obtained using a Taylor expanded version of the integral kernel.

values of the box size L, the results of both calculations agree with each other. For volumes smaller than $1.7a$, the result of the calculation with expansion deviates from the result of the full calculation. For this volume size, the full result differs from the infinite volume binding energy by about 20%. Accordingly, the expansion employed for the integral kernel is not applicable any longer. In Fig. 4.2, results are only depicted for volumes with $L \geq a$. For smaller volumes, the results of calculations using the expansion become cutoff dependent, and are hence not properly renormalized anymore.

In Fig. 4.3, we show our results for the two states Ia and Ib. These states belong to the same physical system characterized by $\Lambda_* a = 5.66$. The volume dependence of the two states is shown for box sizes between $L = 6a$ and $L = a/2$. The curve corresponding to the more deeply bound state Ib shows a behavior that is similar to the one observed for the states II and III. The binding energy remains constant until the volume is small enough to affect the state. This is the case for volumes with $L \approx 0.9a$. When going to even smaller volumes, the energy of the state is more and more diminished.

The behavior of the shallow state Ia is different. In the region $L \approx a$, the binding is not further increased. The results for smaller volumes show a sharp rise of the three-body energy. The
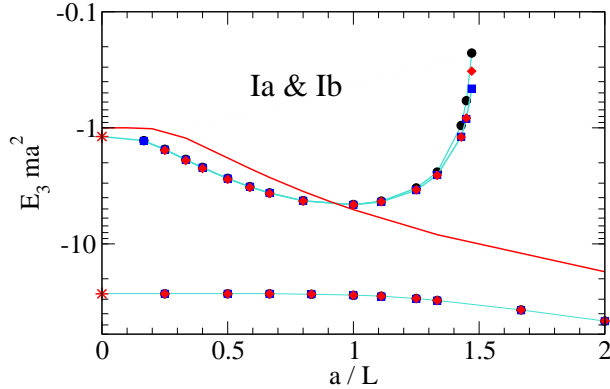
Figure 4.3: Variation of the trimer energy E_3 with the side length L of the cubic volume for the states Ia (upper curve) and Ib (lower curve). Plotted are three datasets for different values of the cutoff parameter Λ, together with the $1/(\Lambda a)$ bands (circles: $\Lambda = 200\,a^{-1}$; squares: $\Lambda = 300\,a^{-1}$; diamonds: $\Lambda = 400\,a^{-1}$). The solid line depicts the diboson energy.

L/a	Λa	$E_3(L)\,ma^2, \quad \ell = 0, 4$	$E_3(L)\,ma^2, \quad \ell = 0$	$E_2\,ma^2$
1.25	200	-4.30392	-4.24545	-3.53099
	200	-4.57097	-4.57753	
1	300	-4.60298	-4.60872	-5.07581
	400	-4.59579	-4.60056	
0.9	200	-4.31223	-4.27927	-6.068

Table 4.2: Energies $E_3(L)$ of state Ia for box sizes near $L = a$ calculated with and without admixture of the $\ell = 4$ amplitude. The dimer energy E_2 is shown for comparison.

energy of the state becomes positive near $L = 0.67a$. State Ia is close to the threshold for boson-diboson scattering in the infinite volume located at $E_D = -1/(ma^2)$. For comparison, we calculated the energy of the physical diboson according to [BBPS04]. The resulting curve is the solid line in Fig. 4.3. Like the energy of the three-body bound states, the energy of the diboson is diminished in finite volumes. For volumes of the size $L \approx 1.2a$, the energy of the three-body state Ia becomes larger than the diboson energy and starts to grow. This behavior is consistent with the observation that states are always shifted away from the threshold in a finite volume. In the two-body sector, for example, continuum states have been shown to have a power law dependence on the volume, while the volume dependence of bound states is dominated by exponentials [BBPS04]. The data shown for state Ia can be explained by an exponential for $L > a$, which characterizes the state as a bound state. For $L < a$, the data is consistent with a power law, indicating the state indeed behaves like a boson-diboson scattering state if its energy is above the diboson energy. However, as has been remarked in Section 3.2.2, the formalism developed in this work is tailored to investigate the behavior of bound states. Other techniques might be needed for a clean access to the boson-diboson scattering sector.

The other investigated states do not show such a transition since their energy is well below the diboson energy for all considered volumes. It is unclear whether other states would show a similar behavior for smaller box sizes. If this is not the case, the transition from bound to unbound would occur only for states with infinite volume binding energies up to a critical value. For a conclusive analysis of the nature of the described transition, more data is still

L/a	Λa	$E_3(L)\,ma^2,\quad \ell = 0,4$	$E_3(L)\,ma^2,\quad \ell = 0$	δ_{rel}
1	200	-11.86	-11.15	6.4%
	400	-11.79	-11.08	6.4%
0.7	200	-19.06	-20.70	-7.9%
	400	-18.97	-20.64	-8.1%

Table 4.3: Energies $E_3(L)$ of state II for box sizes $L = a$ and $L = 0.7a$ calculated with and without admixture of the $\ell = 4$ amplitude. Also given is the relative deviation δ_{rel} between the two energies for each parameter set.

needed. In the investigation of three-nucleon bound states, a similar behavior showed up. This will be discussed in Chapter 6. It would be interesting to see whether such a transition can be seen in lattice data for a state that is very close to the diboson threshold in the infinite volume.

Since the size of the finite volumes where the state crosses the diboson energy is comparable to the size of the state itself, the breaking of the spherical symmetry might be a relevant effect here. To assess the influence of the higher partial waves, calculations including the next partial wave contributing to the trivial representation of the cubic group, namely $\ell = 4$, were performed. The energies of state Ia obtained by this method are summarized and compared to the s-wave only results in Table 4.2. For $L = 1.25a$, the state is still below the dimer state. The inclusion of the higher partial wave leads to a small downward shift in the energy. For $L = a$, we have performed calculations using 3 different cutoffs. The results for different cutoffs agree to two significant digits indicating the results are properly renormalized, but the binding is slightly reduced by the $\ell = 4$ contribution. For $L = 0.9a$, the effect of the higher partial wave is again a small downward shift. All results show only a deviation of about 1% from the s-wave only result. In summary, we find that the correction from the $\ell = 4$ admixture is extremely small. Moreover, the corrections are in the same order of magnitude as the finite cutoff uncertainty of the calculation. In order to establish an estimate of typical corrections from higher partial waves, additional calculations including the $\ell = 4$ contributions for the more deeply-bound state II have been performed. The resulting energies are given in Tab. 4.3. The investigated box sizes are about three times larger than the state itself. The contribution of the higher partial wave is now several percent. This is still a small correction but considerably larger than the finite cutoff uncertainty. This suggests that the extremely small corrections for state Ia are related to its unusual behavior. The dominance of the s-wave may be associated with the closeness of the state to the threshold.

Since the shallow state Ia is more affected by a given finite volume than the more deeply bound state Ib, the ratio of the energies of the states is changing. In the infinite volume, this ratio is 23.08. For $L = 1.5a$, just before the shallow state crosses the dimer energy, the ratio has decreased to 7.4. Note that this ratio differs from the discrete scaling factor $\exp(2\pi/s_0) \approx 515$ even in the infinite volume limit. This behavior is expected for shallow states close to the bound state threshold [BH06]. The ratio $\exp(2\pi/s_0)$ will be approached when deeper states are considered. For example, the infinite volume ratio of state Ib and the much more deeply bound state Ic is 344 and thus already closer to the discrete scaling factor 515.

If we assume that the combination $r = -mE_3^\infty L_{10\%}^2$ is indeed a universal number, we are able to predict $L_{10\%}$ for the states Ia and Ib. The resulting predictions are $L_{10\%} \approx 0.85a$ for state Ib

	$\Lambda a = 4500$		$\Lambda a = 400$	
L/a	$E_3(L)\,ma^2$	δ_{rel}	$E_3(L)\,ma^2$	δ_{rel}
∞	-9440.91	$-$	-9401.32	$-$
1	-9440.91	0%	-9401.36	$\approx 10^{-6}$
0.75	-9440.91	0%	-9400.53	$\approx 10^{-5}$
0.5	-9440.91	0%	-9399.38	0.02%

Table 4.4: Energy E_3 of state Ic for different volume sizes L and two different cutoffs Λ. The relative deviation from the infinite volume value $\delta_{rel} = (E_3 - E_3^\infty)/E_3^\infty$ is also given.

and $L_{10\%} \approx 4a$ for state Ia. The energies calculated for these volumes are $E_3(L = 0.85a) \approx 29.1/(ma^2)$, corresponding to an 8% shift, for state Ib and $E_3(L = 4a) \approx 1.55/(ma^2)$, corresponding to a 30% shift. It should be noted, however, that universal behavior is strongly modified for states close to the threshold already in the infinite volume.

In addition, the dimensionless combination $r' = -mE_3^\infty L_{100\%}^2$ was formed. Here, $L_{100\%}$ is the box side length where the energy of the state is twice the infinite volume value. These values can also be found in Table 4.1. The values obtained are $r' = 6.4, 6.0, 5.6, 6.0$ for the states Ia, II, III and Ib, respectively. Using the value from state II to predict $L_{100\%}$ for the other states yields $2.25a$ for state Ia, which is close to the actual value of $2.32a$. For state III and Ib, the prediction works even better, yielding $0.71a$ and $0.47a$, repectively. The actual value is $0.73a$ for state III and is exactly as predicted for state Ib. These findings support the assumption that the finite volume corrections obey universal scaling relations.

In the infinite volume case, Efimov was able to derive a formula for the binding energies using a hyperspherical formalism. The binding energies are the solutions of

$$mE_3 + 1/a^2 = \mathrm{e}^{\frac{2\pi}{s_0}(n-n_*)} \exp(\Delta(\xi)/s_0)\kappa_*^2, \tag{4.1}$$

where E_3 is the energy of the state measured from the 3-boson threshold that appears also in the variable ξ given by $\tan\xi = -a\sqrt{mE_3}$. The universal function $\Delta(\xi)$ can be parameterized [BHK03]. Thus, the binding energies are fixed as soon as the binding momentum κ_* of the n_*th Efimov trimer is known. If the finite volume effects are indeed universal, it should be possible to find the binding energies in a finite volume by solving an equation similar to (4.1), where the universal function Δ depends now also on the size of the volume under consideration.

The states Ia and Ib appear in the same physical system characterized by $\Lambda_* a = 5.66$. In this system, an even more deeply bound state, denoted state Ic, is present. In the infinite volume, the energy of this state is $E_3^\infty = -9401.32/(ma^2)$. This corresponds to a binding momentum of $97a^{-1}$. Since this is already comparable to the momentum cutoffs of a few hundred inverse scattering lengths employed before, an additional, much larger cutoff of $4500\ a^{-1}$ was used for calculations of this state. The three-body force for this cutoff has been fixed such that the energy of the most shallow state Ia is reproduced. The resulting energy of state Ic is then $-9440.91/(ma^2)$. This differs from the energy obtained using the smaller cutoff by 0.4%. This difference can be attributed to effects stemming from the finiteness of the cutoff. The energy of this state has been calculated for finite volumes of the sizes $L = a$, $L = 0.75a$ and $L = 0.5a$. The results of this calculations are summarized in Table 4.4. The values obtained using the large cutoff $\Lambda a = 4500$ show no effect of the finite volume at all. From the infinite
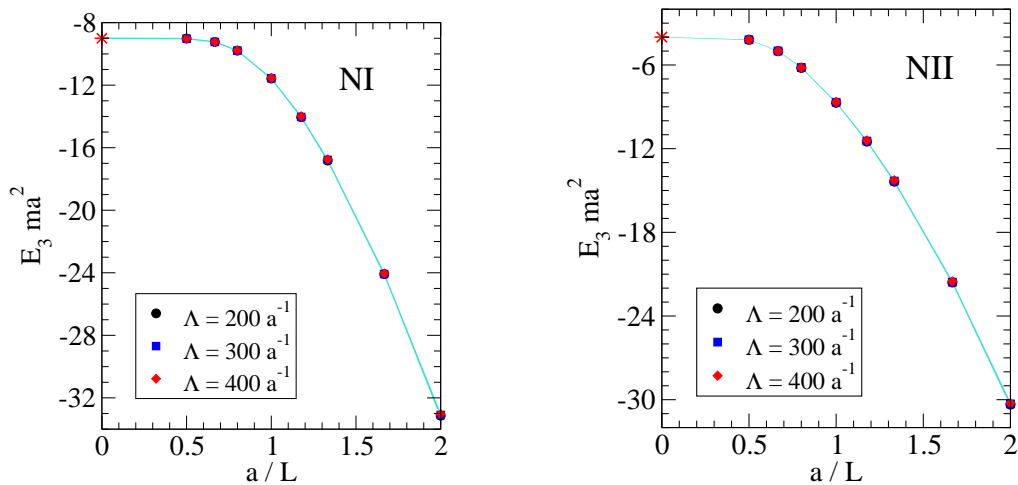
Figure 4.4: Variation of the trimer energy E_3 with the side length L of the cubic volume for the states NI (left) and NII (right). Plotted are three datasets for different values of the cutoff parameter Λ, together with the $1/(\Lambda a)$ bands. The point $a/L = 0$ corresponds to the infinite volume limit.

volume binding energy, the size of the state can be estimated via $(mE_3^\infty)^{-1/2}$ to be $0.01a$. Therefore, no visible effect is expected since the finite volume is fifty times larger than the state itself. However, for the smaller cutoff $\Lambda a = 400$, there are very small deviations from the infinite volume energy. But these deviations are smaller than the uncertainty stemming from the finiteness of the cutoff, which is estimated to be of order $1/(\Lambda a) = 0.25\%$.

4.2 Negative scattering length

In the following, systems with negative two-body scattering length will be investigated. In this regime, the two-body interaction is attractive but no diboson bound state exists in the infinite volume limit. The only possible breakup process for a three-boson bound state is therefore the breakup into three single bosons. The threshold for this process is $E = 0$. As in the case with positive scattering length, we choose states with different energies in the infinite volume:

$$\begin{array}{llll} \text{NI:} & E_3^\infty = -9/(ma^2), & \Lambda_* a = 5.55, \\ \text{NII:} & E_3^\infty = -4/(ma^2), & \Lambda_* a = 4.23, \\ \text{NIII:} & E_3^\infty = -0.2/(ma^2), & \Lambda_* a = 2.60. \end{array}$$

Here, E_3^∞ is the trimer energy in the infinite volume. For each of these states, its energy in a finite cubic volume has been calculated for various values of the box side length L. In order to check the consistent renormalization of the results, the calculation was carried out for several cutoff momenta Λ. For each state, the three-body interaction parameterized by $H(\Lambda)$ has been adjusted such that the infinite volume binding energies given above are reproduced for all considered cutoffs.

The results for the states NI and NII are shown in Fig. 4.4 for box sizes between $L = 2a$ and $L = a/2$. The results for the state NIII with box sizes between $L = 8a$ and $L = a/2$
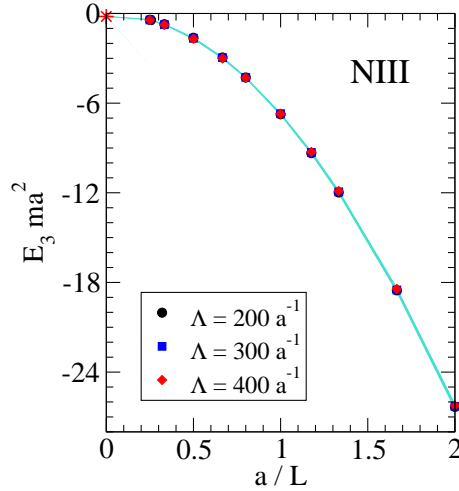
Figure 4.5: Variation of the trimer energy E_3 with the side length L of the cubic volume for the state NIII. Plotted are three datasets for different values of the cutoff parameter Λ, together with the $1/(\Lambda a)$ bands.

State	NI	NII	NIII
$E_3^\infty \, ma^2$	-9	-4	-0.2
$E_3(L=a)\, ma^2$	-11.6	-8.7	-6.7
δ_{rel}	29%	118%	3250%
$L_{10\%}/a$	1.2	1.8	7.2
$L_{100\%}/a$	0.7	1.05	4.2

Table 4.5: For the states NI, NII and NIII, the infinite volume energy E_3^∞ and the energy in a finite volume with side length $L = a$ are shown together with the relative deviation from the infinite volume value $\delta_{rel} = (E_3(L=a) - E_3^\infty)/E_3^\infty$. Also given are the box sizes leading to an energy shift of 10% and 100%, respectively.

are depicted in Fig. 4.5. The energies obtained using different cutoffs agree with each other within the bands representing uncertainties due to finite cutoff effects. This verifies the proper renormalization of the finite volume theory. All three states smoothly approach the infinite volume limit. As the box size becomes smaller the energy of the state is more and more diminished. This corresponds to the intuitive picture that the finite volume "squeezes" the bound state. The overall behavior resembles the behavior in the positive scattering length case as described in the previous section.

Naively, the more deeply bound a state is in the infinite volume, the smaller is its spatial extent. Estimating the size via the formula $(-mE_3^\infty)^{-1/2}$ yields $a/3$ for state NI, $a/2$ for state NII, and $2.2a$ for state NIII. A given finite volume should therefore affect state NII more than state NI, and state NIII should be the most affected. When considering a cubic volume with side length $L = a$, we find the energies given in Table 4.5. The relative deviation of state NI is indeed four times smaller than the shift for state NII and a hundred times smaller than the shift for the shallow state NIII. On the other hand, the box length $L_{10\%}$, for which the energy of each states deviates 10% from its infinite volume value, is smaller the more deeply bound a state is. These values are also given in Table 4.5.

As for positive scattering length, the dimensionless combination $r = -mE_3^\infty L_{10\%}^2$ was inves-

tigated in order to look for hints of universal behavior in the finite volume theory. The value $r \approx 13$ was obtained from the data for state NI. This value is used to predict $L_{10\%} = 1.8a$ for state NII and $L_{10\%} = 8a$ for state NIII. These predictions are in good agreement with the explicitly calculated values shown in Table 4.5. The 10% deviation for the shallowest state can, as was already state for the shallowest state with positive scattering length, be attributed to the largeness of non-universal effects close to the threshold. Again, also the dimensionless combination, $r' = -mE_3^{\infty}L_{100\%}^2$ was formed. For the three investigated states, $L_{100\%}$ is also given in Table 4.5. The value for the state NI yields $r' \approx 4.4$. This value corresponds to a predicted $L_{100\%} = 1.05a$ for state NII and $L_{100\%} = 4.7a$ for state NIII. The value for state NII is as predicted, whereas the value for state NIII is again about 10% off the prediction from universal scaling.

For states far away from the threshold, the regimes of negative and positive scattering length are expected to be governed by the same scaling factor. Therefore, the dimensionless combination r should, for such deeply bound states, have a common value for both signs of a. For positive scattering lengths, state Ib is an example of a rather deeply bound state. For this state, $L_{10\%}$ is found to be $0.79a$. This leads to $r = 16.8$. The very deeply bound state Ic experiences a 10% shift for a volume with side length $0.0427a$, corresponding to $r = 17.2$. With regard to the vast difference of binding energies, the value $r \approx 17$ may be seen as the universal value for this dimensionless variable. For negative scattering lengths, a state with $E_3^{\infty} = -27/(ma^2)$ is present without need for a three-body force when setting $\Lambda_* a = 8.54$. The energy of this state is shifted by 10% in a volume with side length $0.73a$, yielding $r = 14.4$. The values of r for these three states with different signs of the scattering length are indeed close to each other. This behavior provides numerical evidence for the universality of finite volume effects for both positive and negative scattering lengths.

In this chapter, the bound state spectrum in a finite volume was calculated for different physical systems with positive and negative scattering length. The renormalization of the results was verified explicitly. For small shifts up to 15%, an expanded version of the integral kernel can be used to reduce the numerical effort. Typically, the binding energy increases as the box size is reduced. One state showed a peculiar threshold crossing behavior that is not associated with the neglect of higher partial waves and will be further investigated. The effects from higher partial waves are accessible, but require a careful numerical treatment. They were shown to be typically in the order of several percent. Finally, the results provided numerical evidence for a universal scaling of the finite volume effects. Building on these results, the formalism was extended to describe the three-nucleon system.

Chapter 5

EFT for three nucleons in finite volume

The study of the Efimov effect in finite cubic volumes is of particular interest for three-nucleon systems. The Efimov trimers can be identified as the isospin doublet containing the triton and the ^{3}He nucleus. Because the Coulomb interaction complicates the study of the latter, the focus of this work is on the triton. Following the strategy outlined in the bosonic case, the effects of momentum quantization and the breakdown of rotational symmetry lead to an infinite set of coupled integral equations.

5.1 Lagrangian and Nucleon-Dinucleon Amplitudes

In the three-nucleon sector, additional degrees of freedom, namely spin and isospin of the nucleon, have to be taken into account. The general structure of the EFT describing the short-ranged nucleonic interactions, however, strongly resembles the EFT for three identical bosons.

As was stated in Subsection 2.2.3, there are two scattering channels present in NN scattering due to the spin and isospin degrees of freedom. One is the spin-singlet, isospin-triplet ($^1S_0$) channel, the other one is the spin-triplet, isospin-singlet ($^3S_1$) channel. In the latter exists a shallow two-body bound state, the deuteron. In both channels, the two-body scattering length is large compared to the natural length scale of the system given by m_π^{-1}. Accordingly, instead of a single auxiliary diboson field, the Lagrangian will feature two di-nucleon fields corresponding to the two scattering channels.

The Lagrangian of the three-nucleon EFT is to leading order given by [BHvK00]

$$
\begin{aligned}
\mathcal{L}_{3N} =& N^\dagger \left(i\partial_t + \frac{1}{2}\nabla^2 \right) N + \frac{g_T}{2}\vec{T}^\dagger\vec{T} + \frac{g_S}{2}\mathbf{S}^\dagger\mathbf{S} \\
& - \frac{g_T}{2}\left(\vec{T}^\dagger N^T \tau_2 \vec{\sigma}\sigma_2 N + \text{h.c.} \right) - \frac{g_S}{2}\left(\mathbf{S}^\dagger N^T \sigma_2 \boldsymbol{\tau}\tau_2 N + \text{h.c.} \right).
\end{aligned}
\tag{5.1}
$$

Here, N is the isospin doublet containing the neutron and the proton field. The di-nucleon field $\vec{T}$ has the quantum numbers of the deuteron, namely spin 1 and isospin 0. Accordingly,

41

S is the di-nucleon in the $^1S_0$ channel. The $\vec{\sigma}$ ($\boldsymbol{\tau}$) are the Pauli matrices in spin (isospin) space, respectively. Up to now, no isospin breaking effects have been incorporated into this framework. The leading order lagrangian corresponds to the zero-range model. Effects from finite range can be incorporated as higher orders of the Effective Theory.

The two coupling constants in (5.1) have to be matched to two two-body inputs. These can be the scattering lengths or, in case of g_T, the binding energy of the deuteron. As stated in Subsection 2.2.3, range corrections are important in order to reproduce the deuteron binding energy when using the scattering length as input. Since the present work is concerned with leading order calculations only, the deuteron binding energy will be the preferred input in order to correctly reproduce the breakup threshold for the three-nucleon bound state. In the spin-quartet channel of the three-body sector, this is sufficient to renormalize the theory. In the spin-doublet channel that contains the triton, however, the amplitudes calculated with this theory show a strong cutoff dependence. The case of three identical bosons provides the remedy to this problem: An additional three-body force is needed. As it was shown in [BHvK00], a single SU(4)-symmetric three-body interaction is sufficient to renormalize the theory. To leading order, this interaction is given by

$$
\mathcal{L}_{\text{3-body}} = -\frac{2H(\Lambda)}{\Lambda^2}\left(g_T^2 N^\dagger (\vec{T} \cdot \vec{\sigma})^\dagger (\vec{T} \cdot \vec{\sigma})N + \frac{1}{3}g_T g_S \left(N^\dagger (\vec{T} \cdot \vec{\sigma})^\dagger (\mathbf{S} \cdot \boldsymbol{\tau})N + \text{h.c.} \right) \right.
$$
$$
\left. + g_S^2 N^\dagger (\mathbf{S} \cdot \boldsymbol{\tau})^\dagger (\mathbf{S} \cdot \boldsymbol{\tau})N \right).
\tag{5.2}
$$

As in the three-boson case, the dimensionless function $H(\Lambda)$ needs one three-body datum as additional input.

SU(4)-symmetry is a generalization of the SU(2)×SU(2) symmetry of spin and isospin that was introduced by Wigner in 1937 [Wig37]. Although, in order to be an exact symmetry, the two-body scattering lengths have to be equal, their unnatural largeness makes it an approximate symmetry that is satisfied to a high degree in the spectra of nuclei. Group theoretical arguments show that the three-body force given in Eq. (5.2) is the only such force that can be written down to leading order and that the force itself has to be SU(4)-symmetric. In Section 6.2, a possible scenario explaining the approximate SU(4)-symmetry of nuclear physics will be discussed.

The renormalization of the theory absorbs the high-energy behavior of the underlying theory into a few low-energy coefficients. The finite volume, on the other hand, modifies the infrared properties of the system. As has been argued in Chapter 3, the renormalization from the infinite volume should therefore also apply in the finite volume. This is under the premise that the ultraviolet regime, characterized by the momentum cutoff Λ, and the infrared regime, characterized by the scale of momentum quantization $2\pi/L$, are well separated. In Chapter 4, the renormalization of the results for three identical bosons was explicitly shown. The renormalization of the results from the three-nucleon sector has also been explicitly verified. This will be shown in the next chapter where the results are presented.

In analogy to the three-boson case, it is necessary to calculate the full di-nucleon propagators in finite volume. These quantities are obtained by dressing the constant bare propagators
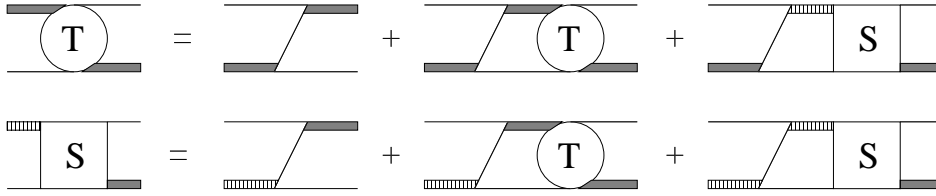
Figure 5.1: Coupled integral equations for the dinucleon-nucleon scattering amplitudes in the $S = \frac{1}{2}$ channel. Single lines denote nucleons, the shaded (full) bars correspond to dinucleons in the $^3S_1$ ($^1S_0$) channel. For the sake of simplicity, the three-body force has been omitted in this diagrammatical representation.

with nucleonic loops. The result is

$$D_{S,T}(E) = \frac{8\pi}{g_{S,T}^2} \left[\frac{1}{a_{S,T}} - \sqrt{-E} + \frac{1}{L} \sum_{\substack{\vec{j} \in \mathbb{Z}^3 \\ \vec{j} \neq \vec{0}}} \frac{1}{|\vec{j}|} e^{-|\vec{j}| L \sqrt{-E}} \right]^{-1}, \tag{5.3}$$

where D_S (D_T) denotes the spin-singlet (spin-triplet) di-nucleon propagator and $a_{S,T}$ is the two-nucleon scattering length in the corresponding channel. In the triplet channel, it is advantageous to use the deuteron binding momentum $\sqrt{mB_d}$ instead of the inverse scattering length. The volume dependent term in the full propagator vanishes in the limit $L \to \infty$, thus reproducing the infinite volume result.

The triton is a $\frac{1}{2}^+$ state. In order to investigate this bound state, the nucleon-dinucleon scattering amplitudes with the appropriate quantum numbers have to be written down. Since the triton can be seen as a single neutron interacting with a proton-neutron pair in either the $^3S_1$ or the $^1S_0$ partial wave, there are two relevant amplitudes. These are the amplitude with an incoming and outgoing dinucleon field $\vec{T}$ (denoted t_T in the following) and the amplitude with an incoming dinucleon field $\mathbf{S}$ and an outgoing field $\vec{T}$ (denoted t_S). The two amplitudes are coupled and the corresponding integral equation is depicted diagramatically in Fig. 5.1. In this diagrammtical representation, the contributions from the 3-body force (5.2) have been omitted for sake of simplicity. As in the three-boson case, the loop momenta are quantized due to the finite volume resulting in loop sums rather than loop integrals. For the internal di-nucleon lines, the full di-nucleon propagators (5.3) have to be used.

In order to write down the integral equation explicitly, kinematics are assigned as follows. The ingoing nucleon line has momentum $-\vec{p}$ and spin (isospin) α (a). The outgoing nucleon line has momentum $-\vec{k}$ and spin (isospin) β (b). Both nucleons are on shell. The ingoing (outgoing) di-nucleon carries momentum $\vec{p}$ ($\vec{k}$) and remains off-shell. This introduces the total energy of the system, E, as an additional parameter of the amplitude. The spin component of ingoing (outgoing) spin-triplet fields is denoted i (j), while the isospin component of the ingoing (outgoing) spin-singlet field is A (B).

With these conventions, the spin-isospin structure of the tree-level diagrams in Fig. 5.1 can be calculated. The results are

$$\begin{array}{lll}
\text{(a)} & N\vec{T} \to N\vec{T}: & g_T^2 \, (\sigma^j \sigma^i)_{\alpha\beta} \, \delta_{ab} \\[2mm]
\text{(b)} & N\mathbf{S} \to N\mathbf{S}: & g_S^2 \, \delta_{\alpha\beta} \, (\tau^B \tau^A)_{ab} \\[2mm]
\text{(c)} & N\vec{T} \to N\mathbf{S}: & g_T g_S \, (\sigma^i)_{\alpha\beta} \, (\tau^B)_{ab} \\[2mm]
\text{(d)} & N\mathbf{S} \to N\vec{T}: & g_T g_S \, (\sigma^j)_{\alpha\beta} \, (\tau^A)_{ab}
\end{array}$$

The momentum space part of all these diagrams reads $i/(E - (p^2 + \vec{p} \cdot \vec{k} + k^2))$. The spin-isospin structure of the contact interactions derived from (5.2) is identical in the cases (a) and (b). In the cases (c) and (d), an additional factor $\frac{1}{3}$ is present. The momentum space part of the contact interaction is given by $-i2H(\Lambda)/\Lambda^2$.

After these preparations, the integral equations for the amplitudes t_T and t_S can be written down. The integration over the unquantized energy of the internal nucleon can be performed via the residue theorem. The result is

$$t_T^{ij}(\vec{p}, \vec{k}; E)_{ab}^{\alpha\beta} = g_T^2 \, (\sigma^j \sigma^i)_{\alpha\beta} \, \delta_{ab} \left(\mathcal{Z}_E(\vec{p}, \vec{k}) - \frac{2H(\Lambda)}{\Lambda^2} \right)$$

$$+ L^{-3} \sum_{\vec{q} \in \mathbb{Z}^3} 8\pi \, (\sigma^k \sigma^i)_{\alpha\gamma} \left(\mathcal{Z}_E(\vec{p}, \vec{q}) - \frac{2H(\Lambda)}{\Lambda^2} \right) d_T(q; E) t_T^{kj}(\vec{q}, \vec{k}; E)_{ab}^{\gamma\beta}$$

$$+ L^{-3} \sum_{\vec{q} \in \mathbb{Z}^3} 8\pi \, \frac{g_T}{g_S} (\sigma^i)_{\alpha\gamma} (\tau^C)_{ac} \left(\mathcal{Z}_E(\vec{p}, \vec{q}) - \frac{2H(\Lambda)}{3\Lambda^2} \right) d_S(q; E) t_S^{Cj}(\vec{q}, \vec{k}; E)_{cb}^{\gamma\beta}$$

$$\text{(5.4a)}$$

$$t_S^{Aj}(\vec{p}, \vec{k}; E)_{ab}^{\alpha\beta} = g_S g_T \, (\sigma^j)_{\alpha\beta} \, (\tau^A)_{ab} \left(\mathcal{Z}_E(\vec{p}, \vec{k}) - \frac{2H(\Lambda)}{3\Lambda^2} \right)$$

$$+ L^{-3} \sum_{\vec{q} \in \mathbb{Z}^3} 8\pi \, \frac{g_S}{g_T} (\sigma^k)_{\alpha\gamma} (\tau^A)_{ac} \left(\mathcal{Z}_E(\vec{p}, \vec{q}) - \frac{2H(\Lambda)}{3\Lambda^2} \right) d_T(q; E) t_T^{kj}(\vec{q}, \vec{k}; E)_{cb}^{\gamma\beta}$$

$$+ L^{-3} \sum_{\vec{q} \in \mathbb{Z}^3} 8\pi \, (\tau^C \tau^A)_{ac} \left(\mathcal{Z}_E(\vec{p}, \vec{q}) - \frac{2H(\Lambda)}{\Lambda^2} \right) d_S(q; E) t_S^{Cj}(\vec{q}, \vec{k}; E)_{cb}^{\alpha\beta},$$

$$\text{(5.4b)}$$

where

$$\mathcal{Z}_E(\vec{p}, \vec{k}) = \left[p^2 + \vec{p} \cdot \vec{k} + k^2 - E \right]^{-1} \tag{5.5}$$

and $d_{S,T}(q; E) = g_{S,T}^2/(8\pi) \, D_{S,T}(E - 3/4q^2)$. Note that the two equations transform into each other under $S \leftrightarrow T$. This is a signature of the approximate SU(4)-symmetry of NN-interactions discussed above.

In the vicinity of a bound state with binding energy B_3, the amplitudes $t_{S,T}^{(A,i)j}$ [1] develop a simple pole in the energy. Moreover, the incoming and outgoing quantum numbers separate:

$$t_{S,T}^{(A,i)j}(\vec{p}, \vec{k}; E)_{ab}^{\alpha\beta} \to \frac{\mathcal{F}_{S,T}^{(A,i)}(\vec{p})_a^\alpha \, \mathcal{F}_{S,T}^j(\vec{k})_b^\beta}{E + B_3} + \text{regular terms, as } E \to -B_3 \tag{5.6}$$

---

[1]This is to be read as a summarizing notation for t_S^{Aj} and t_T^{ij}.

Using this behavior in Eqs. (5.4) and comparing the residues of the poles on both sides yields two coupled equations for the bound state amplitudes $\mathcal{F}_{S,T}$:

$$\mathcal{F}_T^i(\vec{p})_a^\alpha = 8\pi L^{-3} \sum_{\vec{q}\in\mathbb{Z}^3} \Big[(\sigma^k\sigma^i)_{\alpha\gamma} \left(\mathcal{Z}_{-B_3}(\vec{p},\vec{q}) - \frac{2H(\Lambda)}{\Lambda^2} \right) d_T(q;-B_3)\mathcal{F}_T^k(\vec{q})_a^\gamma$$

$$+ (\sigma^i)_{\alpha\gamma}(\tau^C)_{ac} \left(\mathcal{Z}_{-B_3}(\vec{p},\vec{q}) - \frac{2H(\Lambda)}{3\Lambda^2} \right) d_S(q;-B_3)\mathcal{F}_S^C(\vec{q})_c^\gamma \Big] \tag{5.7a}$$

$$\mathcal{F}_S^A(\vec{p})_a^\alpha = 8\pi L^{-3} \sum_{\vec{q}\in\mathbb{Z}^3} \Big[(\sigma^k)_{\alpha\gamma}(\tau^A)_{ac} \left(\mathcal{Z}_{-B_3}(\vec{p},\vec{q}) - \frac{2H(\Lambda)}{3\Lambda^2} \right) d_T(q;-B_3)\mathcal{F}_T^k(\vec{q})_c^\gamma$$

$$+ (\tau^C\tau^A)_{ac} \left(\mathcal{Z}_{-B_3}(\vec{p},\vec{q}) - \frac{2H(\Lambda)}{\Lambda^2} \right) d_S(q;-B_3)\mathcal{F}_S^C(\vec{q})_c^\alpha \Big] \tag{5.7b}$$

Here, the amplitudes have been redefined in order to absorb the ratios of coupling constants appearing in Eqs. (5.4) by

$$\mathcal{F}_T^i \rightarrow \sqrt{\frac{g_S}{g_T}}\mathcal{F}_T^i \text{ and } \mathcal{F}_S^A \rightarrow \sqrt{\frac{g_T}{g_S}}\mathcal{F}_S^A. \tag{5.8}$$

The next step is to project Eqs. (5.7) on total spin $\frac{1}{2}$ and total isospin $\frac{1}{2}$ by

$$(\mathcal{F}_T)_{t_3}^{m_s} = (\sigma^i)_{m_s\alpha}\,\delta_{t_3a}\,\big(\mathcal{F}_T^i\big)_a^\alpha \tag{5.9a}$$

$$(\mathcal{F}_S)_{t_3}^{m_s} = \delta_{m_s\alpha}\,(\tau^A)_{t_3a}\,\big(\mathcal{F}_S^A\big)_a^\alpha. \tag{5.9b}$$

Here, m_s and t_3 are the 3-components of the triton in spin and isospin space, respectively. In order to perform the projection explicitly, the following relations for Pauli matrices are employed:

$$(\sigma^i)_{m_s\alpha}(\sigma^k\sigma^i)_{\alpha\gamma} = -(\sigma^k)_{m_s\gamma} \text{ and} \tag{5.10}$$

$$(\sigma^i)_{m_s\alpha}(\sigma^i)_{\alpha\gamma} = 3\,\delta_{m_s\gamma}. \tag{5.11}$$

The resulting coupled equations for the $S = \frac{1}{2}$ bound state amplitudes in finite volume are

$$\mathcal{F}_T(\vec{p})_{t_3}^{m_s} = 8\pi L^{-3} \sum_{\vec{q}\in\mathbb{Z}^3} \Big[\left(-\mathcal{Z}_{-B_3}(\vec{p},\vec{q}) + \frac{2H(\Lambda)}{\Lambda^2} \right) d_T(q;-B_3)\mathcal{F}_T(\vec{q})_{t_3}^{m_s}$$

$$+ \left(3\mathcal{Z}_{-B_3}(\vec{p},\vec{q}) - \frac{2H(\Lambda)}{\Lambda^2} \right) d_S(q;-B_3)\mathcal{F}_S(\vec{q})_{t_3}^{m_s} \Big] \tag{5.12a}$$

$$\mathcal{F}_S(\vec{p})_{t_3}^{m_s} = 8\pi L^{-3} \sum_{\vec{q}\in\mathbb{Z}^3} \Big[\left(3\mathcal{Z}_{-B_3}(\vec{p},\vec{q}) - \frac{2H(\Lambda)}{\Lambda^2} \right) d_T(q;-B_3)\mathcal{F}_T(\vec{q})_{t_3}^{m_s}$$

$$+ \left(-\mathcal{Z}_{-B_3}(\vec{p},\vec{q}) + \frac{2H(\Lambda)}{\Lambda^2} \right) d_S(q;-B_3)\mathcal{F}_S(\vec{q})_{t_3}^{m_s} \Big] \tag{5.12b}$$

The spin and isospin indices will be supressed in the following. In the next section, the cubic symmetry of the system is employed to make Eqs. (5.12) accessible for a numerical treatment.

5.2   Consequences of cubic symmetry

In a finite cubic box, spherical symmetry is broken down to cubic symmetry. As a consequence, the infinitely many irreducible representations of the double cover of the rotational group, SU(2), become reducible in terms of the eight irreducible representations of the double cover of the cubic group, ^2O. The triton is mainly, and for this work we will assume solely, a $j = \frac{1}{2}$ state. This partial wave is contained in the G_1^+ representation, which also contains $j = 7/2, 9/2, \dots$ [Joh82]. Assuming that the triton amplitude in finite volume transforms under the G_1^+ representation, it is possible to decompose it into the different partial waves [vdLB47, BLMR08] as

$$\mathcal{F}(\vec{y}) = \sum_{j=\frac{1}{2},\frac{7}{2},\dots}^{(G_1^+)} \sum_t F^{(j,t)}(y) \sum_{m_j} \tilde{C}_{jtm_j} |jm_j\rangle. \tag{5.13}$$

The coefficients $\tilde{C}_{jtm_j}$ can be determined by explicitly decomposing the reducible representations of SU(2) in terms of the irreducible representations of ^2O [BLMR08]. The sum over t is needed if a partial wave is contained more than once. Since this is not the case for partial waves less than $13/2$, this index will be omitted in the following. The vectors $|jm_j\rangle$ are given by

$$|jm_j\rangle = \sum_{m=-(j\pm\frac{1}{2})}^{j\pm\frac{1}{2}} \sum_{s=\pm\frac{1}{2}} C^{jm_j}_{j\pm\frac{1}{2}m\frac{1}{2}s} |j\pm\frac{1}{2}m\rangle \otimes |\frac{1}{2}s\rangle, \tag{5.14}$$

where the C's are Clebsch-Gordan coefficients, The $|\ell m\rangle$ are spherical harmonics and $|\frac{1}{2}s\rangle$ is a spin-$\frac{1}{2}$ spinor. The sign of $\ell(j) = j \pm \frac{1}{2}$ has to be chosen such that the result is even in order to get the positive parity of the triton. Details on the construction of the basis functions together with the group theoretical background are presented in Appendix A.

With the expansion in spherical harmonics, the angular dependence of the bound state amplitude has been explicitly extracted. In order to make use of this, the sums over integer vectors in Eqs. (5.12) are rewritten into sums of integral equations using Poisson's resummation formula (3.14). After expanding $\mathcal{Z}_{-B_3}(\vec{p}, \vec{q})$ as in Eq. (3.17) and the exponential from Poisson's formula as in Eq. (3.18), the angular integration can be performed analytically.

Performing the angular integrations and projecting out the Jth partial wave yields an infinite set of coupled equations:

$$\begin{pmatrix} F_T^{(J)}(y) \\ F_S^{(J)}(y) \end{pmatrix} = \frac{4}{\pi} \int_0^\Lambda dy\, y^2 \sum_j^{(G_1^+)} \left(\begin{pmatrix} -1 & 3 \\ 3 & -1 \end{pmatrix} Z_{-B_3}^{(\ell(J))}(p,y) + \begin{pmatrix} 1 & -1 \\ -1 & 1 \end{pmatrix} \frac{2H(\Lambda)}{\Lambda^2}\delta_{\ell(J),0} \right)$$

$$\times \begin{pmatrix} \frac{d_T(y;-B_3)}{2\ell(J)+1} F_T^{(j)}(y) \\ \frac{d_S(y;-B_3)}{2\ell(J)+1} F_S^{(j)}(y) \end{pmatrix} \left[\delta_{Jj} + \sum_{\substack{\vec{n}\in\mathbb{Z}^3 \\ \vec{n}\neq\vec{0}}} \sqrt{4\pi} \sum_{\ell'} i^{\ell'} j_{\ell'}(L|\vec{n}|y) \sqrt{\frac{(2\ell(j)+1)(2\ell'+1)}{2\ell(J)+1}} \right.$$

$$\times \sum_{m=-\ell(j)}^{\ell(j)} \sum_{s=\pm\frac{1}{2}} \frac{\tilde{C}_{j,m+s}}{\tilde{C}_{JM}} Y^*_{\ell'(M-s-m)}(\hat{n}) C^{JM}_{\ell(J)(M-s)\frac{1}{2}s} C^{j,m+s}_{\ell(j)m\frac{1}{2}s}$$

$$\left. \times\, C^{\ell(J)0}_{\ell(j)0\ell'0} C^{\ell(J)(M-s)}_{\ell(j)m\ell'(M-s-m)} \right]. $$

$$\tag{5.15}$$

The partial waves of $\mathcal{Z}$ are given by

$$\frac{Z_{-B_3}^{(\ell)}(p,y)}{2\ell+1} = \frac{1}{py}Q_\ell\left(\frac{p^2+y^2+B_3}{py}\right), \tag{5.16}$$

where Q_ℓ is a Legendre function of the second kind. Note that the first term in Eq. (5.15) reproduces the infinite volume result.

This equation is now specialized to the $J = \frac{1}{2}$ case:

$$\begin{pmatrix} F_T^{(\frac{1}{2})}(y) \\ F_S^{(\frac{1}{2})}(y) \end{pmatrix} = \frac{4}{\pi}\int_0^\Lambda \mathrm{d}y\, y^2 \sum_j^{(G_1^+)} \left(\begin{pmatrix} -1 & 3 \\ 3 & -1 \end{pmatrix} Z_{-B_3}^{(0)}(p,y) + \begin{pmatrix} 1 & -1 \\ -1 & 1 \end{pmatrix} \frac{2H(\Lambda)}{\Lambda^2} \right)$$

$$\times \left[\delta_{j\frac{1}{2}} + \sum_{\substack{\vec{n}\in\mathbb{Z}^3 \\ \vec{n}\neq\vec{0}}} \sqrt{4\pi}\, i^{\ell(j)} j_{\ell(j)}(L|\vec{n}|y) \sum_{m=-\ell(j)}^{\ell(j)} (-1)^m \tilde{C}_{j,m+M} C_{\ell(j)m\frac{1}{2}M}^{j,m+M} Y_{\ell(j)m}(\hat{n}) \right]$$

$$\times \begin{pmatrix} d_T(y;-B_3)F_T^{(j)}(y) \\ d_S(y;-B_3)F_S^{(j)}(y) \end{pmatrix}. \tag{5.17}$$

The lowest partial wave that is mixed with $J = \frac{1}{2}$ is the $j = 7/2$ wave. Since the leading term in the expansion of the Bessel functions in Eq. (5.17) is $1/(L|\vec{n}|y)$, the contributions from higher partial waves are suppressed by at least a/L. They will be small for volumes not too small compared to the size of the bound state. Moreover, contributions from higher partial waves will be suppressed kinematically for shallow states with small binding momentum. This is ensured by the spherical harmonic in the second term of Eq. (5.17). Only for small lattices, i.e. when a/L is large, this behavior is counteracted by terms stemming from the spherical Bessel function $j_{\ell(j)}(L|\vec{n}|y)$ and higher partial waves may contribute significantly. Therefore, the contributions from higher partial waves are neglected for a first approach. This is encouraged by the results for the bosonic case that were presented in Chapter 4. In this case, calculations including one more partial wave yielded corrections on the percent level even for small volumes [KH10]. Thus, only two coupled integral equations remain to be solved.

The numerical methods needed to solve the coupled integral equations are described in Section 3.3. In addition, a coupled channel approach is used to solve both equations simultaneously. This approach has also been outlined in the description of the bosonic case, where it has been used to solve for two partial wave amplitudes simultaneously. In the three-nucleon case, however, the structure of the equations allows for the calculation of four matrix elements at once. Thus, the runtime is not increased in contrast to the s-wave onl bosonic case. The calculation of a single data point for the triton in finite volume takes about 8 to 10 hours. The results are presented in the following chapter.

Chapter 6

Results for three-nucleon bound states in finite volume

The framework described in the previous chapter has been used to calculate the finite volume energy of the triton. After presenting the results for the physical triton, the pion-mass dependence of the triton spectrum is studied. This is motivated by the possibility that QCD lies close to the critical trajectory for an infrared limit cycle in the 3-nucleon sector. In order to study this conjecture with the methods of Lattice QCD, finite volume effects have to be under control.

6.1   The triton in finite volume

In the following, the results for the energy of the triton for cubic volumes with various side lengths L are presented. In order to verify that the results are renormalized, two data sets have been produced. For one set, the cutoff was set to $\Lambda = 600$ MeV and the three-body coupling was chosen such that the triton binding energy, $B_3^\infty = 8.48182$ MeV, is reproduced in the infinite volume. For the other set, the cutoff was set such that there is no need for a three-body force to obtain the correct triton binding energy in the infinite volume. This is always possible due to the ultraviolet renormalization group limit cycle.

Fig. 6.1 shows the triton binding energy for finite cubic volumes with side lengths ranging from 17 fm down to 2 fm. As has been stated in Section 2.1, volumes of $2.5 - 4$ fm are typical for present day lattice calculations. The values from the two data sets are in good agreement, indicating that our results are indeed renormalized. For large volumes, the deviation of the triton energy from its infinite volume value is small. When going to volume side lengths smaller than about 10 fm, the energy of the state strongly decreases. At $L_{100\%} = 5.62$ fm, the shift is already 100%.

The dependence of the energy on L can be nicely fitted to a function of the form $E(L) = E(L = \infty) - b\frac{e^{-cL}}{L}$, thus corresponding to the volume dependence of a two-body bound state [BBPS04, Lee]. This exponential decay was also observed in Chiral Effective Theory calculations on the lattice [EKLM09]. As in the bosonic case, the dimensionless variable $r' = mE_3^\infty L_{100\%}^2$ is formed in order to investigate the aspect of universality. The resulting
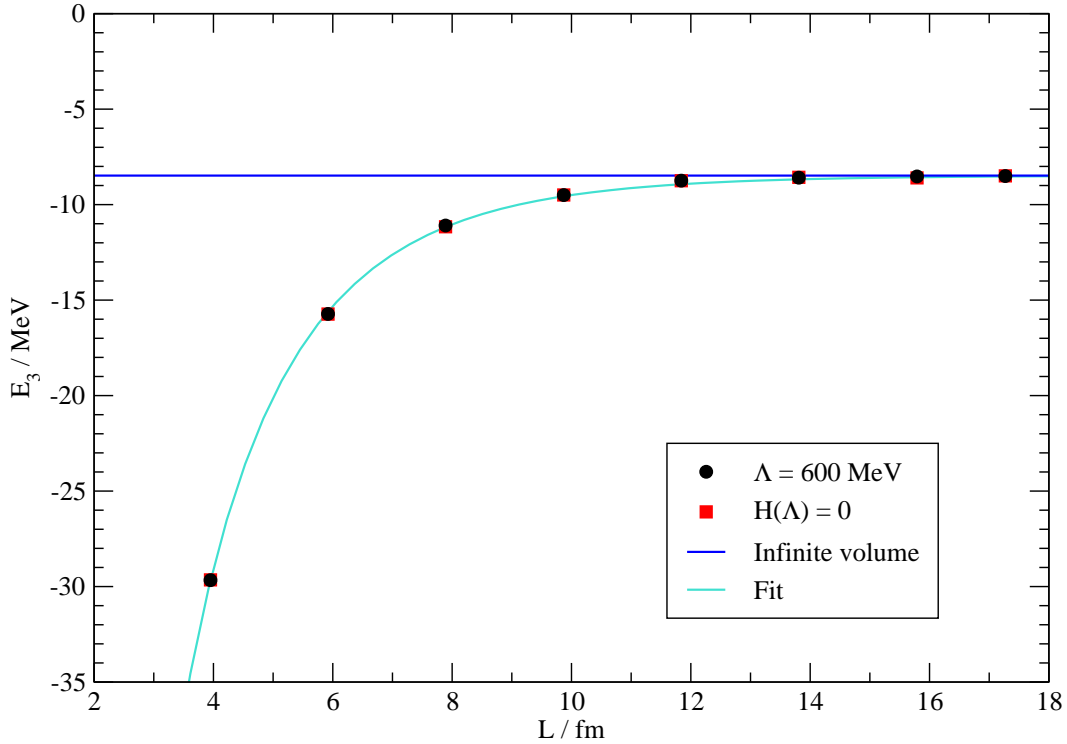
Figure 6.1: Triton energy for different side lengths of the finite cubic volume. Plotted are to data sets obtained with two different renormalization procedures. The horizontal line is the infinite volume triton binding energy.

number is $r' = 6.47$. This value is comparable to the value obtained in the bosonic case. More data points for this dimensionless combination are obtained from the ground state of the triton for varying pion mass, which will be investigated in the following section.

6.2   Pion-mass dependence of the triton spectrum

In 2004, Braaten and Hammer conjectured that QCD is close to the critical trajectory for an infrared renormalization group (RG) limit cycle [BH03]. The theory can be tuned on the critical trajectory by varying the light quark masses or, equivalently, the pion mass. The closeness to the critical trajectory explains the success of the leading order $\not\pi$EFT-calculations in the three-nucleon sector, which correspond to Efimov's program. This is because on the critical trajectory, the scattering lengths in boths channel diverge simultaneously. Such a behavior is indeed consistent with chiral extrapolations to pion masses larger than the physical one. The closeness to the critical trajectory of physical QCD explains the unnatural largeness of the scattering lengths which places the theory close to the unitary limit. Moreover, the ultraviolet RG limit cycle that appears in $\not\pi$EFT would be a signature of the infrared limit cycle of QCD. At the critical pion mass, nuclear physics would be exactly SU(4)-symmetric, and Wigner's approximate SU(4) symmetry can be seen as a remnant of this.

The two-nucleon scattering lengths $a_{s,t}$ can be extrapolated to unphysical pion masses using χEFT [BBSvK02, BS03, EMG03]. The results suggest that the two scattering lengths might
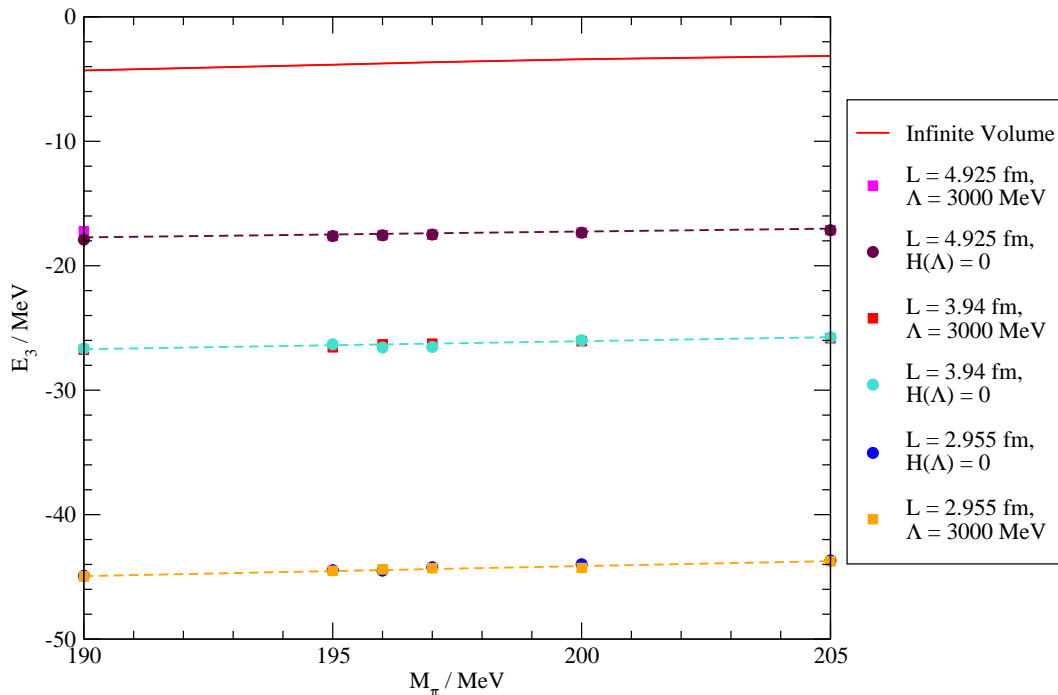
Figure 6.2: Pion-mass dependence of the triton energy. Plotted are the results for three different volumes and two different renormalization procedures alongside the infinite volume curve.

indeed diverge at pion masses not much larger than the physical pion mass. It should be noted, however, that these results come with large error bands due to two not well determined low-energy constants. The mass difference between up- and down-quark can be used in these calculations as an additional tuning parameter to render both scattering lengths infinite at the same critical pion mass m_π^{crit}.

If both scattering lengths diverge at the same pion mass, the Efimov effect occurs. There are two two-body bound states directly at threshold and a below a tower of geometrically spaced three-body bound states with an accumulation point at threshold. This means that the triton gets excited states for pion masses close to the critical one.

An earlier publication [HPP07] used a particular scenario of χEFT results where the singlet and triplet scattering length diverge simultaneously at a critical pion mass $m_\pi^{\mathrm{crit}} = 197.8577$ MeV. For this scenario, the input quantities for the low-energy EFT using only contact interactions where determined for various pion masses. The input quantities are two two-body scattering length or, if applicable, the pole position of the two-body bound state, and one three body datum, for example the triton ground state binding energy or the neutron-deuteron scattering length.

In the following, the study of [HPP07] is extended to finite volumes. As stated above, no additional input is needed to produce renormalized finite volume results. The pion mass dependence of the triton ground state is shown in Fig. 6.2 for volumes with side lengths of 3, 4 and 5 fm. Such sizes are typical in present day lattice calculations. Again, two data sets are plotted that were obtained using two different methods to fix the three-body coupling as described above. The most pronounced effect of the finite volume is a strong downward

	Slopes for data set	
L / fm	$H(\Lambda) = 0$	$\Lambda = 3000$ MeV
∞	0.0783	0.0783
4.925	0.0467	0.0467
3.94	0.0644	0.0639
2.955	0.0770	0.0838

Table 6.1: Slopes obtained by linear fits to the pion-mass dependence of the triton energy in finite and infinite volume near the critical pion mass as shown in Fig. 6.2.

m_π	E_3^∞ / MeV	E_3^∞/B_2	$L_{100\%}$ / fm	$E_3(L_{100\%})$ / MeV	r'
phys.	8.48	3.8	5.62	16.95	6.47
190	4.31	93	7.62	8.63	6.03
195	3.85	613	8.05	7.69	6.01
196	3.74	1,407	8.13	7.50	5.97
197	3.65	6,374	8.25	7.30	5.98
200	3.41	26,368	8.52	6.80	5.97
205	3.14	2,092	8.82	6.29	5.90

Table 6.2: Numerical evidence for universal scaling of the finite volume corrections. For different pion masses, the triton ground state energy in infinite volume, E_3^∞, is given in MeV and in units of the binding energy B_2 of the physical two-body bound state. Further given is the volume size $L_{100\%}$ yielding a shift of 100% with the corresponding energy $E_3(L_{100\%}$ in MeV. Finally, the dimensionless combination $r' = mE_3^\infty L_{100\%}^2$ is shown.

shift, as was expected from the results for the triton at the physical point. However, there is a more subtle effect which is a modification of the slope of the almost linear pion-mass dependence. This effect is summarized in Table 6.1.

The effect on the slopes is supposedly due to the vast difference of the triton ground state energies for different pion masses when expressed in the intrinsic energy scale of the system, namely the binding energy of the physical two-body bound state. The infinite volume energy of the triton for the six investigated pion masses in units of the physical two-body bound state is given in Table 6.2. The physical two-body bound state is the deuteron for $m_\pi < m_\pi^{\rm crit}$ and the spin-singlet dibaryon for $m_\pi > m_\pi^{\rm crit}$. The different binding energies, however, are spread over more than three orders of magnitude in terms of the intrinsic energy scale of the system.

This vast difference offers the possibility to study the presence of universal scaling for the triton ground state. For the various investigated pion masses, the box sizes $L_{100\%}$ yielding an energy shift of 100% compared to the infinite volume value E_3^∞ are given in Table 6.2. The values of $r' = mE_3^\infty L_{100\%}^2$ obtained for the six different unphysical pion masses differ by about 1% from the central value 5.98. The very good agreement between the different values of r' strongly suggests that the finite volume corrections are subject to universal scaling. The central value found for the six ground states differs from the value found for the physical triton, $r' = 6.47$, by 8%. This can be explained by comparing to the bosonic case. Here, the universal behavior has been found to be obscured for states close to the threshold. As can be seen from Table 6.2, all the ground states near the critical pion mass are rather deeply bound states. The physical triton has an infinite volume binding energy of $E_3^\infty(m_\pi^{\rm phys}) \approx 4B_2$

L/fm	$B_3^{(1)}/\mathrm{MeV}$	B_2/MeV
∞	0.052	0.047
19.7	0.742	0.486
14.8	0.890	0.823
14.4	0.884	0.865
14.2	N/A	0.888

L/fm	$B_3^{(1)}/\mathrm{MeV}$	B_2/MeV
∞	0.016	0.006
29.6	0.383	0.198
19.7	0.686	0.431
14.8	0.761	0.753
14.4	N/A	0.794

L/fm	$B_3^{(1)}/\mathrm{MeV}$	B_2/MeV
∞	0.009	5.7×10^{-4}
39.5	0.184	0.105
27.6	0.240	0.211
26.4	0.233	0.231
26.2	N/A	0.234

L/fm	$B_3^{(1)}/\mathrm{MeV}$	B_2/MeV
∞	0.038	1.3×10^{-4}
29.6	0.355	0.182
19.7	0.625	0.407
15.6	0.662	0.651
15.4	N/A	0.668

Table 6.3: Volume dependence of the first excited state of the triton for pion masses of $m_\pi = 190$ MeV (upper left), 195 MeV (upper right), 197 MeV (lower left) and 200 MeV (lower right). The two-body energy has been obtained by the method described in [BBPS04].

in units of the deuteron binding energy B_2. This renders the physical triton a rather shallow trimer for which the universal scaling is obscured.

The behavior of the first excited state when put inside a finite volume differs from the behavior of the ground state. For large volumes, the state remains again unaffected at first. When going to smaller volumes, the energy starts to strongly decrease. But eventually the "breakup threshold", i.e. the energy of the two-body bound state in finite volume, becomes equal to the three-body energy. For pion masses smaller than m_π^{crit}, the two-body bound state corresponds to the deuteron, while for $m_\pi > m_\pi^{\mathrm{crit}}$, there is a bound state in the $^1S_0$-channel and the deuteron has become a virtual state. For even smaller volumes, the excited three-body bound state has disappeared. This is shown in Fig. 6.3, in which the energies of the two-body bound states in finite volume are calculated according to [BBPS04]. Supposedly, the state has crossed into the scattering regime where it would be driven away from threshold. We previously observed such a behavior in our investigation of three-boson bound states inside finite volumes [KH10]. The volume dependence for the investigated pion masses is summarized in Table 6.3. Whether there is a universal relation between the binding energy in infinite volume and the volume size, at which the state disappears, is an interesting question that will be investigated in the future.

The very weakly bound second excited state, that appears in the infinite volume for pion masses very close to the critical one, could not be observed for the volumes with side lengths of several fm that were investigated and has by the above reasoning crossed the threshold already at some much larger volume.

In this chapter, the physical triton was investigated as well as the triton spectrum for unphysical pion masses close to the critical pion mass. The renormalization of the finite volume results was explicitly verified. All states experience a downward shift when decreasing the volume size. For the ground states, the slope of the pion-mass dependence is slightly modified by the finite volume. A possible explanation for this is that, when varying the pion mass, the binding energy of the ground states varies over several orders of magnitude when expressed in terms of the intrinsic energy scale of the system. Strong numerical evidence for
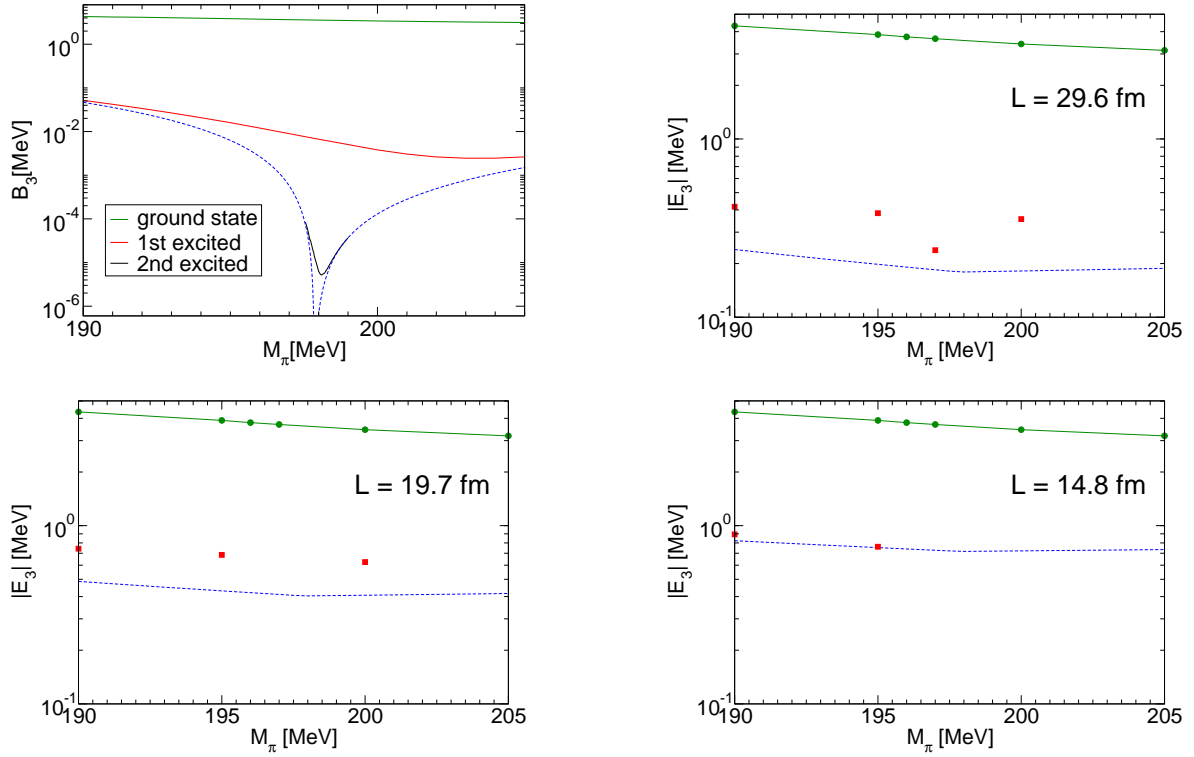
Figure 6.3: Pion-mass dependence of the triton spectrum for the infinite volume (upper left) and finite volumes with side lengths of $L = 29.6, 19.7, 14.8$ fm (upper right, lower left, lower right, respectively). The blue dashed lines are the energies of the physical di-nucleon state. The infinite volume plot is taken from [HPP07].

a universal scaling of the finite volume corrections has been provided. In particular, given an infinite volume binding energy, the volume corresponding to a 100% shift in the energy can be inferred with high accuracy. The excited states of the triton showed the threshold crossing behavior that was already observed for shallow three-boson bound states and will be further investigated. The next step is the inclusion of higher partial waves, which is straightforward but numerically tedious. The knowledge of the volume dependence of the triton binding energy is crucial to the understanding of lattice simulations in this channel. Since, in contrast to the two-body sector, the three-body amplitude can only be determined numerically, the generalization of Lüscher's formula (2.7) to three-body systems cannot be written down in closed form. Nonetheless, the infinite volume scattering properties are implicitly encoded in the volume dependence of the finite volume states.

Chapter 7

Summary and Outlook

In this work, bound-states of resonantly interacting three-body systems were investigated inside a finite cubic volume with periodic boundary conditions. Since the s-wave scattering length is large compared to the natural length scale of the interaction, such systems are well suited for an description within an Effective Field Theory. This approach also allowed for the study of universal behavior of the finite volume corrections. Universality in this context means independence of the details of the underlying interaction.

At first, systems of three identical bosons were studied in order to gain an initial understanding of Efimov physics in finite volumes. To this end, an infinite set of coupled integral equations for the partial waves of the bound state amplitude was derived from the leading order Lagrangian of the EFT. The coupling of the different partial waves is a consequence of the breakdown of rotational symmetry inside the finite cubic volume. The numerical methods needed to determine binding energies from these equations were discussed in detail.

Specializing to the $\ell = 0$ case, the spectrum has been calculated for both positive and negative scattering lengths. It was explicitly demonstrated that the finite volume results are correctly renormalized. For small shifts of up to 15%, an expansion can be used to reduce the numerical effort. Typically, the binding of all three-body states increases as the box size is reduced.

The spectrum for positive and negative scattering length was studied in detail and numerical evidence for a universal scaling of the finite volume effects has been provided. The scaling properties can be quantified by the dimensionless product r (r') of the three-body binding energy in the infinite volume limit and the square of the box side length corresponding to a finite volume shift of 10% (100%) of the infinite volume energy. For states sufficiently far away from the threshold, numerical evidence was obtained that the values of r and $'$ approach universal numbers for both signs of the scattering length. These findings suggest that the finite volume properties of deeper states can be obtained by a simple rescaling and do not require explicit calculations. A more detailed analysis of this issue along the lines of [BHK03] is a future project.

For positive scattering lengths, a system with a spectrum containing three states was investigated. The state closest to the dimer energy, which constitutes the break-up threshold for three-body bound states, drastically changes its behavior as soon as its energy becomes equal to the dimer energy in finite volume. At this point, the energy of the shallowest three-body

state starts to grow and eventually becomes positive. The observed behavior is consistent with exponential suppression of the finite volume corrections below the dimer energy and power law suppression above.

The effect of the admixture of the $\ell = 4$ partial wave has been investigated for two different three-body states for box sizes of the order of the state's size. For a generic state well seperated from the threshold, corrections of the order of a few percent were found for volumes about three times as large as the state itself. For the state closest to threshold, the effect of this admixture turned out to be surprisingly small. For volumes about as large as the state itself, the shift was found to be less than 1%. As the finite cutoff corrections for this state are about the same size, a more quantitative study requires an improved treatment of these corrections. The small effect of higher partial waves might be associated with the closeness of the state to the threshold.

Subsequently, the formalism was extended to systems of three nucleons inside a finite cubic volume. Due to the additional degrees of spin and isospin, there are now two independent two-body scattering channels. Each channel is characterized by a scattering length, both of which happen to be unnaturally large. There are two bound state amplitudes with the quantum numbers of the triton. The equations governing these amplitudes are coupled. The decomposition into partial waves is more involved due to the coupling of spin and angular momentum. After overcoming these additional complications, an infinite set of coupled equations for the partial waves of the bound state amplitude were derived analoguously to the bosonic case.

Neglecting higher partial waves as in the case of three bosons, the triton energy was calculated for several finite volumes in the order of magnitude typical for present Lattice QCD calculations. The results were explicitly verified to be renormalized. The overall behavior of the triton state was found to be similar to that in the bosonic case. That is, decreasing the box size leads to an increased binding.

Additionally, the triton spectrum was investigated near the critical pion mass where both scattering lengths might diverge simultaneously. For the ground states, strong numerical evidence for a universal scaling of the finite volume effects was provided. The dimensionless combination r' seems to be a universal number. For states with binding energies ranging over more than three orders of magnitude when expressed in terms of the intrinsic energy scale of the system, the values that have been found for r' agree within about 1%. For every excited state, there is a volume size for which the state crosses the threshold. This means that its energy becomes equal to the energy of the bound two-nucleon state in this specific volume, and the state can not be found below the two-body energy when further decreasing the volume size. For the first excited state, this has been studied quantitatively. The second excited state always has already crossed the threshold when reaching volumes even a magnitude larger than those which are used in present day lattice calculations.

The next step is the inclusion of higher partial waves in the nucleonic case, which is straightforward but numerically tedious. Also, since range corrections are sizable in the NN-interaction, higher orders of the EFT should be included in the framework. Finite temperature effects should also be taken into account, as lattice calculations are always performed at small, non-zero temperatures.

The framework should be extended in order to describe scattering states. Since, in this case, the analytic structure of the infinite and finite volume amplitude is different, it is not sensible

to use Poisson's equation. With such a framework, it would be possible to investigate, for example, nucleon-deuteron scattering in finite volumes. The results could subsequently be compared to the two-body Lüscher formula in order to look for effects from the three-body force.

With high statistics lattice QCD simulations of three-baryon systems within reach [B$^+$09], the calculation of the structure and reactions of light nuclei appears now feasible within the intermediate future [BDOS10]. The results of this work demonstrate that the finite volume corrections for such simulations are calculable and under control. It was shown that this is also the case if the conjecture of an infrared renormalization group limit cycle in QCD for quark masses slightly larger than the physical values [BH03] is tested.

Appendix A

Representations of the Cubic group

This appendix gives an overview on the cubic group O, its double cover ^2O and the theory of their representations. The informations given here are an important ingredient in the formalism laid out in this work, as they serve to disentangle the contributions from different partial waves. The discussion given here relies on [Joh82] and [BLMR08].

A.1 The Cubic Group and its double cover

The cubic group O is the point group of rotational symmetries of a cube. The group has 24 elements falling in five conjugacy classes. These are, in the notation nC_m, where n is the number of elements in this class and m the order of each element:

- I: identity

- $3C_2$: rotations by π about three coordinate axes

- $6C_4$: rotations by $\pm\frac{\pi}{2}$ about three coordinate axes

- $8C_3$: rotations by $\pm\frac{2\pi}{3}$ about four body diagonals

- $6C_2'$: rotations by π about diagonals connecting centers of opposing edges

Since O is a finite group, the number of its conjugacy classes equals the number of its irreducible representations (irreps). These are the trivial representation A_1, the alternating representation A_2, E, the fundamental representation T_1 and T_2, which is connected to T_1 in the same way as A_2 is connected to A_1. The characters of these irreps are summarized in Table A.1. The dimension of the irrep can be read off from the character of the identity.

The double cover of the cubic group is constructed by adding a negative identity J for 2π rotations. This is analoguous to the construction of the spin group SU(2) from the rotational group SO(3). Of course, this comes as no surprise. Since the cubic group is a subgroup of the continuous rotational group SO(3), the double cover of O has to be a subgroup of the double cover of SO(3). The double cover ^2O contains 48 elements. The extension by a negative

	I	$3C_2$	$6C_4$	$8C_3$	$6C_2'$
A_1	1	1	1	1	1
A_2	1	1	-1	1	-1
E	2	2	0	-1	0
T_1	3	-1	1	0	-1
T_1	3	-1	-1	0	1

Table A.1: Characters of the irreducible representations of O. The character of the identity gives the dimension of the representation.

	I	J	$6C_4$	$8C_3$	$8C_6$	$6C_8$	$6C_8'$	$12C_4'$
G_1	2	-2	0	-1	1	$-\sqrt{2}$	$\sqrt{2}$	0
G_2	2	-2	0	-1	1	$\sqrt{2}$	$-\sqrt{2}$	0
H	4	-4	0	1	-1	0	0	0

Table A.2: Characters of the irreducible representations of ^2O. The character of the identity gives the dimension of the representation.

identity J, which corresponds to a rotation about 2π, yields two new conjugacy classes plus the negative identity itself. Thus, the double cover has eight irreps, namely the five of the cubic group and three more. These are labelled G_1, G_2 and H. The irreps G_1 and G_2 are again related as are A_1 and A_2. The conjugacy classes of ^2O and their characters for the three additional irreps are given in Table A.2.

The rotational group SO(3) has infinitely many irreps, labeled by non-negative integers $\ell = 0, 1, 2, \ldots$, with dimension $2\ell + 1$. These representations become (in general) reducible under the action of the cubic group and can be decomposed in terms of the five irreps of O. This decomposition is the subject of the next section.

The double cover of the rotational group, namely SU(2), has the same irreps as SO(3) and infinitely many additional irreps labeled by half-integer values $j = \frac{1}{2}, 3/2, 5/2, \ldots$, with dimension $2j + 1$. Accordingly, these representations can also be decomposed in terms of irreps of ^2O. But, in order to preserve the completeness relations of O, the additional reducible representations can only contain the three additional irreps of the double cover of the cubic group.

A.2   Decomposition of reducible representations

A given representation of SO(3), labeled by ℓ, acts on a $2\ell + 1$-dimensional vector space. A basis of this vector space is given by $|\ell m\rangle$, where m runs from $-\ell$ to ℓ. The reducibility of the representation means that there are subspaces which are invariant under irreps of O. In the following will be shown how to construct bases for these subspaces.

In order to perform the decomposition of the representation ℓ of SO(3), the projection operator

$$(P_{\alpha\beta}^{\Gamma,\ell})_{mm'} = \sum_{R \in O} (R^{(\Gamma)})_{\alpha\beta} D_{mm'}^{\ell}(R), \tag{A.1}$$

is defined, where the sum runs over all group elements R. The $R^{(\Gamma)}$ is the matrix that respresents R in the irrep Γ and the $D^{\ell}_{mm'}(R)$ are Wigner's D-function associated with R when it is considered as a rotation. The indices α, β run over the dimensionality of the irrep Γ, while m and m' run, as usual, from $-\ell$ to ℓ. The matrix form of the irreps is as follows:

- $\underline{A_1}$: $R^{(A_1)} = 1$ for all $R \in O$

- $\underline{A_2}$: $R^{(A_2)} = -1$ if R is in the conjugacy class $6C_4$ or $6C_2'$, $R^{(A_2)} = 1$ otherwise

- $\underline{E}$: There are six different matrices in this representation. Each matrix is real and represents four elements of O:

  - $R^{(E)} = \mathbf{1}$ for the identity and the matrices in $3C_2$
  - $R^{(E)} = \sigma_3$ for the two rotations in $6C_4$ about the z-axis and the two rotations in $6C_2'$ about axes orthogonal to the z-axis
  - $R^{(E)} = -\cos(\pi/3)\mathbf{1} - \sin(\pi/3)\sigma_1$ for rotations as above, with the z-axis replaced by the x-axis
  - $R^{(E)} = -\cos(\pi/3)\mathbf{1} + \sin(\pi/3)\sigma_1$ for rotations as above, with the z-axis replaced by the y-axis
  - $R^{(E)} = -\cos(\pi/3)\mathbf{1} + i\sin(\pi/3)\sigma_2$ for the four rotations in $8C_3$ with angle $\frac{2\pi}{3}$ $(-\frac{2\pi}{3})$ if the axis vector has an odd (even) number of minus signs.
  - $R^{(E)} = -\cos(\pi/3)\mathbf{1} - i\sin(\pi/3)\sigma_2$ for the remaining four rotations in $8C_3$, corresponding to switching the sign of the rotation angles in the description above.

- $\underline{T_1}$: For each group element, the representation is given by the corresponding rotation matrix in SO(3).

- $\underline{T_2}$: Like T_1, with an additional minus sign for the elements from the conjugacy classes $6C_4$ and $6C_2'$.

The basis vectors spanning the invariant subspaces are then obtained by acting with the linear operator (A.1) on an arbitrary linear combination ψ of the $|\ell m\rangle$

$$(e^{\Gamma,\ell,\beta}_{\alpha})_m = \mathcal{N} \sum_{m'} (P^{\Gamma,\ell}_{\alpha\beta})_{mm'} \psi_{m'}. \tag{A.2}$$

Different bases are mapped out by fixing different values of β and letting α run from 1 to the dimension of Γ. The normalization constant $\mathcal{N}$ is fixed such that the basis is orthonormal

$$\sum_m (e^{\Gamma',\ell,\beta}_{\alpha'})^*_m (e^{\Gamma,\ell,\beta}_{\alpha})_m = \delta_{\Gamma'\Gamma}\delta_{\alpha'\alpha}. \tag{A.3}$$

If Γ is not part of ℓ, then the application of the projector on any ψ yields 0. If the representation Γ enters multiple times in ℓ, an additional orthogonalization of the generated basis vectors is necessary. The eigenvectors needed in this work are, in the notation from above, $e^{A_1,0}$ and $e^{A_1,4}$. Both are given as linear combinations of the $|\ell m\rangle$ in Table A.3.

The extension to the decomposition of representations j of the double cover of SO(3), namely SU(2), is then straightforward. For integer values of j, the decomposition yields identical

Γ	j	α	$e_\alpha^{\Gamma,j}$
A_1	0	1	$\lvert 0,0\rangle$
A_1	4	1	$\frac{\sqrt{30}}{12}(\lvert 4,-4\rangle + \lvert 4,4\rangle) + \frac{\sqrt{21}}{6}\lvert 4,0\rangle$
G_1	$\frac{1}{2}$	1	$\lvert \frac{1}{2},\frac{1}{2}\rangle$
		2	$\lvert \frac{1}{2},-\frac{1}{2}\rangle$
G_1	$\frac{7}{2}$	1	$\frac{\sqrt{15}}{6}\lvert \frac{7}{2},-\frac{7}{2}\rangle + \frac{\sqrt{21}}{6}\lvert \frac{7}{2},\frac{1}{2}\rangle$
		2	$-\frac{\sqrt{15}}{6}\lvert \frac{7}{2},\frac{7}{2}\rangle - \frac{\sqrt{21}}{6}\lvert \frac{7}{2},-\frac{1}{2}\rangle$

Table A.3: Basis functions of A_1 (G_1) for the two lowest partial waves in terms of $\lvert jm_j\rangle$.

results as in the case above. Only the additional representations of the double cover, corresponding to half-integer values, have to be considered. These can in turn only be reducible in terms of the irreps of ^2O that are not contained in O, namely G_1, G_2 and H.

Eq. (A.1) is generalized for the double cover to

$$(P_{\alpha\beta}^{\Gamma,j})_{mm'} = \sum_{R\in{}^2O} (R^{(\Gamma)})_{\alpha\beta} D_{mm'}^j(R). \tag{A.4}$$

The matrices of the three additional irreps is given in the following.

- $\underline{G_1}$: For each group element, the matrix is given by the corresponding SU(2) matrix.

- $\underline{G_2}$: As in G_1, with sign changes for the conjugacy classes $6C_8$, $6C_8'$ and $12C_4'$.

- $\underline{H}$: For each group element, the matrix is given by the corresponding matrix in the $j = \frac{3}{2}$ representation of SU(2).

As in the SO(3) case, the basis is produced by acting with the projector (A.4) on a linear combination of the basis vectors $\lvert jm_j\rangle$ as defined in Eq. (5.14). In Table A.3, the basis vectors $e_\alpha^{G_1,\frac{1}{2}}$, $\alpha = 1,2$, and, for convenience, the basis vectors of the next higher partial wave, $e_\alpha^{G_1,\frac{7}{2}}$, $\alpha = 1,2$ are given as linear combinations of the spinors $\lvert jm_j\rangle$. The table for all irreps of ^2O for partial waves up to $j = 4$ can be found in [BLMR08]

Appendix B

Numerical Evaluation of Fourier Integrals

The formalism laid out in this work requires the computation of integrals with a rapidly oscillating kernel. This problem can be solved with high numerical efficiency by applying a method based on the use of Fast Fourier Transform (FFT). This technique is described in Section B.1. Its application to the evaluation of Fourier integrals is depicted in Section B.2. The presentation given here follows [PTVF07], wherein many more details on the method and additional references can be found.

B.1 Fast Fourier Transform (FFT)

For a discrete sample of data, f_n, with $n = 0, \ldots, N - 1$, the discrete Fourier Transform (DFT) is defined as

$$h_k = \sum_{n=0}^{N-1} f_n e^{i2\pi kn/N}, \quad k = 0, \ldots, N - 1. \tag{B.1}$$

When implemented naively, this is a rather expensive process of the order $O(n^2)$. In 1965, however, an algorithm put forward by Cooley und Tukey became widely known under the name of Fast Fourier Transform (FFT) [CT65]. This algorithm allowed the computation of a DFT in $O(N \log_2 N)$. Since then, many different algorithms have been found with the same complexity. The method of Cooley and Tukey has been previously discovered and forgotten, the first time by Gauß in 1805 [Gau66]. The FFT algorithm relies on a divide-and-conquer strategy. The algorithm described in the following is the original Cooley-Tukey version.

Assuming N is even, consider splitting the sum into sums over odd and even indices

$$
\begin{aligned}
h_k &= \sum_{m=0}^{N/2-1} f_{2m} e^{i2\pi k\, 2m/N} + \sum_{m=0}^{N/2-1} f_{2m+1} e^{i2\pi k\,(2m+1)/N} \\
&= \sum_{m=0}^{N/2-1} f_{2m} e^{i2\pi km/(N/2)} + e^{i2\pi k/N} \sum_{m=0}^{N/2-1} f_{2m+1} e^{i2\pi km/(N/2)}.
\end{aligned}
\tag{B.2}
$$
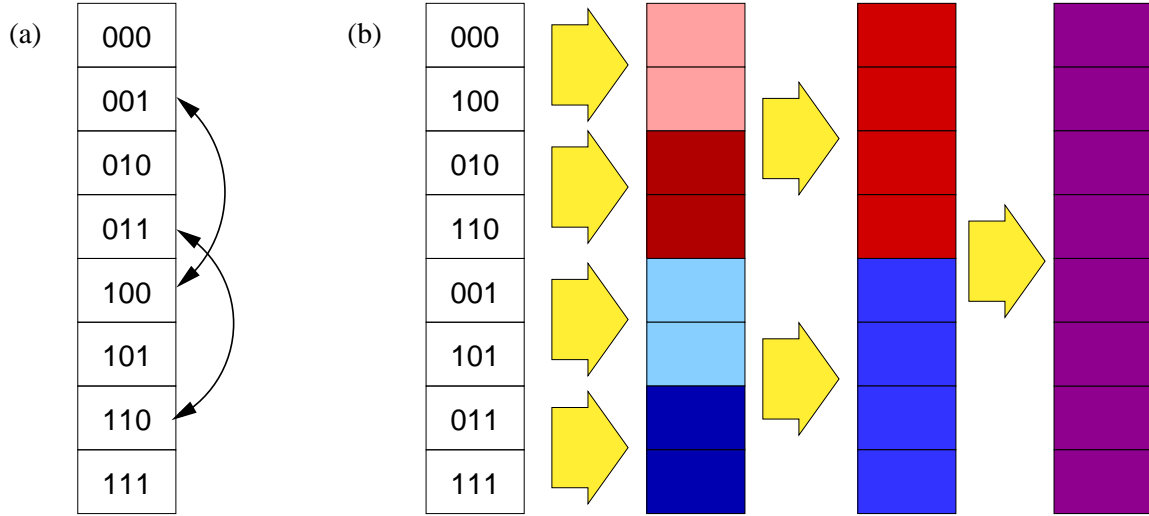
Figure B.1: Illustration of the Cooley-Tukey FFT algorithm for a sample of size $N = 8$. (a) The bit reversal. (b) Subsequent combination of adjacent blocks into four DFTs of length 2, two DFTs of length 4 and the final DFT of the complete sample.

Clearly, the sums in the last line are just the DFTs of the data with even and odd index, respectively. By this means, the values h_k are obtained for $k = 0, \ldots, (N/2) - 1$. The remaining $N/2$ values are obtained by noting that for $k \geq N/2$

$$e^{i2\pi(k+N/2)/N} = -e^{i2\pi k/N},$$

while the sums remain unchanged due to the periodicity of the DFT. Therefore, flipping the sign in front of the second sum yields the missing values.

By setting N to a power of 2, this procedure can be carried out recursively down to a DFT of size 1, which is just the identity operation. The sample can always be increased to a size which is a power of 2 by padding the array with zeros.

From an algorithmic point of view, it is convenient to rearrange the sample such that there is one block containing the originally even indices and another one collecting the odd indices. This should be done in such a manner that it holds in every level of the recursion. The way to achieve this is surprisingly simple. When writing an index in binary notation, the last bit characterizes whether the index is odd (the last bit is 1) or even (the last bit is 0) in the upmost level of the recursion. For the next level, this is determined by the penultimate bit, and so forth. Therefore, by inverting the order of the bits and rearranging the data points accordingly, the blocks of even-indexed and odd-indexed data that are to be merged at a certain step in the algorithm are always adjacent. This makes it easy to implement the algorithm iteratively instead of recursively. In addition, it allows to perform the algorithm in-place, i.e. using the input array as output array, lowering the memory cost by a factor 2. The rearrangement procedure is called bit-reversal. The strategy of Cooley-Tukey algorithm is illustrated in Figure B.1. There are $\log_2 N$ stages where odd- and even-indexed blocks are combined into a single DFT. At each merging stage, there $O(N)$ operations are necessary. This renders the total algorithm to be of order $O(N \log_2 N)$.

B.2   Computing Fourier Integrals

As has been stated above, the FFT is a powerful device to perform a DFT. In the framework presented in this work, it is necessary to compute integrals of the form

$$I_s = \int_0^\Lambda h(y) \sin(\omega y) \mathrm{d}y, \qquad I_c = \int_0^\Lambda h(y) \cos(\omega y) \mathrm{d}y, \tag{B.3}$$

where h is a smooth real function. Such integrals arise from the Bessel functions in Eq. (3.19). The integrals I_s and I_c can be seen as the imaginary and real part, respectively, of

$$I_s = \int_0^\Lambda h(y) \mathrm{e}^{i\omega y} \mathrm{d}y. \tag{B.4}$$

It is desirable to apply the FFT method in order to evaluate this integral.

The intuitive approach is to replace the integral by a sum like

$$I \approx \Delta \sum_{j=0}^{M-1} h_j \mathrm{e}^{i\omega y_j}, \tag{B.5}$$

where $\Delta = \frac{\Lambda}{M}$, $y_j = j\Delta$ and $h_j = h(y_j)$. For the special values of ω

$$\omega_m \Delta = \frac{2\pi m}{M}, \quad m = 0, 1, \dots, (M/2) - 1, \tag{B.6}$$

the sum can then be evaluated using the FFT method via

$$I(\omega_m) \approx \Delta \sum_{j=0}^{M-1} h_j \mathrm{e}^{i2\pi mj/M} = \Delta \left[\mathrm{DFT}(h_0, \dots, h_{M-1}) \right]_m. \tag{B.7}$$

This procedure is surprisingly inaccurate. The reason for this is the oscillatory nature of the integrand. If ω is large enough to yield several cycles inside the integration range, I typically becomes very small. In this case, it is easily dominated by the truncation error introduced by the approximation with a sum. This truncation error is moreover dominated by the combination $\omega \Delta$, which can be as large as π, as can be seen from Eq. (B.6).

It is therefore necessary to significantly reduce the truncation error. To do so, approximate the function $h(y)$ for a given y by an interpolation on the h_j. This may be in written down as

$$h(y) \approx \sum_{j=0}^{M} h_j \psi \left(\frac{y - y_j}{\Delta} \right) + \sum_{j \in \{\text{endpoints}\}} h_j \phi_j \left(\frac{y - y_j}{\Delta} \right). \tag{B.8}$$

The function $\psi(s)$ can be seen as a kernel function of the interpolation. It is characteristic for the employed interpolation scheme. For all schemes holds $\psi(0) = 1$ and $\psi(\pm m) = 0$ for $m = 1, 2, \dots$, in order to reproduce the sampling points exactly. For a linear interpolation, for example, $\psi(s)$ is just piecewise linear, rising from 0 to 1 for s between -1 and 0, and falling from 1 to 0 for s between 0 and 1. For higher order interpolation schemes, $\psi(s)$ is given by piecewise polynomials, joined at integer values of s where the set of points used for the interpolation changes discretely.

Near the endpoints of the integration interval $[0, \Lambda]$, the interpolation scheme has to be non-centered in order to achieve the same accuracy. This is taken into account by the second sum with the kernels $\phi_j(s)$. The number of endpoints included in this second sum is determined by the interpolation scheme, and the index j reflects the dependence on the distance from the edge of the integration interval. The endpoint kernels ϕ_j are actually the differences between the true endpoint kernels and $\psi(s)$ such that the first sum runs over all points, which will prove to be convenient.

The integral operator $\int_0^\Lambda \mathrm{d}y \exp(i\omega y)$ is now applied to Eq. (B.8). After interchanging summation and integration and changing variables to $s = (y - y_j)/\Delta$ in the first sum and $s = y/\Delta$ in the second sum, the relation

$$I \approx \Delta \left[W(\theta) \sum_{j=0}^{M} h_j \mathrm{e}^{ij\theta} + \sum_{j \in \{\mathrm{endpoints}\}} h_j \alpha_j(\theta) \right] \tag{B.9}$$

is obtained. Here, $\theta = \omega \Delta$ and

$$W(\theta) = \int_{-\infty}^{\infty} \mathrm{d}s \, \mathrm{e}^{i\theta s} \psi(s) \tag{B.10}$$

$$\alpha_j(\theta) = \int_{-\infty}^{\infty} \mathrm{d}s \, \mathrm{e}^{i\theta s} \phi_j(s - j). \tag{B.11}$$

The integrals can be extended to infinite range since the interpolation kernels vanish far away from $s = 0$. Eqs. (B.10) and (B.11) can be worked out once for any given interpolation scheme. In this work, cubic interpolation was used. As this is a symmetric scheme, it follows that $\psi(s) = \psi(-s)$, which renders $W(\theta)$ real. The α_j at the right end of the interval are related to those on the left, also by symmetry, since $\alpha_{M-j}(\theta) = \exp(iM\theta)\alpha_j^*(\theta) = \exp(i\omega\Lambda)\alpha_j^*(\theta)$. The results for cubic order are given by [PTVF07]

$$W(\theta) = \left(\frac{6 + \theta^2}{3\theta^4} \right) (3 - 4\cos\theta + \cos 2\theta),$$

$$\alpha_0(\theta) = \frac{(-42 + 5\theta^2) + (6 + \theta^2)(8\cos\theta - \cos 2\theta)}{6\theta^4} + i\frac{(-12\theta + 6\theta^3) + (6 + \theta^2)\sin 2\theta}{6\theta^4},$$

$$\alpha_1(\theta) = \frac{14(3 - \theta^2) - 7(6 + \theta^2)\cos\theta}{6\theta^4} + i\frac{30\theta - 5(6 + \theta^2)\sin\theta}{6\theta^4},$$

$$\alpha_2(\theta) = \frac{-4(3 - \theta^2) + 2(6 + \theta^2)\cos\theta}{6\theta^4} + i\frac{-12\theta + 2(6 + \theta^2)\sin\theta}{6\theta^4},$$

$$\alpha_3(\theta) = \frac{2(3 - \theta^2) - (6 + \theta^2)\cos\theta}{6\theta^4} + i\frac{6\theta - (6 + \theta^2)\sin\theta}{6\theta^4}.$$

The first sum in Eq. (B.9) is evaluated with FFT. To this end, an $N > M$ is chosen which is a power of 2. The sample is filled up with zeros for $M + 1 < j \le N$. Then, the sum can be done for the special frequencies $\theta_n = \Delta \frac{2\pi n}{N}$, $n = 0, 1, \ldots, (N/2) - 1$. Eq. (B.9) is a prescription how to apply endpoint corrections to the sum that is done via FFT. The result for general ω is then obtained by interpolation. In general, an oversampling by a factor of 4, i.e. $N > 4M$, is advantageous such that the sampling in frequency space is fine enough to allow for an accurate interpolation. The value of M determines the highest possible frequency, as the largest possible value of $\omega\Delta$ is just below π, and therefore

$$\omega_{\mathrm{max}} \lesssim \frac{\pi M}{\Lambda} \quad \Rightarrow \quad M > \frac{\omega_{\mathrm{max}}\Lambda}{\pi}. \tag{B.12}$$

The algorithm laid out in this section is a central mechanism in obtaining the numerical results presented in this work.

Bibliography

[AC65]   S. L. Altmann and A. P. Cracknell. *Lattice Harmonics 1. Cubic Groups.* Rev. Mod. Phys. **37** 19–32 (1965).

[B⁺64]   V. E. Barnes et al. *Confirmation of the existence of the Ω^- hyperon.* Phys. Lett. **12** 134–136 (1964).

[B⁺69a]   Elliott D. Bloom et al. *High-Energy Inelastic ep Scattering at 6 degrees and 10 degrees.* Phys. Rev. Lett. **23** 930–934 (1969).

[B⁺69b]   Martin Breidenbach et al. *Observed Behavior of Highly Inelastic electron-Proton Scattering.* Phys. Rev. Lett. **23** 935–939 (1969).

[B⁺08]   Silas R. Beane et al. *Precise Determination of the I=2 $\pi\pi$ Scattering Length from Mixed-Action Lattice QCD.* Phys. Rev. **D77** 014505 (2008). [arXiv:0706.3026].

[B⁺09]   Silas R. Beane et al. *High Statistics Analysis using Anisotropic Clover Lattices: (II) Three-Baryon Systems.* Phys. Rev. **D80** 074501 (2009). [arXiv:0905.0466].

[BBOS06]   S. R. Beane, P. F. Bedaque, K. Orginos, and M. J. Savage. *Nucleon-nucleon scattering from fully-dynamical lattice QCD.* Phys. Rev. Lett. **97** 012001 (2006). [arXiv:hep-lat/0602010].

[BBPS04]   S. R. Beane, P. F. Bedaque, A. Parreno, and M. J. Savage. *Two Nucleons on a Lattice.* Phys. Lett. **B585** 106–114 (2004). [arXiv:hep-lat/0312004].

[BBSvK02]   S. R. Beane, Paulo F. Bedaque, M. J. Savage, and U. van Kolck. *Towards a perturbative theory of nuclear forces.* Nucl. Phys. **A700** 377–402 (2002). [arXiv:nucl-th/0104030].

[BDOS10]   S. R. Beane, W. Detmold, K. Orginos, and M. J. Savage. *Nuclear Physics from Lattice QCD.* 2010. [arXiv:1004.2935].

[BDS07]   Silas R. Beane, William Detmold, and Martin J. Savage. *n-Boson Energies at Finite Volume and Three-Boson Interactions.* Phys. Rev. **D76** 074507 (2007). [arXiv:0707.1670].

[BH03]   Eric Braaten and H. W. Hammer. *An infrared renormalization group limit cycle in QCD.* Phys. Rev. Lett. **91** 102002 (2003). [arXiv:nucl-th/0303038].

[BH06]   Eric Braaten and H.-W. Hammer. *Universality in few-body systems with large scattering length.* Physics Reports **428** 259–390 (2006).

[BHK03]   Eric Braaten, H. W. Hammer, and M. Kusunoki. *Universal Equation for Efimov States.* Phys. Rev. **A67** 022505 (2003). [arXiv:cond-mat/0201281].

[BHvK98]   Paulo F. Bedaque, H. W. Hammer, and U. van Kolck. *Effective Theory for Neutron-Deuteron Scattering: Energy Dependence.* Phys. Rev. **C58** 641–644 (1998). [arXiv:nucl-th/9802057].

[BHvK99a]   Paulo F. Bedaque, H. W. Hammer, and U. van Kolck. *Renormalization of the three-body system with short-range interactions.* Phys. Rev. Lett. **82** 463–467 (1999). [arXiv:nucl-th/9809025].

[BHvK99b]   Paulo F. Bedaque, H. W. Hammer, and U. van Kolck. *The Three-Boson System with Short-Range Interactions.* Nucl. Phys. **A646** 444–466 (1999). [arXiv:nucl-th/9811046].

[BHvK00]   Paulo F. Bedaque, H. W. Hammer, and U. van Kolck. *Effective Theory of the Triton.* Nucl. Phys. **A676** 357–370 (2000). [arXiv:nucl-th/9906032].

[BKM95]   V. Bernard, Norbert Kaiser, and Ulf-G. Meißner. *Chiral dynamics in nucleons and nuclei.* Int. J. Mod. Phys. **E4** 193–346 (1995). [arXiv:hep-ph/9501384].

[BLMR08]   V'eronique Bernard, Michael Lage, Ulf-G. Meißner, and Akaki Rusetsky. *Resonance properties from the finite-volume energy spectrum.* JHEP **08** 024 (2008). [arXiv:0806.4495].

[BLRM08]   V. Bernard, M. Lage, A. Rusetsky, and U.-G. G. Meißner. *Analysis of the Delta-resonance in a finite volume.* Eur. Phys. J. **A35** 281–285 (2008).

[BM07]   V'eronique Bernard and Ulf-G. Meißner. *Chiral perturbation theory.* Ann. Rev. Nucl. Part. Sci. **57** 33–60 (2007). [arXiv:hep-ph/0611231].

[BS03]   Silas R. Beane and Martin J. Savage. *The quark mass dependence of two-nucleon systems.* Nucl. Phys. **A717** 91–103 (2003). [arXiv:nucl-th/0208021].

[BvK98]   Paulo F. Bedaque and U. van Kolck. *Nucleon deuteron scattering from an effective field theory.* Phys. Lett. **B428** 221–226 (1998). [arXiv:nucl-th/9710073].

[CGL01]   G. Colangelo, J. Gasser, and H. Leutwyler. $\pi\pi$ *scattering.* Nucl. Phys. **B603** 125–179 (2001). [arXiv:hep-ph/0103088].

[CT65]   James W. Cooley and John W. Tukey. *An algorithm for the machine calculation of complex fourier series.* Mathematics of Computation **19** 297–301 (1965).

[DS08]   William Detmold and Martin J. Savage. *The Energy of n Identical Bosons in a Finite Volume at $O(L^{-7})$.* Phys. Rev. **D77** 057502 (2008). [arXiv:0801.0763].

[Efi70]   V. Efimov. *Energy levels arising form the resonant two-body forces in a three-body system.* Phys. Lett. **B33** 563–564 (1970).

[Efi79]   V. Efimov. *Low-Energy properties of three resonantly interacting particles.* Sov. J. Nucl. Phys. **29** 546 (1979).

[EKLM09]   Evgeny Epelbaum, Hermann Krebs, Dean Lee, and Ulf-G. Meißner. *Lattice chiral effective field theory with three-body interactions at next-to-next-to-leading order.* Eur. Phys. J. **A41** 125–139 (2009). [arXiv:0903.1666].

[EMG03]   Evgeny Epelbaum, Ulf-G. Meißner, and Walter Gloeckle. *Nuclear forces in the chiral limit.* Nucl. Phys. **A714** 535–574 (2003). [arXiv:nucl-th/0207089].

[Epe06]   Evgeny Epelbaum. *Few-nucleon forces and systems in chiral effective field theory.* Prog. Part. Nucl. Phys. **57** 654–741 (2006). [arXiv:nucl-th/0509032].

[FGML73]   H. Fritzsch, M. Gell-Mann, and H. Leutwyler. *Advantages of the Color Octet Gluon Picture.* Phys. Lett. **B47** 365–368 (1973).

[FJR10]   Xu Feng, Karl Jansen, and Dru B. Renner. *The $\pi^+\pi^+$ scattering length from maximally twisted mass lattice QCD.* Phys. Lett. **B684** 268–274 (2010). [arXiv:0909.3255].

[FP67]   L. D. Faddeev and V. N. Popov. *Feynman diagrams for the Yang-Mills field.* Phys. Lett. **B25** 29–30 (1967).

[Gau66]   C. F. Gauß. Nachlass: Theoria interpolationis methodo novo tractata. In *Carl Friedrich Gauß, Werke, Band 3*, pages 249–253. Königliche Gesellschaft der Wissenschaften, 1866.

[GL84]   J. Gasser and H. Leutwyler. *Chiral Perturbation Theory to One Loop.* Ann. Phys. **158** 142 (1984).

[GL85]   J. Gasser and H. Leutwyler. *Chiral Perturbation Theory: Expansions in the Mass of the Strange Quark.* Nucl. Phys. **B250** 465 (1985).

[GM62]   Murray Gell-Mann. *Symmetries of baryons and mesons.* Phys. Rev. **125** 1067–1084 (1962).

[GM64]   Murray Gell-Mann. *A Schematic Model of Baryons and Mesons.* Phys. Lett. **8** 214–215 (1964).

[GW73]   D. J. Gross and Frank Wilczek. *Ultraviolet behavior of non-Abelian gauge theories.* Phys. Rev. Lett. **30** 1343–1346 (1973).

[HPP07]   H. W. Hammer, Daniel R. Phillips, and L. Platter. *Pion-mass dependence of three-nucleon observables.* Eur. Phys. J. **A32** 335–347 (2007). [arXiv:0704.3726].

[Joh82]   R. C. Johnson. *Angular momentum on a lattice.* Physics Letters **B114** 147–151 (1982).

[KH09]   Simon Kreuzer and H. W. Hammer. *Efimov physics in a finite volume.* Phys. Lett. **B673** 260–263 (2009). [arXiv:0811.0159].

[KH10]   Simon Kreuzer and H. W. Hammer. *On the modification of the Efimov spectrum in a finite cubic box.* Eur. Phys. J. **A43** 229–240 (2010). [arXiv:0910.2191].

[KMW$^+$05] T. Kraemer, M. Mark, P. Waldburger, J. G. Danzl, C. Chin, B. Engeser, A. D. Lange, K. Pilch, A. Jaakkola, H. C. Naegerl, and R. Grimm. *Experimental evidence for efimov quantum states.* Nature **440** 315–318. 17 p (2005).

[KSW98a]   David B. Kaplan, Martin J. Savage, and Mark B. Wise. *A new expansion for nucleon nucleon interactions.* Phys. Lett. **B424** 390–396 (1998). [arXiv:nucl-th/9801034].

[KSW98b]   David B. Kaplan, Martin J. Savage, and Mark B. Wise. *Two-nucleon systems from effective field theory.* Nucl. Phys. **B534** 329–355 (1998). [arXiv:nucl-th/9802075].

[Lee]   Dean J. Lee. Personal Communication. April 2010.

[Lüs91a]   Martin Lüscher. *Signatures of unstable particles in finite volume.* Nucl. Phys. **B364** 237–254 (1991).

[Lüs91b]   Martin Lüscher. *Two particle states on a torus and their relation to the scattering matrix.* Nucl. Phys. **B354** 531–578 (1991).

[Ne'61]   Yuval Ne'eman. *Derivation of strong interactions from a gauge invariance.* Nucl. Phys. **26** 222–229 (1961).

[Nec08]   Silvia Necco. *Chiral low-energy constants from lattice QCD.* PoS CONFINEMENT8 024 (2008). [arXiv:0901.4257].

[PC07]   L. Pricoupenko and Y. Castin. *Three fermions in a box at the unitary limit: universality in a lattice model.* Journal of Physics **A40** 12863–12872 (2007). [arXiv:0705.1502].

[Pol73]   H. David Politzer. *Reliable perturbative results for strong interactions?* Phys. Rev. Lett. **30** 1346–1349 (1973).

[PTVF07]   William H. Press, Saul A. Teukolsky, William T. Vetterling, and Brian P. Flannery. *Numerical Recipes: The Art of Scientific Computing, Third Edition.* Cambridge University Press, 2007.

[Roy71]   S. M. Roy. *Exact integral equation for pion pion scattering involving only physical region partial waves.* Phys. Lett. **B36** 353 (1971).

[Tan07]   Shina Tan. *Three-boson problem at low energy and Implications for dilute Bose-Einstein condensates.* 2007. [arXiv:0709.2530].

[vdLB47]   Fred C. von der Lage and H. A. Bethe. *A Method for Obtaining Electronic Eigenfunctions and Eigenvalues in Solids with An Application to Sodium.* Phys. Rev. **71** 612–622 (1947).

[vK97]   U. van Kolck. *Nucleon nucleon interaction and isospin violation.* 1997. [arXiv:hep-ph/9711222].

[vK99]   U. van Kolck. *Effective field theory of short-range forces.* Nucl. Phys. **A645** 273–302 (1999). [arXiv:nucl-th/9808007].

[WC06]   Felix Werner and Yvan Castin. *The unitary three-body problem in a trap.* Phys. Rev. Lett. **97** 150401 (2006). [arXiv:cond-mat/0507399].

[Wei79]   Steven Weinberg. *Phenomenological Lagrangians.* Physica **A96** 327 (1979).

[Wig37]   E. Wigner. *On the consequences of the symmetry of the nuclear hamiltonian on the spectroscopy of nuclei.* Phys. Rev. **51** 106–119 (1937).

[Wil74]   Kenneth G. Wilson. *Confinement of quarks.* Phys. Rev. **D10** 2445–2459 (1974).

List of Tables

List of Figures

Danksagung

Am Ende dieser Dissertation möchte ich die Gelegenheit nutzen, meine Dankbarkeit denen gegegnüber auszudrücken, die auf die eine oder andere Art ihren Anteil an der Fertigstellung dieser Arbeit hatten.

Mein erster Dank gilt Hans-Werner. Ich habe mich die gesamte Zeit gut betreut gefühlt und konnte stets mit Fragen und Problemen bezüglich der Arbeit zu Dir kommen. Auch unsere Gespräche über Themen außerhalb der Physik, natürlich insbesondere über Fußball, habe ich immer sehr genossen.

Ich danke Bernard dafür, dass er sich als zweiter Gutachter zur Verfügung gestellt hat. Aber auch für die vielen Diskussionen über Numerik, spezielle Funktionen und Themen quer durch die Physik möchte ich Dir danken.

Christoph, Michael und Simon danke ich dafür, dass sie unser Büro zu einem Ort gemacht haben an den ich gerne gekommen bin, selbst wenn die Diskussionen mal lauter wurden. Gleichermaßen gilt mein Dank dem gesamten Theorieflur des HISKP für die freundschaftliche Atmosphäre. Insbesondere möchte ich hier David und Kerstin nennen, ihr seid für mich mehr als "nur" Kollegen gewesen. Auch die mittwöchlichen Fußballspieler sollen hier nicht unerwähnt bleiben, es hat immer Spaß gemacht.

I owe many thanks to people who discussed this thesis with me in the last four years. Not seldom this helped me to gain a new perspective, thereby advancing this work. Two of these people I want to mention by name, these are Prof. Dean Lee and Prof. Daniel Phillips.

Meinen Freunden bin ich zu Dank verpflichtet für aufmunternde Worte in schwierigen Phasen und dafür, dass ich die Arbeit auch mal kurz vergessen konnte. Ich bin froh darüber, dass die folgende Liste so lang und doch nicht vollständig ist: Andy, Christoph, Daniel, Donate, Eric, Fabian, Francis, Pütti, Rudi, Sabrina und To. Eine Einzelnennung hat sich Else verdient, danke für alles!

Die Unterstützung meiner Eltern während dieser Arbeit ist nur die Spitze des Eisbergs. Ihr habt mich mein ganzes Leben begleitet und unterstützt. Ohne Euch würde ich diese Sätze nicht schreiben. Ich kann Euch nicht genug danken für alles, was Ihr für mich getan habt. Genauso danke ich meinen Schwestern Sarah, Judith und Rebekka. Ich bin glücklich Euch in meinem Leben zu haben.

Danke, Kerstin, für Deine Liebe, Deine Unterstützung und viel mehr als ich hier aufzählen könnte. Ohne Dich wäre mein Leben nicht so erfüllt und glücklich.

Publications and Talks

Refereed Journals

- S. Kreuzer and H.-W. Hammer, *On the modification of the Efimov spectrum in a finite cubic box*, Eur. Phys. J. A **43** 229 (2010) [arXiv:0910.2191 [nucl-th]]

- S. Kreuzer and H. W. Hammer, *Efimov physics in a finite volume*, Phys. Lett. B **673**, 260 (2009) [arXiv:0811.0159 [nucl-th]].

Proceedings

- S. Kreuzer and H. W. Hammer, *Three-boson bound states in finite volume with EFT*, Proceedings of the 19th International IUPAP Conference on Few-Body Problems in Physics, Bonn, Germany, EPJ Web of Conferences, Volume 3, id.04011 (2010)

Talks

- *The Triton in Finite Volume*, Contributed Talk, Spring Meeting of the Deutsche Physikalische Gesellschaft, Division Hadrons and Nuclei, Bonn, Germany, March 16, 2010.

- *The Efimov effect in Finite Volume*, Invited Talk, INT Workshop on Finite-volume Effects in Few-Body systems, Seattle, WA, USA, April 7, 2010

- *Three-body bound states in Finite Volume with EFT*, Contributed Talk, 19th International IUPAP Conference on Few-Body Problems in Physics, Bonn, Germany, September 1, 2009

- *Three-body bound states in Finite Volume with EFT*, Contributed Talk, Spring Meeting of the Deutsche Physikalische Gesellschaft, Division Hadrons and Nuclei, and EPS European Nuclear Physics Conference, Bochum, Germany, March 17, 2009

- *Three-body bound states in Finite Volume with EFT*, Contributed Talk, Spring Meeting of the Deutsche Physikalische Gesellschaft, Division Hadrons and Nuclei, Darmstadt, Germany, March 13, 2008.